Diatom-Inspired Microfluidic Generation of Tunable Emulsions for Macroporous Silica

Frank Zendejas

Electrical Engineering and Computer Sciences
University of California at Berkeley

Technical Report No. UCB/EECS-2007-84
http://www.eecs.berkeley.edu/Pubs/TechRpts/2007/EECS-2007-84.html

June 19, 2007

Diatom-Inspired Microfluidic Generation of Tunable Emulsions for Macroporous Silica

by

Frank Jesse Zendejas

B.S. (California State University, Fresno) 1999

A dissertation submitted in partial satisfaction of the
requirements for the degree of
Doctor of Philosophy
in
Engineering – Electrical Engineering and Computer Sciences
in the
GRADUATE DIVISION
of the
UNIVERSITY OF CALIFORNIA at BERKELEY

Committee in charge:

Professor Roger T. Howe, Co-Chair
Professor Kristofer S.J. Pister, Co-Chair
Professor Jay D. Keasling
Professor Albert P. Pisano

Spring 2007

The dissertation of Frank Jesse Zendejas is approved:

_____

Co-Chair Date

_____

Co-Chair Date

_____

Date

_____

Date

University of California at Berkeley

Spring 2007

Diatom-Inspired Microfluidic Generation of Tunable Emulsions
for Macroporous Silica

by

Frank Jesse Zendejas

Abstract

Diatom-Inspired Microfluidic Generation of Tunable Emulsions

for Macroporous Silica

by

Frank Jesse Zendejas

Doctor in Philosophy in Electrical Engineering and Computer Sciences

University of California at Berkeley

Professor Roger T. Howe, Co-Chair

Professor Kristofer S.J. Pister, Co-Chair

We present a biomimetic approach, inspired by diatoms, to create synthetically derived silica-based porous materials using bioinspired catalysts and emulsions generated in a microfluidic device as templates for silica deposition. This process occurs at near neutral pH, ambient temperature, and pressure. Our approach employs an axisymmetric microfluidic flow-focusing configuration to generate a steady flow of droplets from co-flowing continuous streams. The dispersed phase flows into a central channel, flanked by faster flows of an immiscible continuous phase. The outer flows focus the inner flow through an orifice into a narrow thread. If the flow conditions within the orifice are such that the viscous stresses exerted by the continuous phase cause an imbalance in the surface tension of the dispersed phase stream, the stream ruptures periodically to produce monodisperse droplets.

With precise control over the size and uniformity of the emulsion droplets, we are able to tailor the pore size and size distribution of the resulting bulk silica gels off-chip. Using triethylenetetramine as a biomimetic catalyst, chosen for its similarity to natural polyamines found to catalyze silica precipitation in diatoms, the gelation reactions occur within minutes at room temperature and neutral pH, in contrast to conventional sol-gel processes. Subsequent drying at 50°C and calcinating at 400°C yields glassy materials with spherical pores where the emulsion droplets had been. Monodisperse porous silica with a range of pore sizes from 5 – 50 μm and polydispersity less than 2.4% have been fabricated.

We also describe a new approach to the formation of macroporous silica particles generated through a two-step emulsification process using a single microfluidic device. The first emulsification step (oil-in-water) is generated using flow-focusing, and the subsequent emulsification step (water-in-oil) occurs downstream at a T-junction. Between the formation of the first and second emulsification steps, orthosilicic acid (1M) and triethylenetetramine (6.7mM) are both introduced into the intermediate phase separately using the two microchannels causing the intermediate phase to form a templated silica gel around the inner monodisperse oil droplets. After calcinations, the resulting porous silica particles were 150 μm in diameter with pore sizes on the order of 5 μm.

The incorporation of gold nanoparticles within the intermediate phase of the double emulsion embedded them within the templated silica. During the calcination

process in air, the gold nanoparticles served as catalysts as was clearly evident from the 20 – 40 μm diameter nanowires observed in the silica.

Using diatoms as inspiration, a new technique was demonstrated to create ordered macroporous materials efficiently, by combing template-directed synthesis and biomimetic chemistry with microfluidics. This technique opens the possibility of tailoring materials specific to their intended applications such as bioseparation filters, high surface area catalytic supports, tissue engineering supports, size-exclusion chromatography, and three-dimensional metamaterials for photonics applications.

_____

Professor Roger T. Howe, Co-Chair Date

_____

Professor Kristofer S.J. Pister, Co-Chair Date

A mi madre, mi padre, mis hermanas y mis hermanos

Contents

List of Figures

List of Tables

Acknowledgements

I would like to begin by thanking my advisor Professor Roger T. Howe for his endless moral support, guidance, and motivation throughout my studies as an academic, and as a person. I would like to thank him for allowing me the freedom to guide the project in the directions that were interesting to me. From the first day I met him, his enthusiasm and vast knowledge have continually fueled my desire to do research. His creative and intuitive mind has taught me to think outside the box, and that it's okay to pursue what others may believe is "wild". I would also like to thank my co-advisor Professor Jay D. Keasling for welcoming me into his group and for his continued guidance, support and helpful advice. I would also like to thank the rest of my dissertation committee Professor Albert P. Pisano and Professor Kristofer S.J. Pister for their endless support and valuable discussions.

I would also like to thank the diatom group. In particular, I am grateful to Dr. Uthara Srinivasan for her close collaboration and support throughout this project. I also would like to thank William J. Holtz and Afshan Shaikh for their useful discussions and advice.

As a graduate student, I have had the pleasure of meeting many wonderful and brilliant graduate students, who have influenced me in many ways, and undoubtedly I may accidentally overlook some in this acknowledgement and I apologize to those of you beforehand. I would like to thank Michel M. Maharbiz for his part in mentoring me when I first arrived to Berkeley. His advice was always encouraging, whether he said it in English or in Spanish, and many times that was all I needed to hear to get refocused. I

would also like to thank Noel Arellano for his support, advice, and for becoming a great friend. We have gone through many challenges together, from courses, and prelims, to quals. My experiences would not have been the same without him, thank you brother. I would like to thank both Wesley Chang and Ming-Ting Wu for their support, helpful discussions, humor, and their friendship. I would like to say thank you to Carrie Low for keeping me company at our cubicle and for encouraging me during this writing process. I am also grateful for John Heck, Michael Helmbrecht, Karen Scott, Justin Black, Sunil Bhave, Turgut Aytur, Hyuck Choo, Debbie Jones, Rishi Kant, Peter Chen, J Provine, and Alvaro Padilla. They have made my experience as a student memorable and have also kept me sane.

I would like to thank all the wonderful people of the Berkeley Sensor & Actuator Center for their kindness and helpfulness. I also owe a great deal of thanks to the staff of the Berkeley Microlab. Special thanks go to Marilyn Kushner, Bob Hamilton, Phil Guillory, and Robert Connolly. They have all gone out of their way to assist me in my processing.

I am forever indebted to Dr. Sheila Humphreys, Dr. Carla Trujillo, (they both have called me Dr. Zendejas since the first day they met me), Mary Byrnes, and Ruth Gjerde. They have always looked out for me and have gone the extra mile to ensure I was doing fine. If I ever had a question, or concern, I could go to them in an instant. Thank you for believing in me.

I would like to thank Eastman Kodak Company, for their financial support in the form of a fellowship. Thank you for allowing me the liberty and freedom to pursue any

project I desired. A special thanks to Gilbert Hawkins, my mentor at Kodak, for his encouragement and helpful advice.

Lastly, I would like to thank my family. The two most important and influential people in my life are my mother, Maria Elena Zendejas, and father, Francisco Zendejas. Thank you for raising a young boy, and providing him with all the love, moral and spiritual support, and encouragement needed to grow and succeed. You have always believed in me even when I didn't believe in myself. The phrase I've heard repeatedly from the both of you, "Just do your best, we will be proud of you regardless of the outcome" resonates with me everyday and provides tranquility. I would also like to thank my sisters and brothers who have always supported, motivated, and encouraged me to follow my dreams. Each one of you has served as an endless source of inspiration and I am sincerely grateful.

Chapter 1

Introduction

1.1 MEMS to NEMS

The transition from the micron scale to nanometer scale is driven by the global demand for more functionality in electronic, optical, chemical and biomedical devices. Currently, microfabrication methods are largely based on two-dimensional layer-by-layer processing that relies on the deposition and selective etching of layers. In order to microfabricate dense microelectronics, the resolution limits of ultra violet photolithography are continually being tested. Other alternative lithographic techniques are electron-beam lithography and nanoimprint lithography which both have nanometer resolution; however, electron-beam is a time consuming process and the molds used in nanoimprinting can be damaged after one imprint. Another method commonly used to define nanometer scale features is a technique termed ashing. In this method an existing photoresist feature is etched using oxygen plasma to reduce the overall feature dimension. Although this technique works, a drawback is the difficulty of reproducing

the etch process from run to run. In the overall picture, these techniques remain two-dimensional.

One approach to continue on pace with Moore's Law would be to build three-dimensional microstructures out of the substrate plane. This may sound like science fiction; however there are microorganisms that hold the secrets of how to make three-dimensional nanostructures. By leveraging their fabrication methodologies used to create their structures, this notion of building nanostructures out of plane might be realized.

1.2 Nature's Nanotechnologist

In nature, marine organisms such as diatoms, sponges, and other higher plants, such as grasses, produce biosilica that is essential for the formation of their architecturally diverse and complex shells, spicules, and fibers, respectively. The remarkable control that diatoms and sponges exhibit during the creation of their morphologically ornate structures at nanoscales has attracted a great deal of interest. Consequently, researchers are inspired to study the mechanisms that allow these organisms to form structural features that far exceed the capabilities of present day nanotechnology. In addition, these marine organisms have drawn closer attention because they can create these three-dimensional nanostructures at ambient temperatures and near neutral pH. Present-day processes to form simple silicates require much harsher conditions: extreme pressures, elevated temperatures, and strong acid or alkaline chemicals [1].

Many researchers are currently investigating the biomineralization mechanisms used by sponges [2-5], seashells [6], and higher order plants [7-9]; whereas we on the other hand are drawn to understand the mechanisms used by diatoms to create their highly ordered porous silica shells. We found ourselves asking, "How do diatoms form such an amazingly lace-like structure with nanometer precision; can we better understand the biosilica process in order to explore new methods of mimicking diatoms to create custom tailored porous silica materials?" Before presenting our approach to creating porous silica inspired by diatoms, we briefly review diatoms and the relevant information known about their biosilicification process with the aim of answering our initial questions.

1.3 Diatoms

Diatoms are a group of unicellular brown algae whose ornate nanometer scale shells, known as frustules, are composed of amorphous silica. They are among the most successful organisms on earth; they inhabit most of the world's oceans and fresh waters and account for up to 25% of the world's photosynthesis. As a result, these organisms can fix approximately the same amount of carbon as a terrestrial forest [10-15]. It is not known how many living species of diatoms there are, but it is believed that there are perhaps as many as 100,000 [16, 17].

Diatoms can range in size between 5 μm and 5 mm in diameter and are classified by two main groups: centric or pennate. Centric diatoms possess radial symmetry,

whereas pennate diatoms are elongated and bilaterally symmetrical. In both cases the frustules are composed of two almost equal sized halves where the smaller half fits into the larger half like a petri dish. The two halves are joined together by one or more silica girdle bands. Each species frustules are ornamented with species-specific patterns and structures that consist of rows of pores or slits arranged in a remarkable pattern which results in micro- and nanoporous silica shells with fractal pore structures as small as 5 nm as shown in (Fig. 1.1). These specific patterns make the taxonomic classification of diatoms straightforward [18].

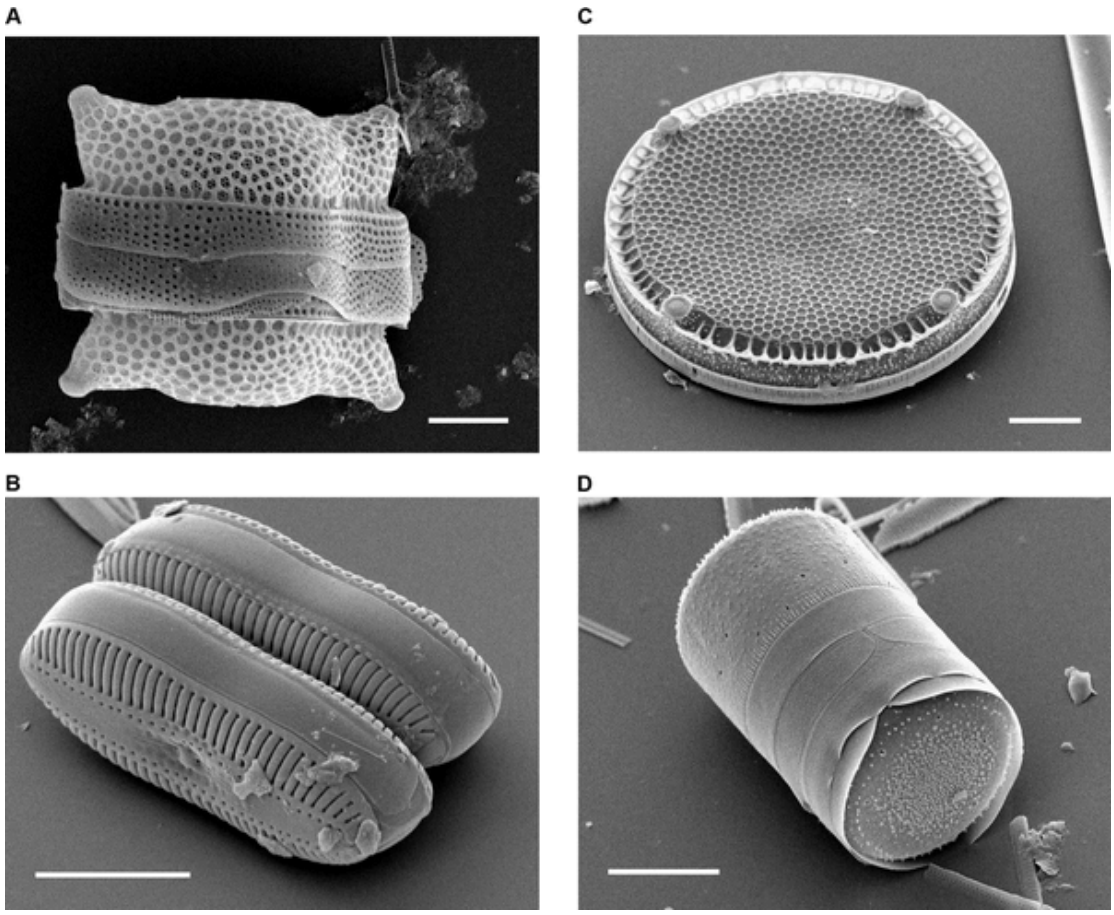

Figure 1.1: Scanning Electron Micrographs of Diatoms. a) Biddulphia reticulata, b) Diploneis sp., c) Eupodiscus radiatus, and d) Melosira varians. Scale bar equals: (10 μm for images a, b, and d) and (20 μm for image c) [19]. (Images courtesy of Mary Ann Tiffany, San Diego State University).

1.3.1 Routes to Elucidating Natures Biosilica Mechanisms

Evolution has had many years to refine the process used by these microorganisms to define their nanostructures, so as nanotechnologists we find ourselves having to cover vast amounts of ground before we can even come close to realizing highly ordered biologically inspired materials. There are a number of approaches that can be taken to

make significant progress in creating biologically inspired materials. One avenue is to study the macromolecules responsible for the precipitation of silica in these microorganisms and learn how to elucidate them to create new structures *in vitro*. A second path is to use analogous synthetic macromolecules that closely resemble the biological molecules responsible for the biogeneses of silica formation to create new structures *in vitro*. Yet another route is to study the genomic sequence of these microorganisms and genetically engineer the microorganism in order to produce tailorable structures *in vivo* specifically designed for further use.

1.3.1.1 Protein-Mediated Biosilica

Until the recent development of advanced biomolecular techniques used to isolate and purify biomolecules and genomic sequencing, little was understood about the molecular mechanisms diatoms use in the formation of their silica structures. Kröger and Sumper were the first to isolate two sets of organic macromolecules from purified diatom, *Cylindrotheca fusiformis*, silica that are responsible in the biogenesis of diatom Biosilica [20-25]. The first set of these macromolecules are polycationic polypeptides named silaffins [20, 22] and the second are long-chain polyamines [24, 25]. It is known that diatoms take up monosilicic acid, which is found in low concentrations and is the predominate form of soluble silicon in natural waters. As a result, Kröger and Sumper found that when either the silaffins or long-chain polyamines were added to a silica precursor, monosilicic acid, a network of nanospheres precipitated in minutes. Other researchers have demonstrated similar results when reacting purified proteins from sea

sponges [3] and monosilicic acid. Since these original findings the chemical structures of the long-chain polyamines have been determined. In contrast, only parts of the silaffins are currently known. A main reason for this shortcoming is that the silaffin extraction and purification process is difficult [23].

1.3.1.2 Biomimetic Silica

Inspired by the observations described above, a number of groups investigated the role that synthetic amino acids, derived peptides, and polyamines play in biomimetic silica precipitation. Taking this approach the complexity of purifying the silaffins is replaced by the simpler task of looking through catalogs of commercially available synthetic molecular structures. However, the question remained whether or not these molecules could catalyze the silica precipitation from monosilicic acid like the silaffins. Most of these synthetic polyamines exhibit long-chain structures analogous to the polyamines found in diatoms. Similar to the silaffins, a number of the polyamines demonstrated fast silica precipitation and flocculation of larger silica aggregates instead of gel formation [26-35]. These results are a positive step in learning the mechanisms responsible for biosilicification, and in developing methods of mimicking the diatom to create custom materials.

1.3.1.3 Genetically Engineering Diatoms

During cell division, creation of a new identical frustule shell for a daughter cell takes place by mitotic cell division. The process of mitotically dividing leads to a reduction in size during successive divisions. As the diatom reaches a critical minimum size, regeneration of a diatom of the original size occurs via sexual reproduction [36]. Diatoms mitotically replicate themselves at roughly three replications a day. As a result, diatoms can be thought of as little factories that continually create identical copies of themselves, as a species, in a massively parallel and precise manner. This has received a great deal of attention because from a fabrication standpoint diatoms can create three-dimensional structures faster than any current layer-by-layer microfabrication process. To gain insight into the replication process used by the diatoms, the genetic code must be carefully studied. As a result, the complete genomic sequence for the marine-centric diatom, *Thalassiosira pseudonana*, has been completed and the genomic sequencing of two other diatoms is currently underway. One of the reasons why *Thalassiosira pseudonana* was chosen to be sequenced is because the entire genome is relatively small at 34 million base pairs, whereas the human genome consists of approximately 3.2 billion base pairs. The motivation for these genomic studies is that once a genome is known, all the proteins of that diatom can be identified and subsequent research can determine the function of each protein.

Hildebrand and coworkers have demonstrated the cloning and isolation of complementary DNA (cDNA) from the diatom *Cylindrotheca fusiformis* [37]. In addition, they are currently using a combination of gene manipulation techniques and

advanced imagining tools to examine the silica frustule formation of the diatom *Thalassiosira pseudonana* [38, 39]. They have successfully isolated genes that encode monosilicic acid transporters which are proteins responsible for transporting silicic acid across the cell's lipid bilayer membrane. In addition, they have observed that during cell division monosilicic acid is collected in a specialized membrane-bound compartment, termed the silica deposition vesicle (SDV), that undergoes movements during the biosilica formation. These intricate movements are believed to play a role in the overall architecture of their nanostructures scaffold; however, there still remains little knowledge of the complete function of each protein and their roles in how diatoms use them to lay down the silica in specific patterns. If one thing is certain, genetically engineering diatoms is a difficult task at present.

1.4 Creating Ordered Nanostructures

Looking closely at the diatom's frustules, they appear to be built from a series of extremely small biosilica particles, roughly 5 nm in diameter, that have aggregated to give a continuous structure. The biomimetic silica particles produced thus far by reacting native proteins or synthetic analogs with monosilicic acid is appreciably larger than the silica particles observed in diatoms. In addition, the surface topography of the biomimetic silica has been observed to be either smooth or very rough depending on which molecule is used to catalyze the reaction. These results have certainly provided

benchmarks; however, the ultimate challenge lies in assembling these silica nanoparticles into three-dimensional networks in a highly controlled manner as the diatoms do.

1.4.1 Directing silica formation

There is no shortage of research devoted towards the development of efficient and innovative fabrication techniques to obtain controlled silica materials with well defined morphologies. A major reason for the growing interest is the large demand for improved silicas with specific properties such as mechanical strength, pore volume, pore-size distribution, and surface area for applications ranging from catalysis, and chromatographic adsorbents. In addition, current industries producing specialty silica globally, under the harsher and environmentally unfriendly conditions, have sales of approximately 2 billion dollars annually [40].

One avenue of interest was manipulating the reaction conditions used during the catalyst and monosilicic acid reaction. For example it was reported that by applying a shearing force, generated by a magnetic stirrer in the reaction vial, elongated fiber-like silica structures were created [41]. Other conditions that have been manipulated are: pH, temperature, reactant concentrations, and aging time [29, 42].

Another avenue takes into account the vast number of templating approaches used to create porous silica such as: using lyotropic liquids [43, 44], block copolymers [45, 46], microemulsions [47-50], foams [51], colloidal arrays [52], surfactants using both micelles and reverse micelles [53-55], viruses [56, 57], bacterial superstructures [58], and

polystyrene spheres [59]; however, these approaches provided porous silica structures with non-uniform shapes, non-uniform pores, varied silica thickness, and which were not structurally stable.

When we started this research our aim was to develop a new approach to the formation of ordered macroporous silica. Unlike conventional methods of creating porous silica, which require harsh conditions, we set out to mimic diatom biosilicification. As micro/nanoemulsions are believed to be central to the diatom's synthetic mechanism in pore structure formation [24], we developed a biomimetic approach to create synthetically derived silica-based porous materials using bioinspired catalysts and emulsions generated in a microfluidic device as templates at near neutral pH, ambient temperature, and pressure. It is our vision that in the future, custom materials may be produced *in situ* within lab-on-a-chip systems and functionalized for use in reaction and separation modules. In addition, a more benign silica process provides a biological friendly environment for the immobilization of enzymes, antibodies and other molecules.

Chapter 2

Microfluidic Emulsification

2.1 Emulsions

As mentioned in the first chapter it has been hypothesized that diatoms use micro/nanoemulsions to template the synthesis of their nanostructured silica frustules [24]. As a result, it is our goal to use a similar approach for the formation of macroporous silica, by using emulsions generated in a microfluidic device as templates for silica deposition. Before describing microfluidic emulsification techniques it is important to first understand the concept of a simple emulsion, how it is created, and the basic principles that govern its stability.

The definition of an emulsion is not straightforward. However, Becher best describes an emulsion as follows, "an emulsion is a heterogeneous system, consisting of at least one immiscible liquid intimately dispersed in another in the form of droplets, whose diameter in general, exceeds 0.1 μm. Such systems possess a minimal stability, which may be accentuated by such additives as surface-active agents, finely divided solids, etc [60]."

There are two main types of emulsions, e.g., oil-in-water (o/w) and water-in-oil (w/o). The droplets in an emulsion are referred to as the dispersed phase, while the surrounding liquid is the continuous phase. Emulsions are traditionally made using one of three mechanical techniques, 1) homogenizers, 2) mixers, or 3) colloid mills. The droplet size of an emulsion can range anywhere from greater than 1.0 μm to less than 50 nm. As a result, the overall appearance of an emulsion can be used to approximate the size of the emulsion droplet according to Table 2.1.

A classic example of an emulsion is oil and vinegar salad dressing. When a salad dressing bottle is left sitting, the oil and vinegar phases separate, so it is necessary to shake the bottle in order to disperse the oil phase into droplets within the continuous vinegar phase before pouring it onto a salad. As soon as the bottle is no longer shaken, the oil droplets begin to recombine and if left long enough, the oil and vinegar phases will again separate. Emulsions are thermodynamically unstable and the recombination of droplets into phase-separated bulk liquids is a natural process. Phase separation can occur via 1) creaming or sedimentation in which drops sink or rise out of the bulk as a result of the density difference between the phases, or 2) flocculation in which the droplets enter an energetically stable situation where the droplets are close to each other but still retain

Droplet Size	**Appearance**
> 1.0 μm	Milky
0.1 – 1.0 μm	Blue-white,(Tyndal effect)
0.05 – 0.1 μm	Grey, (Semi-transparent)
< 0.05 μm	Transparent

Table 2.1: Emulsion droplet size and general appearance.

their integrity. Ultimately, coalescence, the process where drops merge to form larger drops, finally occurs and two distinct immiscible phases form, as shown in (Fig. 2.1). Another process which can occur, but not shown in Figure 2.1, is Ostwald ripening in which larger drops grow and smaller drops shrink due to the larger internal pressure of the smaller drops.

It should be noted here that the emulsions described above are considered macroscopic emulsions because their relative droplet size is on the order of 1 – 10 μm, and are thermodynamically unstable. However, microscopic emulsions have relative droplet sizes on the order of 10 nm, are thermodynamically stable, and form upon simple mixing of the components and do not require the high shear conditions needed to form macroemulsions. The emulsions described in this thesis focus on macroemulsions.

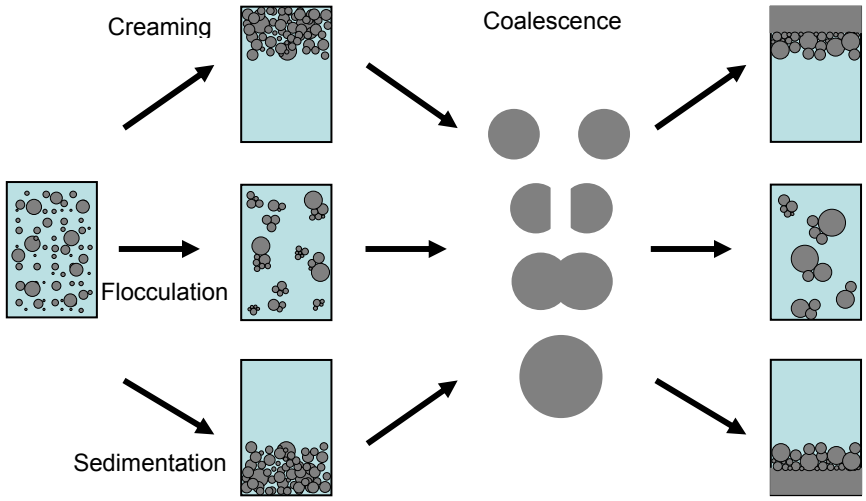

Figure 2.1: Mechanisms of recombination of droplets into phase-separated bulk liquids [60].

A common objective is to keep the emulsion metastable by opposing the mutual approach of the droplets. This is not an easy task to accomplish, especially if no additives are added to the emulsion. The surface area of an emulsion alone is incredible as the following example demonstrates. Suppose 1.0 cm^3 of oil is emulsified into uniform droplets 1.0 μm in diameter. This process generates a total surface area of 6.0 m^2, 10000 times more surface area than the un-emulsified oil. Consequently, it is necessary to introduce surfactants to the emulsion in order to inhibit coalescence by keeping drops from touching through steric or electrostatic repulsion and reduction of the interfacial tension between the liquids.

A surfactant is a surface-active agent, which literally means active at a surface. A characteristic feature of surfactants is their tendency to lower the interfacial free energy of the phase boundary by quickly adsorbing around the dispersed drop as a condensed non-adherent film which will not thin out when two drops collide and thus reducing the coagulation or coalescence between droplets. All surfactant molecules consist of at least two parts, the lyophilic part which is soluble in a specific liquid, while the lyophobic part is insoluble. These two parts are often referred to as the hydrophilic and hydrophobic parts respectively when the fluid is water. A schematic illustration of a surfactant depicting the head and tail group is shown in (Fig. 2.2).

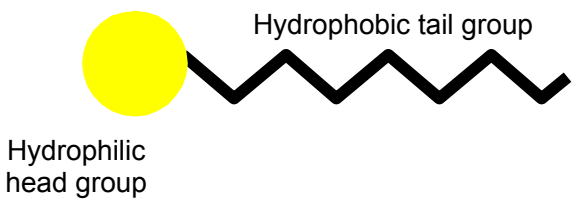

Figure 2.2: Illustration of a surfactant.

Surfactants are classified on the basis of the charge of the polar head group. The common classes are anionic which are negatively charged in solution, cationic which are positively charged in solution, non-ionic which have no electrical charge in solution, and zwitterionics which can be anionic, cationic, or non-ionic in solution depending on the pH of the solution. Surfactants are typically soluble in the continuous phase of the emulsion. At surfactant concentrations below the surfactant molecules are loosely integrated in the water structure and self-assemble at the interface as shown in (Fig. 2.3).

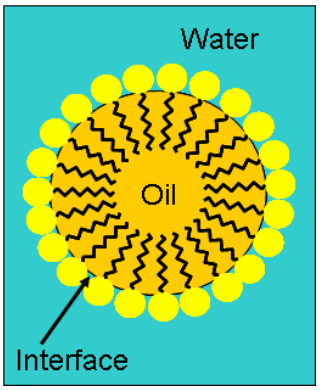

Figure 2.3: Surfactant molecules quickly self-assemble along the water/oil interface.

At higher surfactant concentrations the surfactant structure changes in such a way that the surfactant molecules begin to build up and aggregate into their own structures known as micelles. The point at which surfactants begin to form micelles is known as the critical micelle concentration or CMC. In water, surfactants aggregate with their hydrophobic tail group forming a core while the hydrophilic head group forms the outer shell that maintains favorable contact with water (Fig. 2.4a). In oil, the hydrophilic head group forms the core while the hydrophobic tail group forms the outer shell that maintains favorable contact with oil (Fig. 2.4b). These aggregates are known as reverse micelles.

Lastly, before reviewing microfluidic emulsification techniques, the terminology often used to describe the quality of the emulsion is briefly addressed. Highly uniform emulsions with droplets having narrow size distributions are often referred as monodisperse, whereas non-uniform emulsions are referred to as polydisperse. The degree of droplet uniformity is known as the polydispersity or the coefficient of variation.

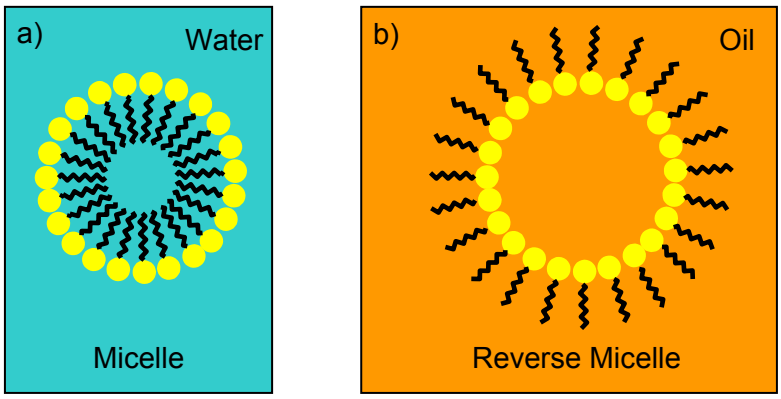

Figure 2.4: Surfactant aggregation upon reaching the critical micelle concentration. a) micelle formed in water, and b) reverse micelle formed in oil.

The value of polydispersity or coefficient of variation is determined by the ratio of the standard deviation of the diameter of a collection of droplets to the average diameter of the same collection. Typically, values below 3% are referred to as monodisperse whereas values greater than 3% are referred to as polydisperse. Microfluidic emulsification techniques have been demonstrated to produce highly uniform emulsions, which are desirable for emulsion templating [61]. These microfluidic emulsification techniques are the subject of the remainder of the chapter.

2.2 Motivation for Microfluidic Emulsification

Emulsions generated using traditional mechanical techniques which include homogenizers, mixers, or colloid mills require a great deal of energy in the form of high shearing forces and pressures. In addition emulsions generated using mechanical techniques produce droplets with a large size distribution, and often the same emulsification is not reproducible when generated under the same conditions [62]. Conversely, microfluidic methods of emulsification are attractive because the emulsion can be generated inside a microsystem, using little energy and microfluidic techniques allow for the precise control of the geometry of the emulsion generator which enables the formation of emulsions with narrow size distributions.

Since the 1980s, a new technology emerged known as micro-electro-mechanical-systems (MEMS), which integrates electronics and mechanical structures using extensions of microelectronic fabrication processes. Subsequently, the same technologies

were used to create devices for controlling fluids at the micron scale which gave rise to the field of microfluidics in the 1990s [63-67]. More recently, research groups have investigated the generation of emulsions using microfluidics for biological and pharmaceutical applications. Microfluidics provides a method of manipulating droplets that are generated using only a minute amount of material, and the droplets can be divided and recombined in a multiplicity of nanoreactors so as to perform high-throughput screening and combinatorial studies.

2.3 Microfluidic Emulsification Techniques

The uniformity of the droplet size is essential for our fundamental emulsion studies for ease of data interpretation and for stability, as Laplace pressure differences between droplets of different sizes can lead to droplet coalescence. With precise control over the size and uniformity of the emulsion droplets, we will be able to tailor the pore size and size distribution of the resulting bulk silica. The current section will review the current microfluidic emulsification techniques.

There are a number of techniques that have been studied to generate emulsions. Early work focused on using porous membranes to generate emulsions [68, 69]. However, with the recent introduction of microfluidics, new techniques for the generation of emulsions have emerged. These microfluidic emulsion generators include: porous membranes, micromachined porous substrates, intersecting channels that form T-junctions, shallow microchannels that approach a ledge, and lastly flow-focusing that

consists of liquid streams that are forced through a single orifice. Each of these techniques will be described further in the following sections. When evaluating the emulsion generating microfluidic devices for our research there are a number of criteria that we considered: 1) the coefficient of variation between droplets (droplet uniformity), 2) droplet size tunability, 3) minimum droplet size, and 4) ease of microfabrication and test setup. With these conditions in mind, we compared microfluidic emulsification techniques to determine which method of generating emulsions is most promising for this application.

2.3.1 Porous Membranes

In membrane emulsification the droplet phase is pushed through a microporous membrane while the continuous phase flows parallel to the membranes surface as illustrated in (Fig. 2.5).

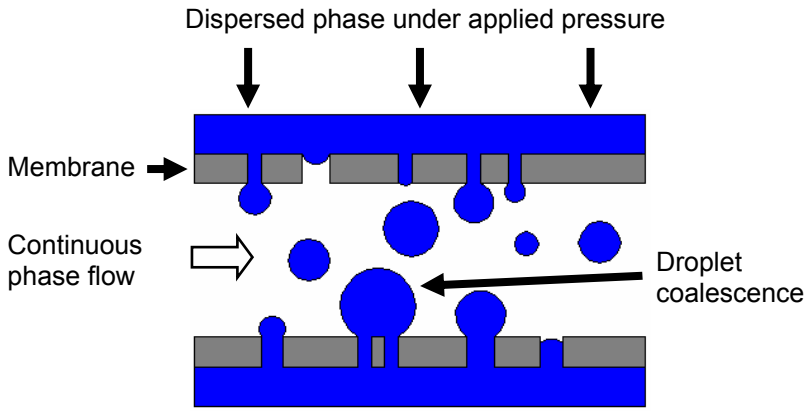

Figure 2.5: Schematic diagram of a traditional membrane emulsification process [68].

As the droplet phase is pushed through the membrane pores, droplets form at the end of each pore and once detached are suspended in the continuous phase. In the literature, there are two common mechanisms that of droplet detachment, the spontaneous transformation-based droplet formation [70, 71] and the second is shear-induced droplet formation [72-74]. In the former, the droplets are generated without the need of a crossing flow from the continuous phase and detach as a result of the minimization of free energy. In the latter, shear induced by the flow of the continuous phase onto the droplet phase causes droplet detachment. The size of the droplets formed due to the shearing flow can be determined by balancing the drag and interfacial tension forces the forces acting on the droplet.

A wide variety of results have been published in the literature with respect to membrane based emulsification. Early work in membrane emulsification focused primarily on the materials chosen for the membranes, such as Shirasu Porous Glass (SPG), glass [75, 76], ceramic [77], and polymeric [72], since the material properties controlled the droplet size rather than the forces induced by the continuous phase. In general, the droplet sizes were determined to be 2-10 times larger than the mean diameter of the membranes pores [76]. The droplet size could not be tuned when the pressure of the droplet phase through the membrane was increased or the shearing force of the continuous phase was varied. The main disadvantage of the membrane emulsification methods was that the coefficient of variation was determined to be greater than 10% [78] and at times up to 50% [72].

2.3.2 Micromachined Porous Substrates

More recently, microfabrication techniques inspired research in silicon-based emulsification membranes. This technique is closely related to the porous membrane method described earlier with the only difference being that the pore geometry and location can be precisely controlled using lithographic and deep reactive ion etching processes. Research done by Kobayashi and coworkers described a silicon substrate with uniformly sized micromachined through-holes, called straight-through microchannels, used to form the emulsification membrane [78-80] as illustrated in (Fig. 2.6).

They reported a coefficient of variation of 1.5 – 5%. Although this does show considerable improvement over conventional porous membranes, the main disadvantage is that the droplet size can not be changed dynamically over the flow rates that were used,

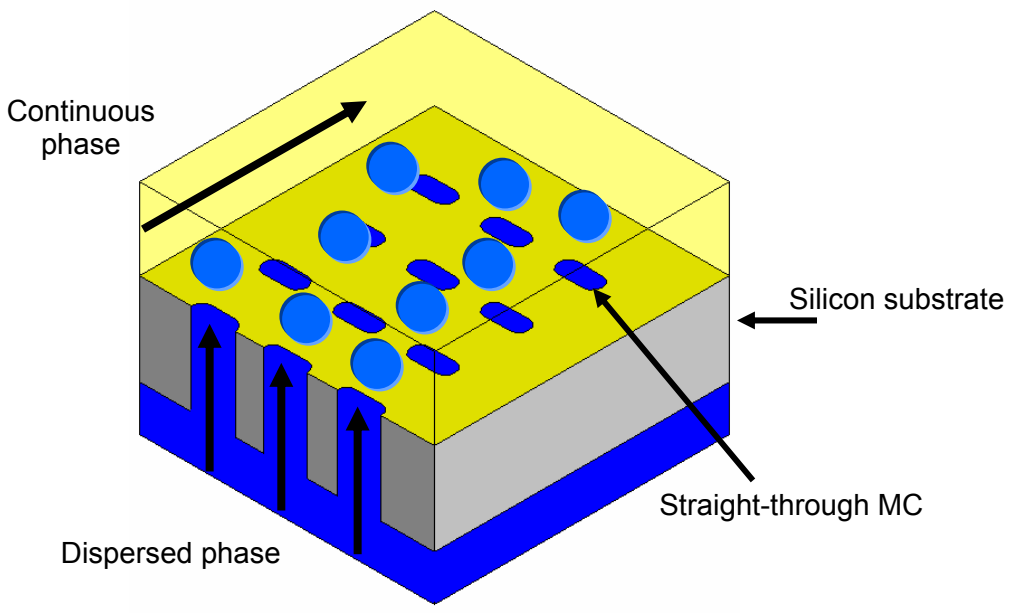

Figure 2.6: Schematic diagram of straight-through microchannel emulsification process [78, 80].

since the droplet size is determined by the geometry of the through-holes. As a result, different silicon etched membranes are required to make varying droplet sizes.

2.3.3 T-junction

A simple microfluidic device for producing droplets is the T-junction. In this emulsification technique two channels intersect one another to form a "T" shape. The droplet phase is flowed through the central channel while the continuous phase is flowed through the main channel (Fig. 2.7). The flow rate of the central channel is in general lower than that of the main channel. As a result, as the droplet phase enters the intersection the continuous phase applies a shearing force causing the generation of droplets. In general the droplet size depends on the flow rates used; however, at relatively low flow rates (low shear), the droplet size depends on the dimensions of the microchannels.

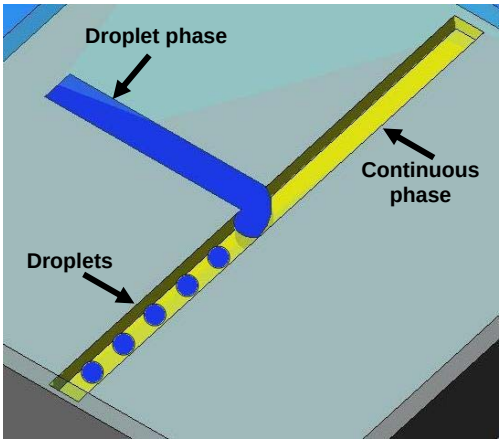

Figure 2.7: Schematic of T-junction droplet formation [81].

Thorsen and coworkers fabricated T-junctions using a micro molding process [81]. Patterned photoresist on a silicon substrate was used to define the microchannel mold. UV curable acrylated urethane was poured over the mold and subsequently exposed to UV light. The molded urethane channels were then encapsulated using a coverslip that had been coated with a thin layer of the urethane and re-exposed to UV light. In their work, they used water as their droplet phase and oil as the continuous phase. It was reported that the droplet size could be controlled by modifying the pressures used for varying the flow rates of both phases. When the pressure of the water phase (P_w), was much less than the pressure of the oil phase (P_o), the water was held in check and no droplets were generated. In the case were P_w was much greater than P_o the water and oil co-flowed through the channels as separate streams. When P_w was equal to P_o a single stream of closely packed droplets that resembled pearl necklaces was generated. Lastly, for the case were P_w was just larger than the critical pressure necessary to force the water phase out into the oil phase, the uniform droplets generated were no longer formed in a single stream like in the pearl necklace case, rather the droplets generated in a zigzag formation. The drop sizes reported ranged between 12.5 ─ 40 μm at oil and water pressures between 8.0 ─ 22.4 psi; however, the coefficient of variation was not reported.

Okushima and coworkers fabricated T-junctions by isotropically etching pyrex substrates or by machine milling Quartz substrates [82, 83]. There was no mention on the method used to encapsulate their channels. In their studies, they used water as the dispersed phase and oils as the continuous phase. They reported generated droplet sizes

between 50 ─ 70 μm with measured coefficient of variation between 2.7 ─ 4.9%. Although the uniformity of the generated droplets is improved, the range of droplet sizes is somewhat limited.

2.3.4 Microchannel Emulsification

In microchannel emulsification an array of shallow narrow microchannels guide the droplet phase onto a terrace ledge where subsequently the droplet phase reaches a deep well where the continuous phase is continually flowed (Fig. 2.8a). A coverslip is used to encapsulate the shallow microchannels. When the droplet phase is forced onto the terrace section of the chip, the dispersed phase begins to form into a distorted disk-like shaped droplet (Fig. 2.8b). As the distorted droplet continues to expand on the terrace there comes a point where the droplet phase reaches the well and at that point spontaneous detachment forms the droplet.

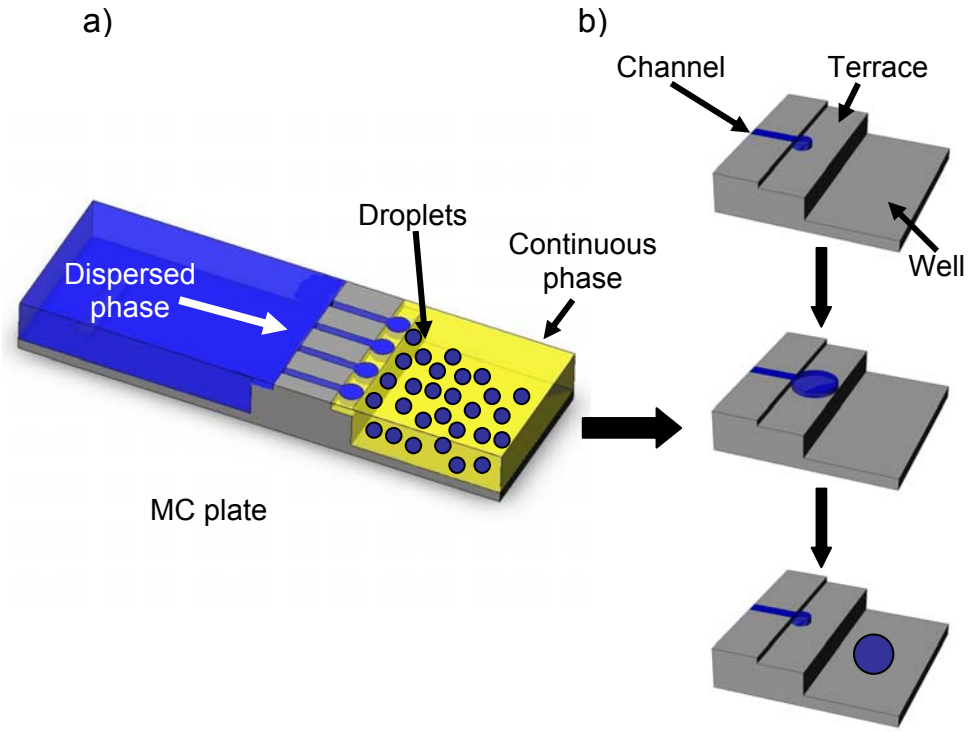

Figure 2.8: (a) Schematic of the microchannel emulsification process. (b) Depiction of the spontaneous detachment process [71].

The distorted disk-like shape plays a critical role in the droplet generation. A disk-like shape has a greater interface area than does a sphere, which results in an instability from the viewpoint of interfacial free energy.

Sugiura and coworkers were the first to propose this technique to prepare uniformly sized droplets with a coefficient of variation of less than 5% at low flow velocities [71]. Their silicon-based emulsification chip was fabricated using a series of deep reactive ion etches to define the microchannels, terrace ledge, and deeply etched well areas. The micromachined chip was then encapsulated by sandwiching it between a

rubber gasket and a glass cover slip in a compact module. In their early work the primary focus was investigating the dependence of the generated droplets to the microchannels length, width, and depth dimensions [71, 84] and by modifying the interfacial tension of the emulsification system [85-87]. They reported no dependence on the microchannel width or length. Uniform droplets, approximately 25 μm in diameter, formed at low flow velocities of between 0.3 ─ 2.0 mm/s [84]. When the depth of the microchannels was varied between 2, 4, 8, and 16 μm, uniform droplets were generated with diameters of 8, 15, 32, and 58 μm, respectively. Therefore, it was reported that the microchannel depth was the dominating factor in determining the droplet size produced. Lastly, for all the cases described above, a critical velocity is reached at flows above 2.0 mm/s. In this regime, the viscous drag forces dominate the interfacial tension and consequently the dispersed phase flows out continuously and produces nonuniform droplets. Although this technique has proven to produce very uniform droplets, its major drawback is that the droplets cannot be tuned, as could be done with the micromachined porous membranes.

2.3.5 Flow-Focusing

Recently, there has been progress in generating droplets using flow-focusing emulsification because such systems generate droplets highly efficiently with tunable sizes ranging from 100's nm to 100's μm and size variation as low as 2 – 5% [61, 88]. In flow-focusing emulsification a dispersed phase flows into a central channel, flanked by faster flows of an immiscible continuous phase. As illustrated in Figure 2.9, the outer flows focus the inner flow through an orifice into a narrow thread. If flow conditions are

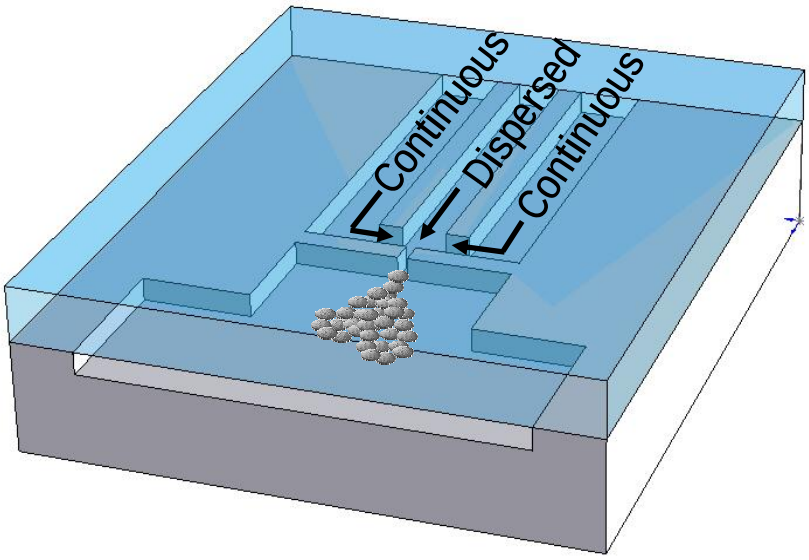

Figure 2.9: Schematic of a flow-focusing device illustrating the three fluids being forced through an orifice producing monodisperse droplets.

such that the viscous stresses exerted by the continuous phase cause an imbalance in the surface tension of the dispersed phase stream, the stream ruptures periodically to produce monodisperse droplets.

In the early 1980's Gañán-Calvo and coworkers demonstrated the generation of monodisperse droplets when a liquid jet is surrounded by an air flow was focused into a thin thread [89, 90]. This process is similar to droplet generation in ink jet printers [91, 92]. In other work, they demonstrated monodisperse gas bubbles by forcing a gas through a capillary tube located upstream of an orifice. The gas and outer liquid streams were forced through the orifice to produce the bubbles [93]. These early works inspired the development of microfluidic flow-focusing.

It must be noted that although flow-focusing has proven to generate monodisperse droplets there is still a great interest in fully understanding the mechanisms responsible for droplet generation. There is a wealth of experimental literature on the topic of flow-focusing. Most of the work has focused on empirically varying parameters such as flow rates [61], liquid viscosities [88], device geometry [94], and liquid-liquid and liquid-gas surface tension [88, 90, 94, 95], to better understand droplet generation. A numerical study of two-phase flow in an axisymmetric flow-focusing device has just been published, which is a promising development [96]. The following section surveys flow-focusing techniques reported in the literature.

2.3.5.1 Flow-Focusing Techniques

Anna and coworkers used soft lithography techniques [97], to fabricate their flow-focusing device out of polydimethylsiloxane (PDMS) in order to generate water-in-oil emulsions [61]. By systematically changing the relative flow rates of the two liquids as well as the total liquid flow rates, they quantified the resulting changes in droplet sizes and size distributions and developed a phase diagram indicating the range of response that was observed. They identified different regions where polydisperse and bi-disperse droplets were generated, and reported a flow rate ratio where monodisperse droplets smaller than the orifice width of 43.5 μm were generated.

Garstecki and coworkers extended the work done by Anna using a similar flow-focusing device to generate gas bubbles in the range of 10 ─ 1000 μm [88]. They

observed two types of bubble generation, which were identified as “period-1” and “period-2”. In period-1 generation, which was observed over a wide range of flow parameters, only a single bubble was formed at the orifice a time. These bubbles had a reported coefficient of variation of 2%. In period-2 generation, which was observed when a critical flow rate was achieved, two bubbles of different sizes formed in the orifice. As a result, the coefficient of variation of the bubble generation increased to more than 15%; however when the coefficient of variation was calculated for the large and small bubbles individually, the coefficient of variation was below 5%. By varying the flow rate and viscosity of the air-liquid phases, they observed that the bubble size was inversely proportional to the product of the viscosity and flow rate. When the surface tension of the system was increased twofold they did not observe any significant change in the bubble size.

Seo and coworkers fabricated a polyurethane flow-focusing emulsification using a molding process to construct two-dimensional oil-in-water lattices [98-101]. Their work was application-focused, rather than directed towards a better understanding of the drop breakup mechanism. A UV curable monomer was used as the dispersed oil phase and water was used as the continuous phase. They generated monomer droplets with a coefficient of variation of 3.0% and high volume fractions. The monomer was photopolymerized downstream of the orifice to form solid lattices.

There is no shortage of applications for very uniform emulsions ranging from foods, pharmaceuticals, and cosmetics to novel engineered materials. Microfluidic

emulsification has provided technologies to produce uniform emulsions that in generally create more stable products.

2.4 Material Selection for Specific Emulsions

The wetting properties of the microfluidic channels play a significant role in determining which of the two immiscible phases will be dispersed as droplets. Therefore, proper considerations need to be taken when selecting the materials used to fabricate a microfluidic emulsification device.

2.4.1 Water-in-Oil or Oil-in-Water

When generating water-in-oil emulsions, hydrophobic materials, including polymers such as, acrylic urethanes, polydimethylsiloxane (PDMS), and polymethylmethacrylate (PMMA), can be used as the substrate. Emulsification devices fabricated from these materials are typically molded from silicon masters since micromachining tools and processes for these materials are immature. The major appeal for these materials is that they are relatively inexpensive and are optically transparent so visual inspection of the droplet generation is facilitated. The reason for requiring a hydrophobic surface to create water-in-oil emulsions is to prevent the wetting by the to-be-dispersed water phase on the substrate since the hydrophobic continuous phase completely wets the microchannels.

For the generation of oil-in-water emulsions, hydrophilic materials such as pyrex, quartz, and oxidized silicon are generally used as the substrates. Emulsification devices fabricated from these materials are typically micromachined using conventional wet, dry, or both etching techniques. Pyrex and quartz substrates like the polymers are optically transparent whereas substrates are not. However, microfluidic devices made from silicon substrates can also provide a means for visual inspection if encapsulated with pyrex or quartz. For reasons similar to the water-in-oil emulsions, a hydrophilic surface is required for oil-in-water emulsions. The continuous water phase in this case wets the microchannels completely while preventing the hydrophobic droplet phase from wetting and becoming pinned on the surface.

There may arise occasions where a particular material must be used as the substrate, even though it may not have the correct surface wetting properties. In this event, there are techniques that can be used to modify the surface properties so that the surface properties become hydrophilic or hydrophobic. Oxygen plasma treatments are commonly used to render hydrophobic polymers hydrophilic [102]. Similarly, for hydrophilic materials such as pyrex, quartz, and oxidized silicon a number of techniques such as applying self-assembled monolayers (SAM's) have been used to render the surface hydrophobic. There are a few drawbacks of having to modify the surface properties of a material. The newly modified surface properties typically last for only a given amount of time and then the original surface properties are restored. For example, the broken polymer chains repair themselves as the SAM's wash away. As a result, the surfaces will frequently need to be retreated.

2.5 Microfluidic Emulsification Using Flow-Focusing

After reviewing the literature on emulsification techniques we determined that the flow-focusing method satisfied all of the criteria that our application would require. Specifically, flow-focusing emulsification has proven to produce very monodisperse droplets, the size of the droplets could be modified dynamically, a single design could produce droplets with sizes in the range between hundreds of microns to tens of microns, and lastly the microfabrication process was fairly straightforward. A schematic image of our microfluidic device is shown in (Fig. 2.10).

The next section describes the process used to microfabricate our microfluidic emulsification device, as well as the bonding process used to encapsulate the microchannels is addressed.

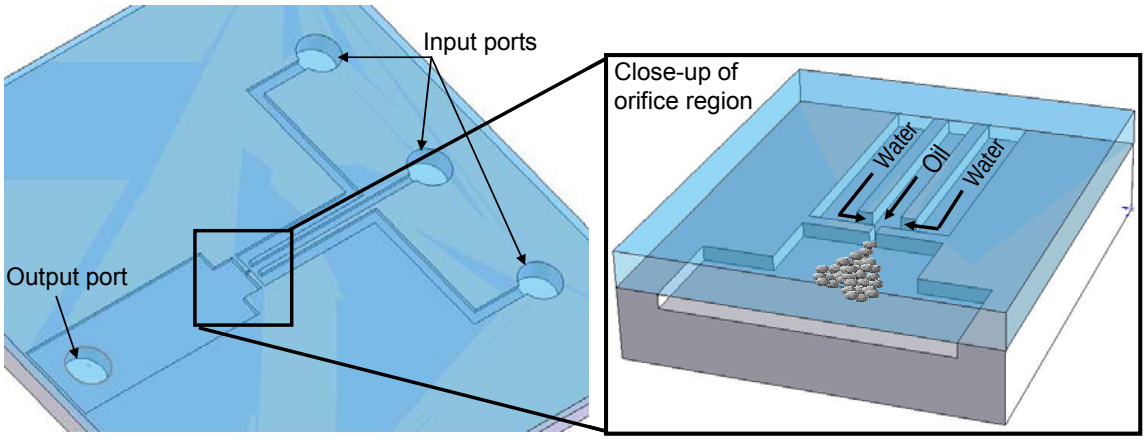

Figure 2.10: A schematic of our flow-focusing microfluidic emulsification device adapted from [61].

2.5.1 Microfabrication and Chip Bonding

2.5.1.1 Fabrication

The microfluidic emulsification chip used in this work was fabricated from silicon (100) substrates using a two-step deep reactive ion etch (DRIE) process. The process flow is depicted in (Fig. 2.11). The microchannels on the bare silicon substrate were defined using a 2.8 μm layer of I-line photoresist. Following photolithographic exposure and development of the first layer pattern the photoresist was baked for 2 hours to provide a durable masking layer. The unprotected areas were etched 120 μm deep in the first of two DRIE steps in an Surface Technology System (STS) advanced silicon etcher using the Bosch process. After the etching was complete the photoresist mask was removed using PRS3000 at 90°C for 2 hours. The substrate was then cleaned in piranha, a 4:1 (vol) solution of concentrated sulfuric acid and 30% hydrogen peroxide to remove any trace organics.

Before patterning the backside of the wafer with photoresist to define the etch locations for the fluidic ports (through-holes), the wafer needed to be bonded to an oxidized silicon handle wafer. This step is necessary because through-wafer etches on single substrates are not allowed in our clean room facility in order to avoid etching the electrostatic clamp. The device substrate was bonded to the handle wafer with the microchannels facing down using standard I-line photoresist as an adhesion layer. The backside of the wafer was then patterned with a 9 μm layer of SPR 220 photoresist (Shipley) and the second DRIE step was used for the through-wafer etch to create the

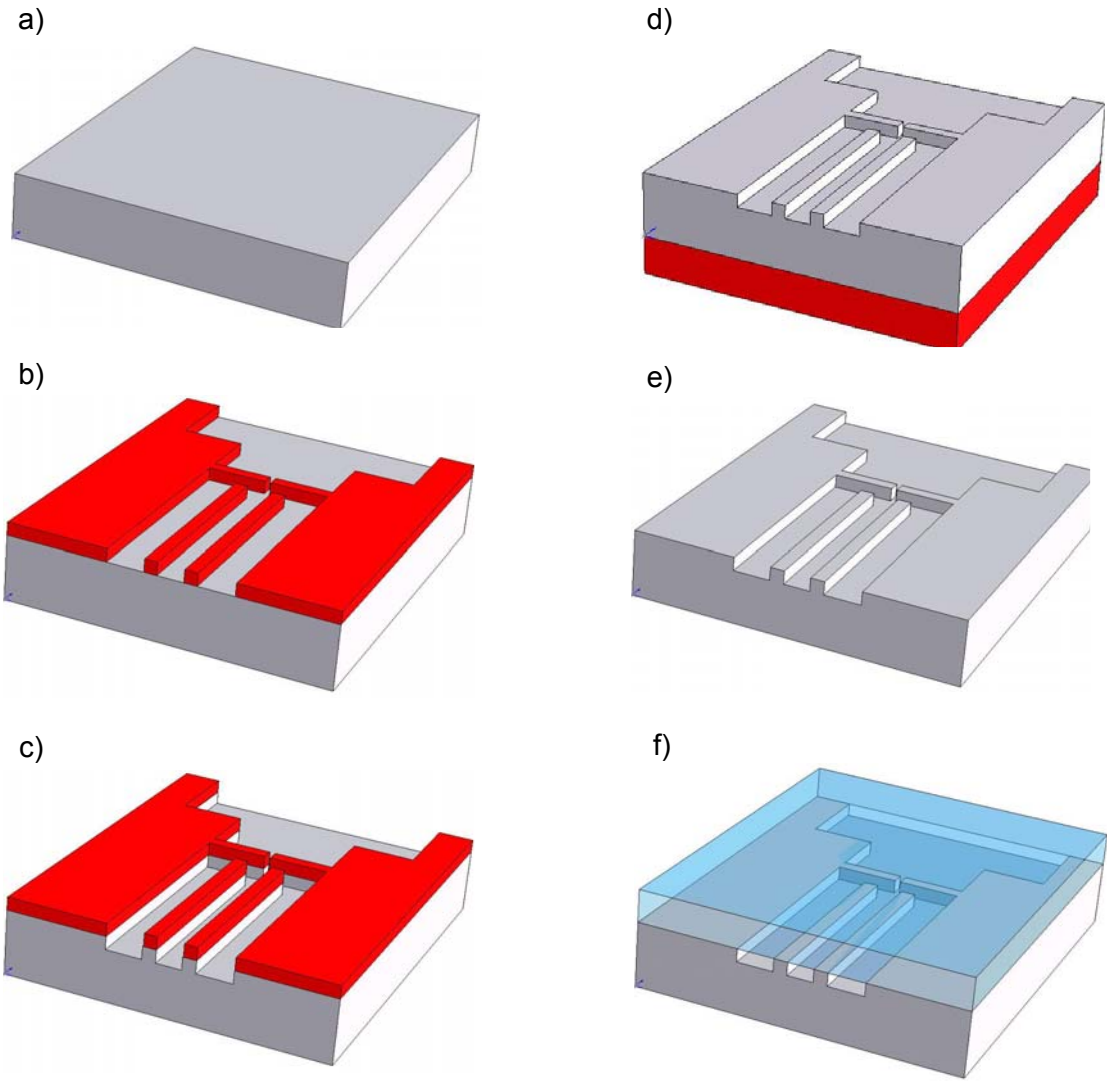

Figure 2.11: Process flow for the fabrication of the flow-focusing emulsification device. (a) The starting substrate is a bare silicon (100) wafer. (b) Photoresist is patterned to define the microchannels, (c) deep reactive ion etching is used to etch the silicon, (d) the first photoresist masking layer is removed and a second layer of photoresist is patterned on the backside of the wafer to define the through-wafer holes, (e) the second photoresist masking layer is removed, (f) the wafer is encapsulated with a glass coverslip.

fluidic ports. The bonded wafers were then separated by immersing the pair in PRS3000 at 90°C for 24 hours.

Due to the handle wafer, the STS wafer holder could not cool the device substrate properly and the photoresist used as the adhesion layer began to burn and roughen the microchannels. By etching the through-wafer holes first and then etching the microchannels, this problem was solved. Also, Cool Grease™ (AI Technology) became available to use as an adhesion layer for wafer to handle wafer bonding. This new material provided two major benefits, better thermal conductivity, so the cooling problems experienced by the substrates in the STS was no longer a problem, and easier separation of the pair of wafers. By immersing the pair in acetone at room temperature under ultrasonication, they could be separated in 30 minutes.

The wafer was then manually recoated with STR-1075 photoresist (Shipley) at 800 RPM on a spin coater to provide a thick protective film for the sawing of 1 cm^2 dice. The dice were then cleaned in PRS3000 at 90°C for 2 hours followed by a 30 minute piranha clean. Lastly, the dice were immersed for 30 seconds in concentrated hydrofluoric acid to remove the native oxide in preparation for coverslip encapsulation. A SEM of a fabricated device is shown in (Fig. 2.12).

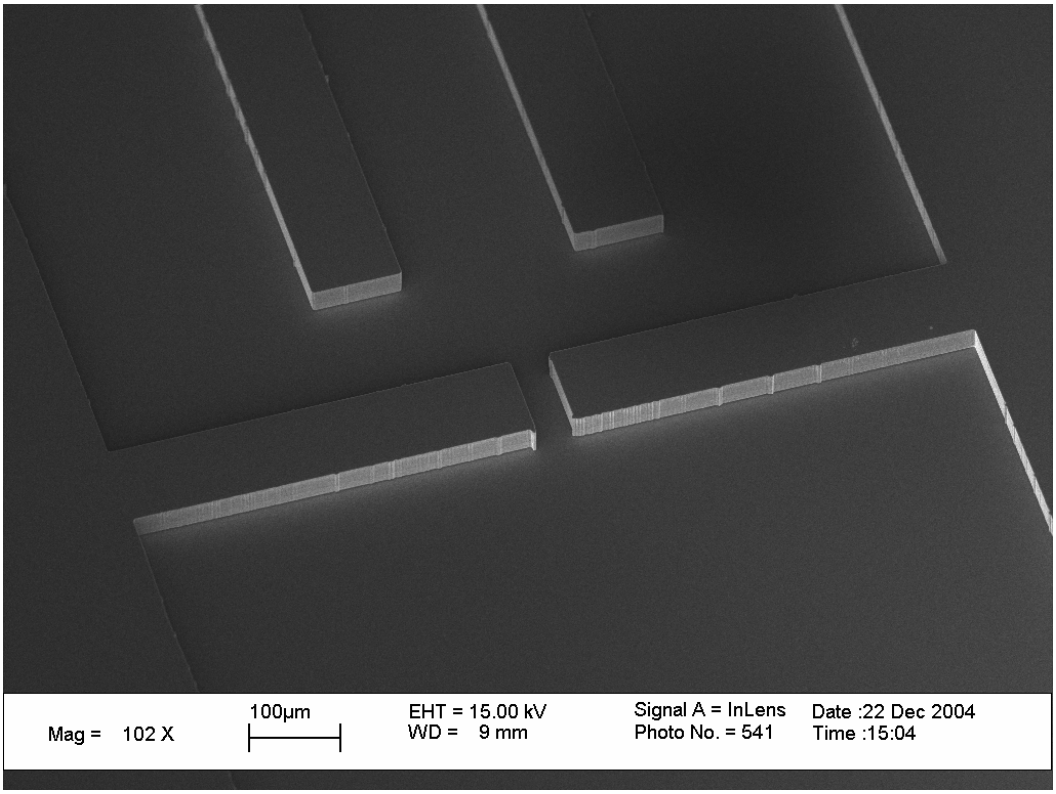

Figure 2.12: SEM micrograph of a fabricated emulsification device depicting the orifice region. The microchannels are 30 μm deep, and the orifice is 105 μm long and 43.5 μm wide.

2.5.1.2 Chip Bonding

After cleaning the dice the channels were sealed by bonding a glass coverslip using a thin layer of RTV615 series polydimethylsiloxane (GE Silicones) as an adhesion layer. We decided to bond the chips in this manner because we wanted to be able to easily remove the coverslip. A piece of dicing tape is applied to the backside of the silicon chip in order to plug the through-wafer holes. The chip is then placed onto an

intermediate glass slide face up, so that the glass coverslip can be placed on it during the bonding process.

A 1 cm^2 area puddle of PDMS is poured onto a 1 $inch^2$ coverslip. The coverslip was manually ramped up at a rate of 333 RPM/s for 15 seconds and then allowed to spin at a constant 5000 RPM for an additional 10 seconds. After coating, the coverslip was then left to sit for 5 minutes in order to let air bubbles outgas and to provide sufficient time for the ripples in the PDMS film to evenly spread out across the coverslip. The coverslip was then placed on a 90°C hotplate for 3 minutes to pre-cure the PDMS. This step causes the PDMS to crosslink; however, it remains very tacky since the polymer is not fully cured.

The coverslip is then carefully placed over the silicon chip paying close attention so as to not press down on the coverslip because doing so will cause the PDMS to fill the channels and ruin the chip. The tacked coverslip/chip pair is flipped so the coverslip side of the pair is resting on the intermediate slide. The intermediate slide including the tacked pair was then placed in an oven at 120°C for 10 minutes to permit the PDMS to fully cure. The dicing tape was then removed and the chip was ready to go through the process used to create the connections for fluidic interfacing between the chip and pumps. Images of several bonded chips are shown in (Fig. 2.13).

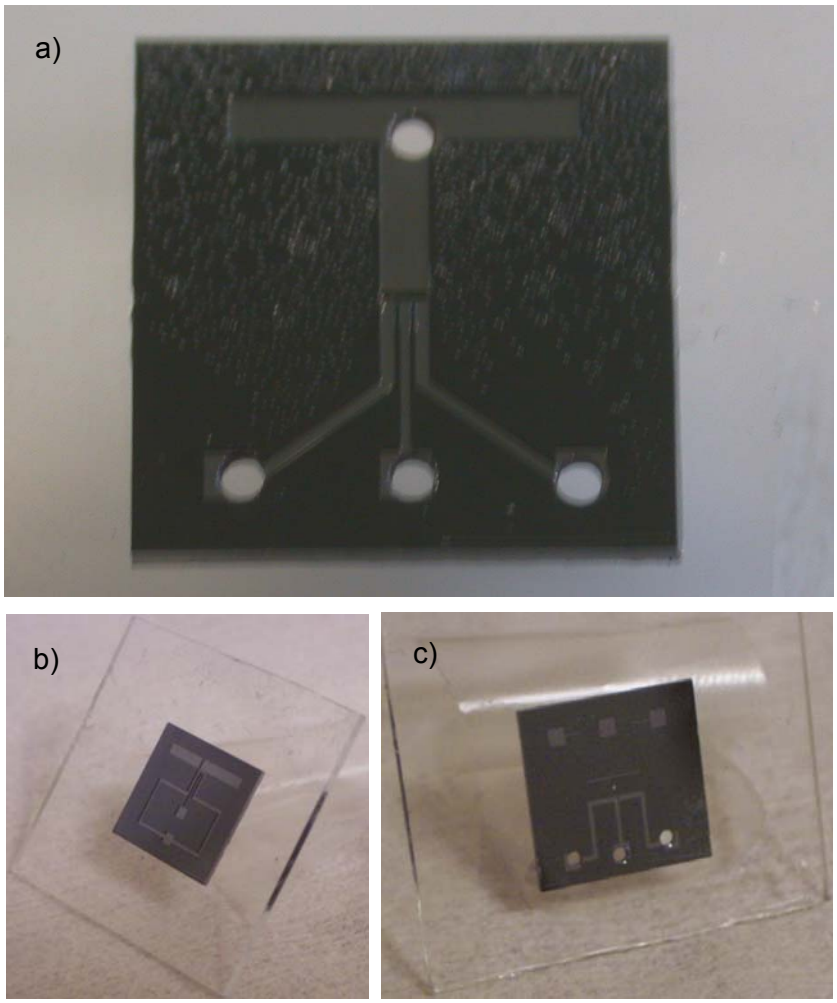

Figure 2.13: Silicon chips bonded to glass coverslips using PDMS as an adhesion layer. (a) Flow-focusing emulsification device, the through-wafer holes in this device were drilled using a 1 mm diamond drill bit. (b) A second version of the flow-focusing device. (c) A microchannel/terrace emulsification device that also had drilled through-wafer holes.

The dicing tape proved to be an important step in the bonding process because anytime the tape was not used the PDMS would fill the microchannels independent of how long we allowed the thin layer of PDMS to pre-cure. The dicing tape provides a method of

trapping air within the through-wafer holes and microchannels when the coverslip is placed over the silicon chip that effectively prevents the pre-cured PDMS from filling the channels.

2.5.2 Fluidic Interfacing

To interface the chip to the pumps we decided to glue blunt luer lock syringe needles to the chip. It was difficult finding needles with the precise outer diameter that matched our through-wafer holes so we developed a process as depicted in Figure 2.14 to glue our syringe needles. Disposable pipette tips were first trimmed so that the tip could fit snugly into the through-wafer hole yet not touch the glass coverslip. The pipette tips were then trimmed at the other end and glued to the silicon chip with epoxy. The syringe

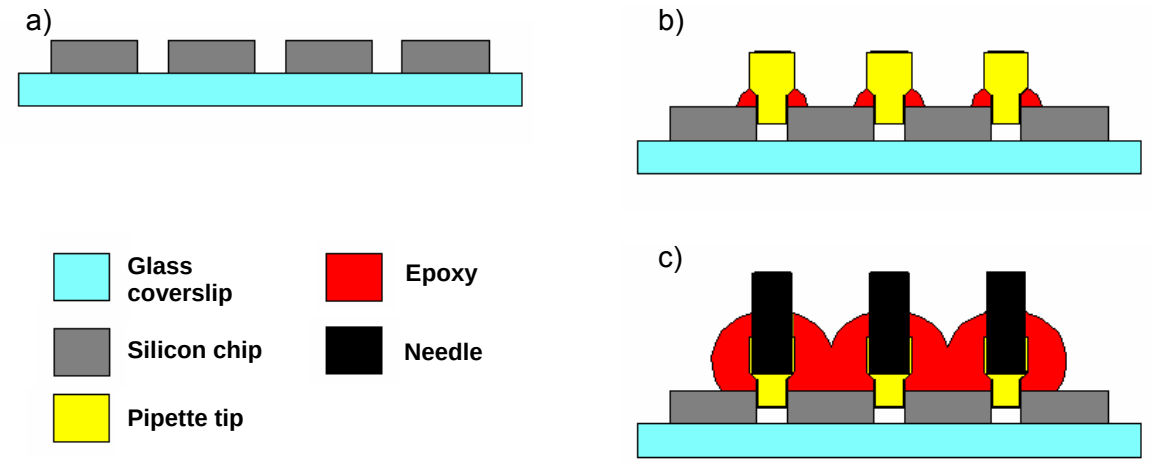

Figure 2.14: Cross-sectional view of the process developed to glue luer lock syringes to silicon chip. (a) PDMS bonded silicon chip. (b) Trimmed pipette tips were wedged into the through-wafer holes and glued in place. (c) Syringe needles were wedged into the glued pipette tips and glued in place with a second epoxy coating.

needles were then inserted snugly into the trimmed pipettes and glued in place using another coat of epoxy. High viscosity quick drying epoxy was the glue of choice at these steps because epoxy with low viscosity (water-like) tends to seep its way through the pipette tip and silicon interface and wets the inside of the channels causing them to plug. Silicone tubing (Cole-Parmer) and conventional luer lock connections were used to interconnect the chip to the pumps.

2.6 Experimental Setup

2.6.1 Liquids and Surfactants Used

We ran the flow-focusing emulsification chip using a number of liquids and surfactants to prepare both oil-in-water and air-in-water emulsions. When generating oil droplets in water we used hexadecane (Sigma-Aldrich) as received for the discontinuous phase while sodium dodecyl sulfate SDS (Sigma-Aldrich) surfactant solubilized in water at concentrations between (0 – 6)% (w/v) were used as the continuous phase. In other experiments where air bubbles in water were generated, compressed air was used as the discontinuous phase while DI water mixed with 52% (w/w) glycerol (Fisher) and 2% (w/w) Tween-20 (Sigma-Aldrich) were used as the continuous phase. The glycerol was used to modify the viscosity of the DI water while Tween-20 was used as the surfactant. All the liquids were filtered through 0.45 μm syringe filters (Cole-Parmer) to remove any aggregates and prevent clogging of the microchannels before being used.

2.6.2 Reynolds Number

The Reynolds number in fluid mechanics is a dimensionless parameter of the ratio of inertial forces to viscous forces and is used for determining whether a flow will be laminar (Re < 2300) or turbulent (Re > 4000). Laminar flow occurs at low Reynolds numbers, where viscous forces are dominant, and is characterized by smooth, constant fluid motion, while turbulent flow, on the other hand, occurs at high Reynolds numbers and is dominated by inertial forces, producing random eddies, vortices and other flow fluctuations. Before running the chip we calculated the Reynolds number for a range of operating flow rates that we expected to use. For our purpose we can express the Reynolds number as follows:

$$R_e = \frac{Q}{\frac{\mu}{\rho} \times h} \tag{2.1}$$

where Q is the flow rate of our liquid, μ is the viscosity of the liquid, ρ is the density of the liquid and *h* is the height of the flow-focusing orifice. Table 2.2 depicts the Reynolds numbers we calculated and as can be seen the chip will be operating under laminar conditions.

10 μL/min <	**Q**	**< 100 μL/min**
0.1	Re (Air)	1
0.23	Re (Water)	2.27
0.13	Re (Oil)	1.35

Table 2.2: Calculated Reynolds numbers for air, water, and hexadecane oil for the expected operating flow rates.

2.6.3 Test Setup

The testing of the flow-focusing emulsification chip was done under a probe station as shown in (Fig. 2.15). The chip was fixed to the probe station using a scratch-built chip holder. Two digitally-controlled syringe pumps (Cole-Parmer) were used to regulate the flow rates of both liquids. Droplet generation was imaged using a high-speed Cohu 2700 video camera with exposure times as short as 100 μs. Droplet diameters were then measured from recorded images using etched features as a reference.

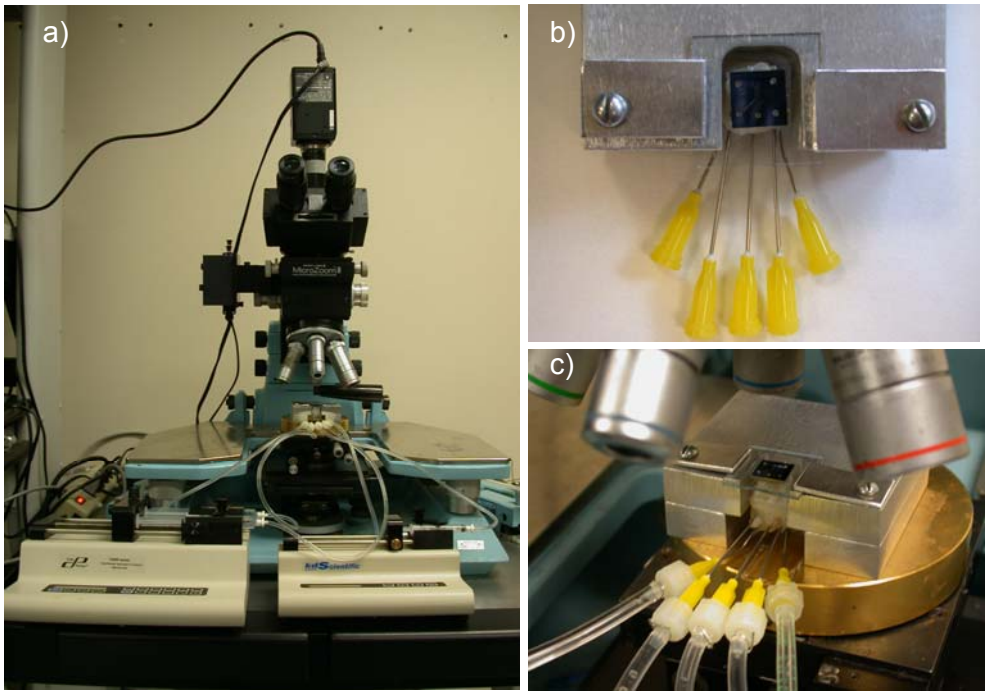

Figure 2.15: Test setup. (a) Two syringe pumps to precisely control flow rates of the oil and water phases, a video camera attached to a microscope for recording drop generation with a VCR. (b) Chip holder. (c) Fluidic connections from the syringe pumps to the emulsification chip were done with glued luer lock syringe needles.

2.6.4 PDMS Chip Bonding Problems

Using the flow-focusing chip, we generated oil-in-water emulsions with varying droplet sizes, size distributions, and droplet generation speeds, similar to work with air-in-water foams in [80] and water-in-oil emulsions in [78]. We quickly began to experience many problems due to the PDMS film used as the adhesion layer. The emulsification device produced non-uniform droplets and in the worst case, completely stopped generating droplets. It is well known that PDMS has a tendency to absorb liquids readily in particular oils; however, when we set out to use a thin film of PDMS as the adhesion layer we did not anticipate that the oil induced swelling would affect our device as much as it actually did. Figure 2.16 shows a close-up of the PDMS bonded chip prior to emulsion generation and a second chip after operation that displays the swelling which causes the flow rates to change in the channels due to the change in the cross-sectional geometry.

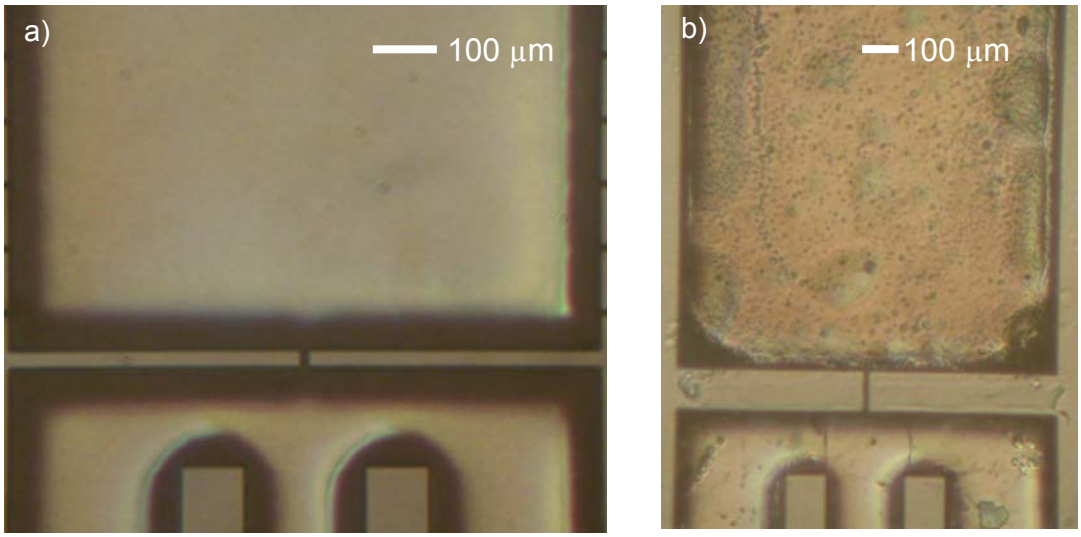

Figure 2.16: Micrographs of PDMS bonded chips. (a) Microfluidic chip prior to operation. (b) A chip after operation showing evidence of oil induced swelling. Consequently shallow (5 – 10) μm channels tend to seal up and our device stops functioning.

A second problem experienced due to the PDMS swelling was that small PDMS particles tore off due to the flow of the liquids through the channels. These particles would then clog the orifice. Since the orifice width of our device is 43.5 μm it took only a single particle tens of microns in size to lodge itself in the orifice and disrupt the flow of liquids through the orifice. When this occurred, it was necessary to remove all the fluidic connections to the chip and force liquids in the reverse direction to try and flush out the debris. Many times the forces necessary to do this ended up creating more particles and worsened the problem.

2.6.5 Chip Bonding Solutions

To solve both the oil induced swelling and the particulate problems experienced using PDMS as an adhesion layer we decided to use an anodic bonding process to encapsulate our device. Anodic bonding of quartz and pyrex to silicon is a standard process [103, 104], where a large voltage potential is applied across the pair of substrates at temperatures starting at 400°C to slightly below the melting temperature of quartz or pyrex.

After cleaning the substrate in piranha, the channels were sealed by anodic bonding of a pyrex wafer using a Suss SB6 Anodic Bonder at a temperature of 400°C, voltage of -450 V, and a maximum current of 1 mA shown in (Fig. 2.17). The benefits of anodic bonding include: 1) the bonding process is less time and process intensive, 2) the microfluidic device can be cleaned after being used with chemicals, such as acetone, which was not otherwise possible due to the PDMS, 3) there are no longer problems with PDMS particulates clogging the orifice, and 4) the channels maintain their geometry during operation, which permits constant flow rates.

Additionally we switched from using glued pipette tips and syringe needles to using NanoPort™ assemblies (Upchurch Scientific). These NanoPort™ assemblies facilitate interconnection to Hamilton gas-tight syringes via Halar tubing (Upchurch Scientific). To apply the NanoPort™ assemblies, the silicon substrate was wiped clean using an acetone damped clean-wipe. Adhesive rings that were provided were placed around each of the fluidic ports on the chip. A provided gasket was then placed just inside of the adhesive ring. The NanoPort™ assemblies were carefully paced over the

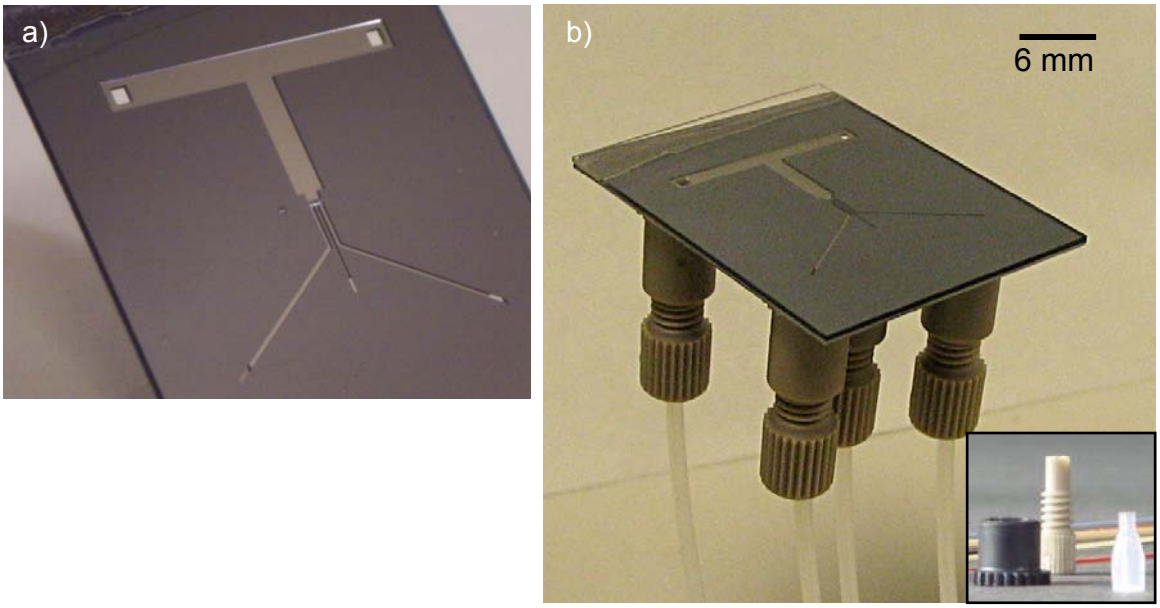

Figure 2.17 Anodic bonded Pyrex to silicon chip with NanoPort™ assemblies used for fluidic interfacing.

adhesive and gasket and held securely to the chip using a large binder clip as a clamp. The final step in the process is a heat curing step to activate the adhesive. Depending on the temperature used (121 ─ 177)°C the curing time can take anywhere between (95 ─ 6) minutes respectively.

2.7 Conclusions

In summary, we decided to pursue flow-focusing emulsification to produce emulsions because it has proven to be a viable technology of producing monodisperse droplets while the size of the droplets could be modified dynamically in a single chip design. We successfully demonstrated the microfabrication of our flow-focusing device,

although we encountered problems due to the oil induced swelling of the adhesion layer. Anodic bonding proved to be the optimal choice for sealing our device because along with the NanoPort™ assembly's we reduced the time required to assemble the fluidic interfacing as well as minimized the risk of debris from the PDMS plug our device.

In the next chapter we focus our efforts on characterizing the generated oil-in-water and air-in-water emulsion droplets/bubbles in order to determine which emulsion will provide a stable template for silica pore formation.

Chapter 3

Droplet Generation and Characterization

3.1 Droplet Generation and Results

Having resolved all the troubles experienced with the first generation chip-bonding process we characterize both air-in-water and oil-in-water emulsions generated from the microfluidic emulsification device. Our aim is to demonstrate that the flow-focusing emulsification device is capable of making porous materials via emulsion templating. Additionally, we demonstrate the ability to generate double emulsions, in which the internal encapsulated droplets serve as templates for forming porous particles.

3.1.1 Air-in-Water Bubble Generation:

To generate an air-in-water foam a filtered solution of DI water, glycerol (52% (w/w)), and Tween-20 surfactant (2% (w/w)) was used as the continuous aqueous phase and an empty gas-tight syringe was used to inject the dispersed gas phase. Glycerol was added to the solution in order to increase the viscosity to μ = 6.1 mPa from that of DI

water μ = 0.92 mPa [88]. Both the liquid and gas phases were pumped into the emulsification device using digitally controlled syringe pumps. To generate bubbles of varying sizes and size distributions, the liquid and gas flow rates were varied, spanning air/water ratios from ~1:1 to 1:80. The dimensions of the emulsification chip used in this work were: microchannel depth of 120 μm, orifice width and length of 43.5 and 105 μm, respectively, and outlet channel length of 30 mm. A micrograph illustrating the gas and water phases including the bubble break-up region is shown in (Fig. 3.1).

To demonstrate control of bubble formation over a range of air flow rates, the average bubble size verses inner air flow rate was measured and plotted, while the outer water flow rate was maintained constant at (40 and 80 μL/min) (Fig. 3.2). The procedure in which the flow rates were varied was as followed. The air flow rate was initially set to

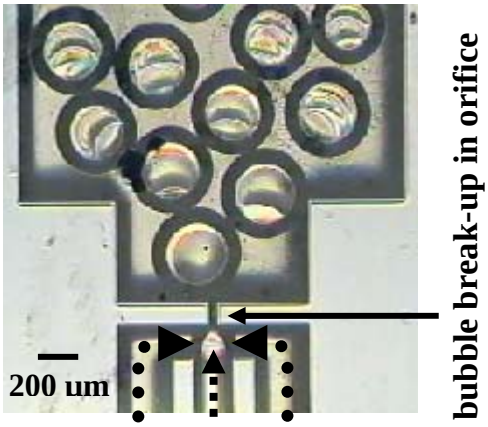

Figure 3.1: Micrograph of flow-focusing device illustrating operation. The continuous water phase (●), flows through the two outer channels while the dispersed gas phase (■), flows through the inner channel. Bubble break-up occurs in the orifice. The dark ring around each air bubble is the result of the bubble being squeezed into a disk-shape.

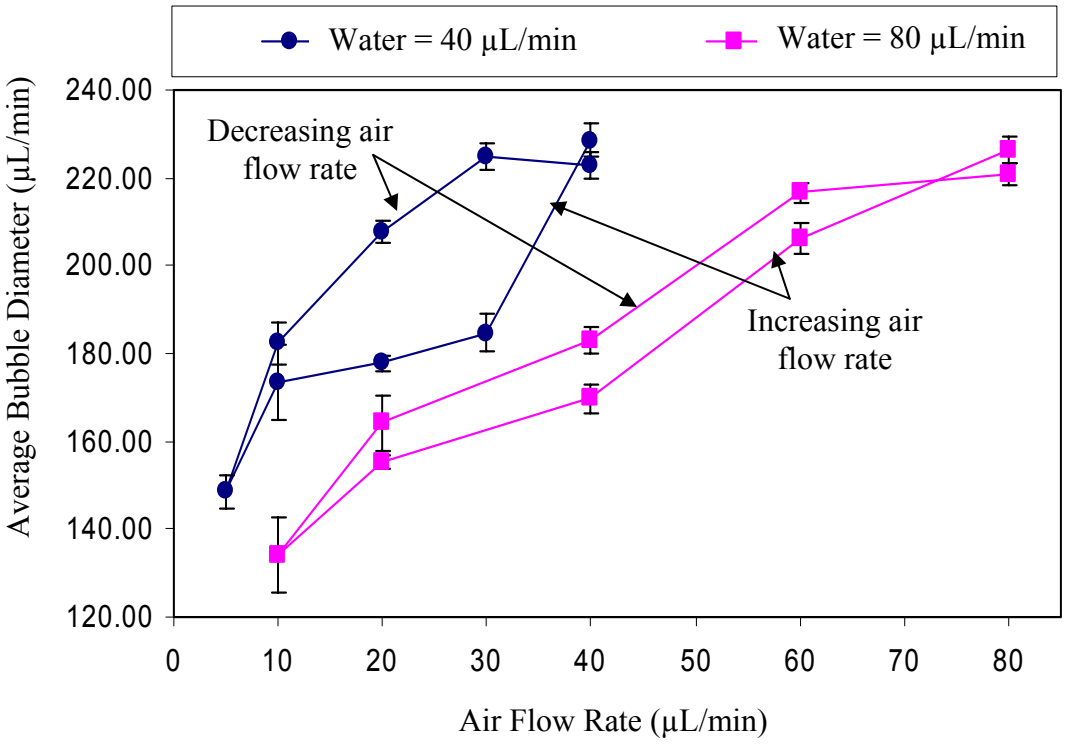

Figure 3.2: Air bubble diameters in air-in-glycerol/water foam (52 wt.% glycerol, 3 wt.% Tween 20) as a function of air flow rate. The water flow rates were held constant at (40 and 80 µL/min), respectively.

equal the respective water flow rate (40 or 80 µL/min) and decreased in (10 or 20 µL/min) increments until the lowest setting of (5 or 10 µL/min) was reached. At that point the air flow rate was increased in (10 or 20 µL/min) increments until the air and water flow rates once again equaled. Bubbles with average diameters between 130 and 230 µm were generated. The plot illustrates noticeable hysteresis which was later determined to be due to not allowing sufficient time (1 minute) between air flow rate changes. In Figure 3.2, bubble sizes were recorded before the pressure in the lines

reached its steady state values, and hence why ($\Delta P < 0$). The calculated polydispersity P of the bubbles, which is defined as the standard deviation of the bubble radii divided by the average radius for a given flow setting ranges from 1.3 to 8.7% indicating a high degree of monodispersity for certain settings and significant polydispersity at others. The large polydispersity however, is more than likely the result of the non-equilibrium pressures in the lines.

The data which were measured after the system was allowed to stabilize properly demonstrated better bubble uniformity. By letting the pressure stabilize for 5 minutes in between flow rate changes and bubble measurements, the hysteresis is eliminated. Air-in-water foams generated in this fashion demonstrated much better polydispersity which ranged between 1.4 to 3.7%. In addition, the bubble size was easily varied over a large range of flow rates. Figure 3.3 shows gas bubbles of average diameters 207, 155, and 134 μm formed at three settings of gas and water flow rates.

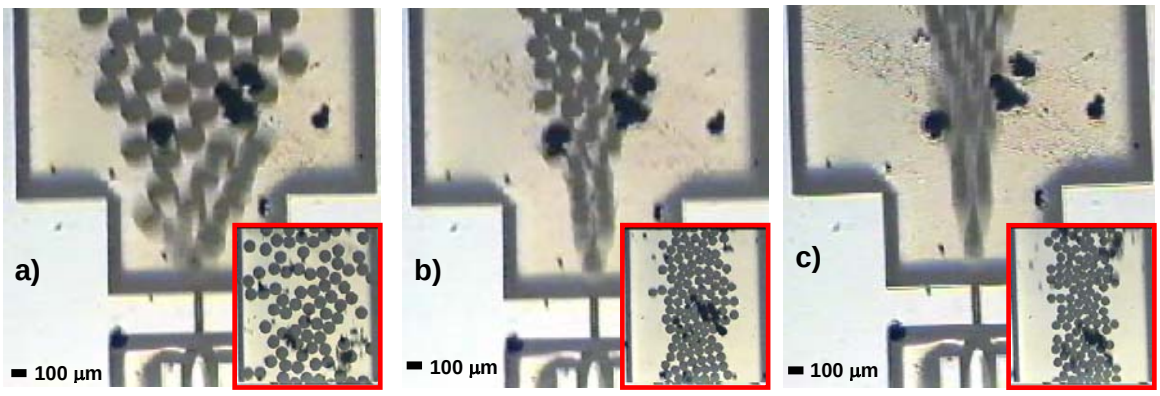

Figure 3.3: Formation of air-in-water foams using the flow-focusing chip at flow ratios of Q_{air} : Q_{water} = a) 20:40, b) 5:40, and c) 20:80 μL/min. The insets are close-up images of the recorded bubbles.

Figure 3.4 shows a plot of the average bubble volume versus air pressure when the water volumetric flow rate was maintained at a constant 80 µL/min while Figure 3.5 shows a plot of the average bubble diameter versus water flow rate when the air pressure was maintained at a constant 5.62 kPa. From Figure 3.4, it can be observed that when the flow rate of the water phase was held constant, the average bubble volume is linearly proportional to the air pressure applied. In the case of Figure 3.5, when the air pressure was maintained constant it is difficult to determine how the average bubble volume scales with water flow rate. Garstecki and co-workers shed some light on the scaling properties of gas bubbles as a function of varying flow rates and air pressures [88]. Their experiment determined the volume of a generated gas bubble when the aqueous fluid was varied.

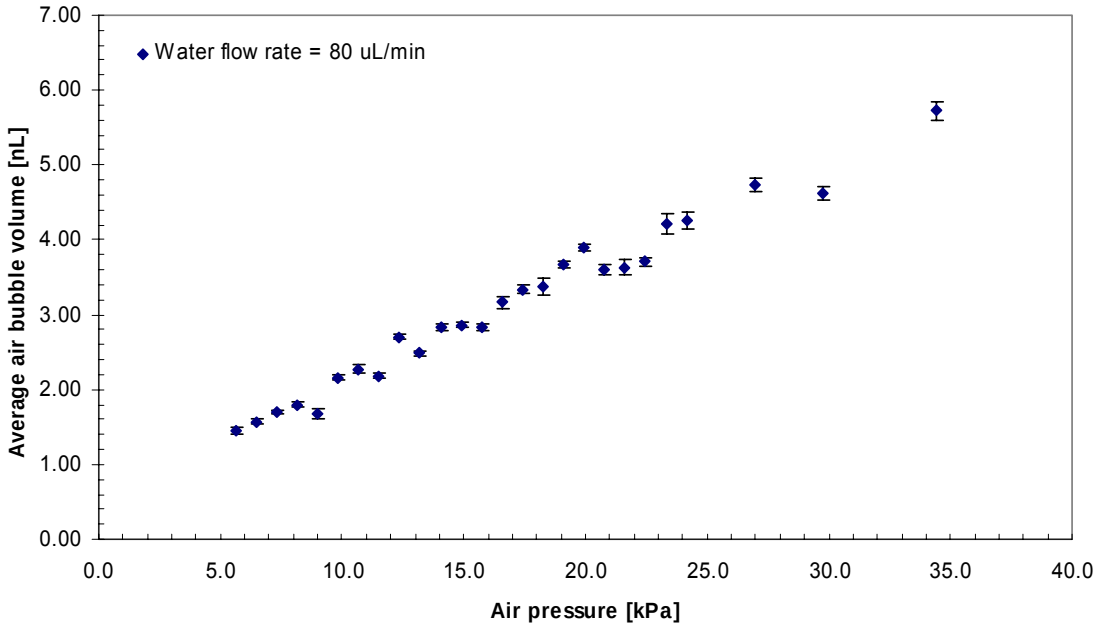

Figure 3.4: Average bubble volume versus air pressure

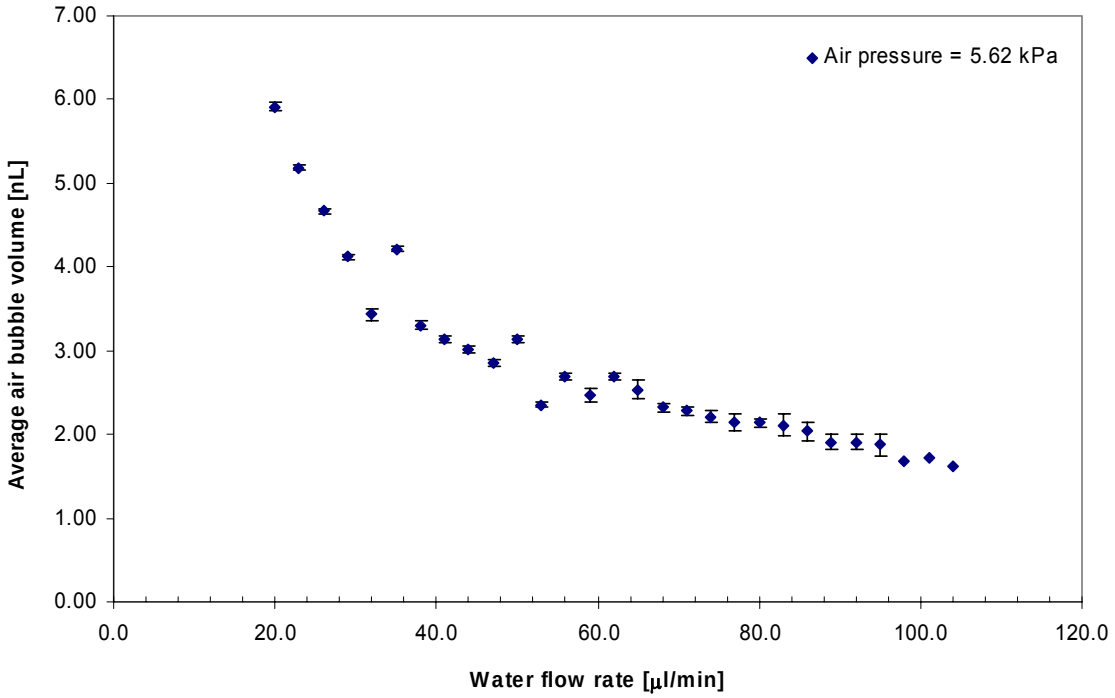

Figure 3.5: Average bubble volume versus water flow rate

The bubble volume is equal to the product of the flow rate of the gas (q_{gas}) and the interval of time (τ) between the formation and the break-up of a generated bubble.

$$V_{bubble} = q_{gas} \times \tau \tag{3.1}$$

As the bubble grows in the orifice and moves downstream in the outlet channel, it experience viscous resistance which can be explained by Poiseuille's equation for a square channel:

$$\Delta P = \frac{12 q \mu_{liquid} L}{W h^4} \tag{3.2}$$

where ΔP is the change in pressure, q is the gas flow rate, μ is the viscosity, L is the length of the outlet channel, W is the width of the orifice, and h is the height of the

channel. As an analogy, Poiseuille's law can be thought to be similar to Ohm's law for electrical circuits ($\Delta V = IR$), where the pressure drop ΔP is analogous to the change in voltage ΔV and the flow rate q is analogous to the current I. With that in mind the resistance R is proportional to $\mu_{liquid}L/h^4$. Therefore the gas flow rate (bubble rate of expansion), as a result of the resistance, can be expressed as:

$$q_{gas} = \frac{p_{gas}}{R} \propto \frac{p_{gas}}{\mu_{liquid}} \tag{3.3}$$

where p_{gas} is the gas pressure and μ_{liquid} is the viscosity of the liquid. Since the velocity of collapse of the gas thread flowing through the orifice is set by the flow rate of the continuous liquid fluid, which yields the time between consecutive generated bubbles:

$$\tau \propto \frac{1}{q_{liquid}} \tag{3.4}$$

By combining equation (3.1) and (3.4) the volume of the generated droplets should scale linearly with the gas pressure or the gas flow rate, and inversely with the flow rate of the continuous liquid phase:

$$V_{bubble} = q_{gas} \times \tau \propto \frac{p_{gas}}{q_{liquid}\,\mu_{liquid}} \tag{3.5}$$

Our results for varying the air pressure applied agree with their scaling equation. However, when the water flow rate was varied we did not match the equation fully because our data is not completely inversely proportional to the water flow rate.

Using gas bubbles for templating pores is very attractive since there is no need to remove the templating liquid, and highly monodisperse bubbles can be formed.

However, there are two main drawbacks: 1) the smallest droplets generated from our device were 120 μm, which are too large for our applications and 2) the gaseous bubbles coalesced very quickly, which makes working with foams as templates difficult. As a result, oil-in-water emulsions were investigated in hopes of generating tunable monodisperse emulsions on the order of tens of microns, or smaller.

3.1.2 Oil-in-Water Droplet Generation: Varying Surfactant Concentration

Filtered hexadecane oil and DI water with SDS surfactant were pumped into the channels using digitally-controlled syringe pumps. In order to generate droplets of varying sizes and size distributions, the liquid flow rates were varied over the same oil/water ratios used for the air-in-water experiments discussed in the previous section. In addition, the total liquid flow rate was varied to generate droplets at higher frequencies. The orifice width, length, and depth used in this work were 43.5, 210, and 30 μm, respectively. A micrograph of the illustrating the oil and water phases including the droplet break-up region is shown in (Fig. 3.6).

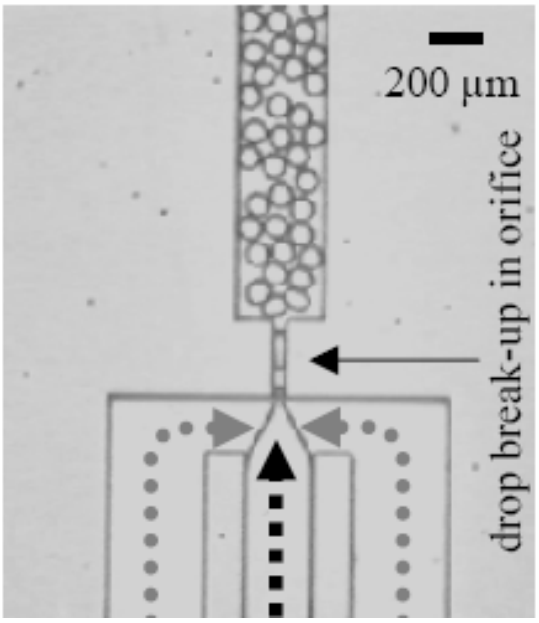

Figure 3.6: Micrograph of flow-focusing device illustrating operation. The continuous water phase (●), flows through the two outer channels while the dispersed phase (■), flows through the inner channel. Droplet break-up occurs in the orifice.

We generated oil-in-water emulsions with varying droplet sizes, size distributions, and droplet generation speeds. Figure 3.7 shows hexadecane-in-water droplets produced by maintaining a constant volumetric flow rate of the inner oil flow ($Q_{hexadecane}$ = 1.4 µL/min) while varying the outer water flows (Q_{water} = 1, 9.5, 17 µL/min). At these settings, hexadecane droplets with average diameters 67, 17, and 11 µm respectively, were formed. The polydispersity of the droplets ranged from 1.7 to 2.4% indicating a high degree of monodispersity. The droplet size decreases as the ratio of water/oil flows increases, as expected; the width of the inner focused flow decreases at higher outer/inner flow ratios, and less volume is available for drop formation [88, 105].

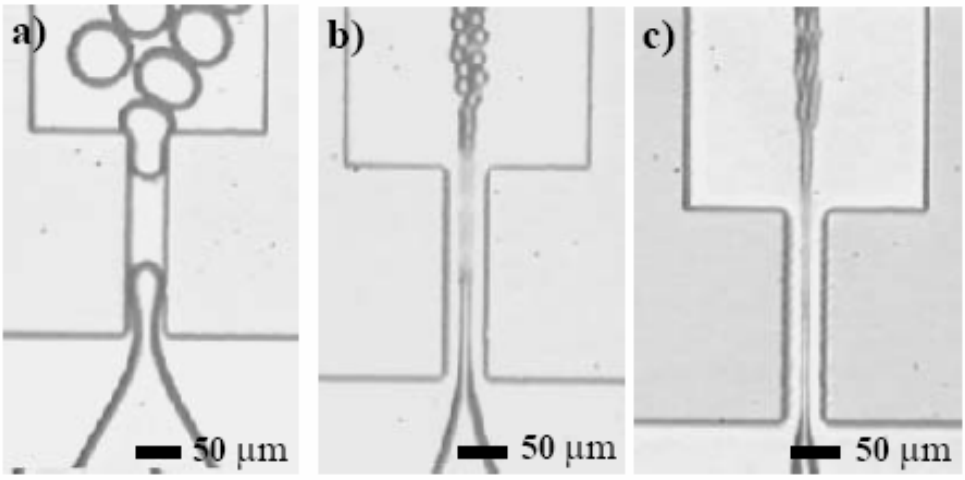

Figure 3.7: Formation of hexadecane-in-water emulsions using the flow-focusing chip at constant $Q_{hexadecane}$, 1.4 μL/min, and Q_{water}: **a)** 1, **b)** 9.5, and **c)** 17 μL/min.

Depending on the dimensions of the outlet channel and the volume fraction of the droplet stream produced, the droplets were observed to pack into ordered arrays after emerging from the orifice, as shown in (Fig. 3.8). These close-packed droplets are promising for use as templates for silica deposition.

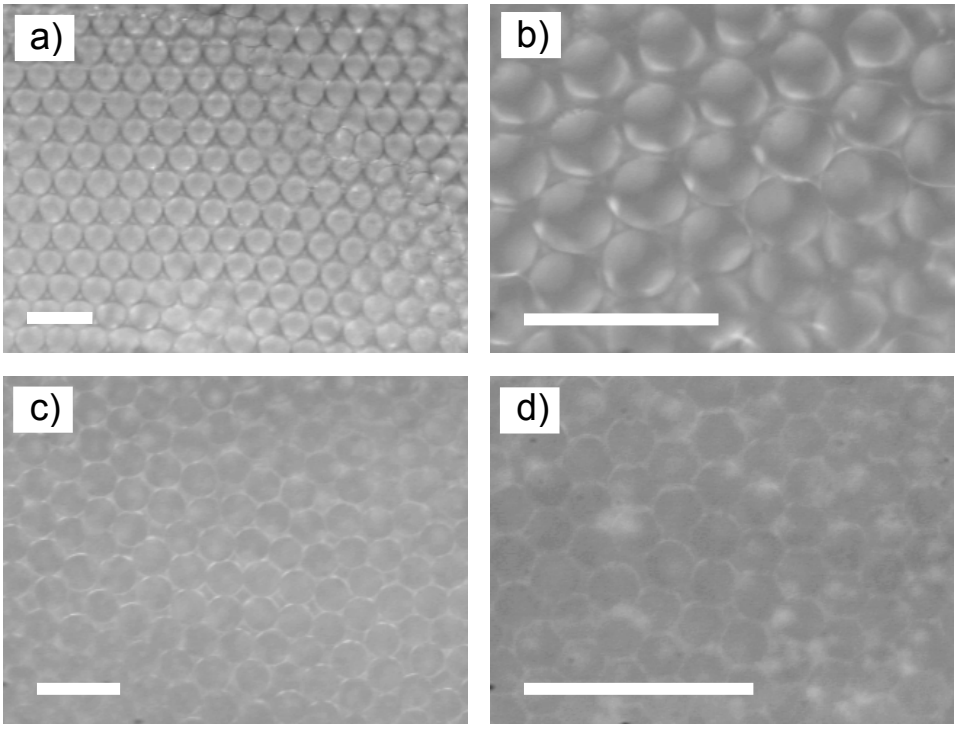

Figure 3.8: Micrographs of droplets packed into ordered arrays a) 40 μm, b) close-up of (a), c) 18 μm and, d) 10 μm. Scale bars are 100 μm for (a and b), and 50 μm for (c and d).

Fine control of droplet size and polydispersity over a range of water/oil flow rates ratios was observed. In addition, to examine the role of interfacial tension in droplet break-up, experiments using different concentrations of SDS surfactant in the water phase were performed. Figure 3.9 shows a plot of average droplet diameter versus water flow rate (oil flow held constant) for 6, 3, 1 and 0% (w/v) SDS/water.

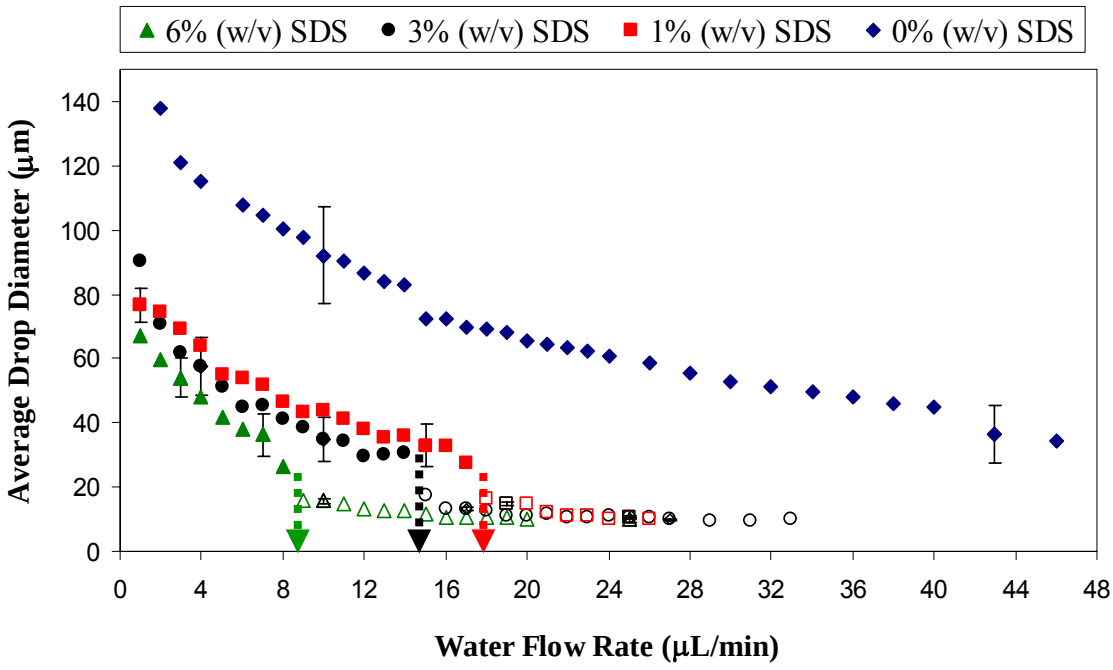

Figure 3.9: Average droplet diameter vs. water flow rate for hexadecane-in-water droplets using the following SDS concentrations in the water phase: 6, 3, 1 and 0 % (w/v). The hexadecane flow rate was held constant at 1.4 µL/min. Monodisperse droplets (P < 3%) are indicated by open symbols, and polydispersity ($P \approx 5 - 15\%$) by filled symbols. Dashed arrows indicate transition points.

Two regimes of drop formation were observed in experiments using the surfactant in the water phase. Operating at low ratios of water/oil flow rates produced polydisperse droplets ($P \approx 5 - 15\%$) until a critical flow rate was reached at which a transition to the generation of monodisperse droplets occurred (P < 3%). In the surfactant-free case, this transition was not observed over the range flows tested, and only polydisperse emulsions were produced.

3.1.2.1 Capillary Number Investigation: Insight Into Droplet Break-up

As the SDS concentration in the water phase was raised, the critical flow rate was observed to fall. For insight into droplet break-up in this case, the relevant dimensionless number is the capillary number,

$$Ca = \frac{\mu v}{\gamma} \tag{3.6}$$

where, μ is the viscosity of the continuous phase, v the linear velocity of the continuous phase through the orifice, and γ the interfacial tension between the dispersed and continuous phases. The Ca number represents the relative importance of viscous stresses exerted by the continuous phase to the surface tension of the oil-water interface. The interfacial tensions between hexadecane droplets and water with various concentrations of SDS surfactant were measured using the pendant drop method in a Kruss goniometer. Table 3.1 lists the ranges of Ca values corresponding to the experiments in Figure 3.9, as well as the values at the transition from polydisperse to monodisperse droplet formation. Images showing polydisperse and monodisperse droplets are shown in (Fig. 3.10).

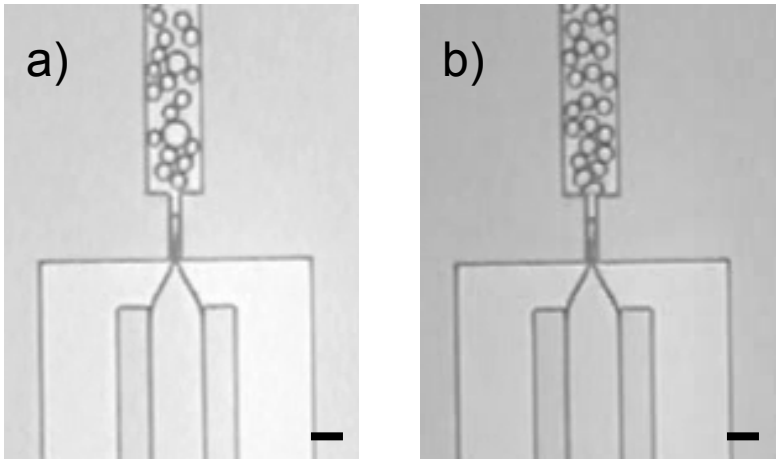

Figure 3.10: Generated droplets transition from (a) polydisperse to (b) monodisperse as the flow rate reaches the critical flow rate as predicted by the capillary number. Scale bars equal 100 μm.

For three experiments with increasing surfactant concentration and thus decreasing interfacial tension, similar values for the critical Ca were found (0.032-0.039). This suggests that at a critical balance between viscous and surface forces, the mechanism of droplet break-up due to capillary instabilities shifts from droplets that are polydisperse to droplets that are monodisperse. Similar transitions have been observed in [106-108]. Calculations for the surfactant-free case suggest the transition to monodisperse droplets

SDS (w/v)	Interfacial Tension (mN/m)	Ca	Critical Ca
0%	52.8	0.001 - 0.02	not reached
1%	11.1	0.023 - 0.06	0.039
3%	9.25	0.003 - 0.083	0.039
6%	7.15	0.004 - 0.089	0.032

Table 3.1: Calculated capillary numbers for emulsification at different SDS concentrations. The critical capillary number is calculated at the transition from polydisperse to monodisperse droplets.

occurs at $Q_{water} \approx 70$ μL/min. Qualitative observation confirms this, but low light at the fast shutter speed of ~10 μs required for imaging these rapid flows prevents video capture.

3.2 Double Emulsions

A double emulsion is simply an emulsion within an emulsion. More specifically, an oil-in-water-in-oil (O/W/O) emulsion consists of internal oil droplets that are dispersed within larger water droplets, which themselves have been dispersed in an external continuous oil phase, as illustrated in (Fig. 3.11a). Similarly, water-in-oil-in-water (W/O/W) emulsions consist of internal water droplets that are dispersed within larger oil droplets, which themselves have been dispersed in an external continuous aqueous phase (Fig. 3.11b). In both cases the internal and external droplets are stabilized by two different surfactants. Double emulsions have been highly investigated in the areas of food science [109, 110], cosmetics [111, 112], and pharmaceuticals [113, 114], since it is convenient to compartmentalize one fluid within a second. Double emulsions provide a vehicle for the controlled release of substances such as flavors and nutrients in foods, scented oils in cosmetic creams, insecticides and herbicides in agriculture sprays or release of therapeutic agents for targeted drug delivery.

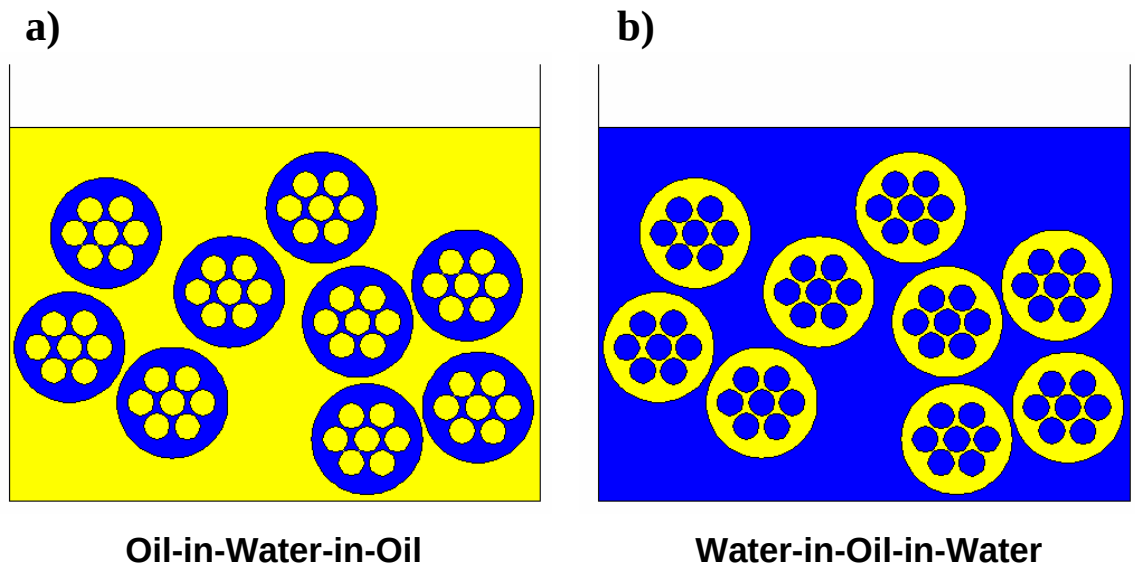

Figure 3.11: Double emulsions. a) O/W/O and b) W/O/W. Both internal and external droplets are stabilized by added surfactants.

3.2.1 Current Techniques

Early work on double emulsions consisted of a two-step emulsification process where the first emulsion is produced by vigorously stirring two immiscible fluids. The second step consisted of taking the first emulsion and dispersing it in a third immiscible fluid using low shearing forces to create the outer most droplets without disrupting the first emulsion. However, this technique leads to poor control of droplet size distributions since both the first and second emulsification steps have a large polydispersity [60, 62].

As opposed to using conventional bulk emulsification devices such as stirring apparatuses, high pressure homogenizers, and rotor stator systems to generate double emulsions recent research has investigated using microfluidic techniques to produce

highly uniform double emulsions. A major challenge faced when using microfluidic emulsification to generate double emulsions is controlling the size and uniformity of both the inner and outer droplets. This proves to be critical for maintaining a stable double emulsion because the Laplace pressure difference between uniformly sized inner droplets is zero, similarly the Laplace pressure difference between similar adjacent outer droplets is zero. In each case, this aids in minimizing coalescence between neighboring inner and outer droplets. Surfactants, which are discussed later, are also used to help minimize coalescence between the inner and outer droplets.

Other concerns when using microfluidic emulsification for generating double emulsions are the narrow range of droplet size distributions that are producible and the wetting properties of the microchannels, of which the latter has proven to be more difficult to overcome. As described in Chapter 2, the wetting properties of the microchannels play a role in which form of emulsion, water-in-oil or oil-in-water, can be formed. In order to generate a double emulsion on a single chip both hydrophobic and hydrophilic regions need to be selectively defined by modifying the channel wall surfaces.

Several promising microfluidic devices for double emulsion generation have been described recently [82, 83, 115-120]. When evaluating these double emulsification techniques a number of criteria were examined: 1) inner and outer droplet uniformity, 2) control of inner and outer droplet tunability, and 3) techniques used to selectively functionalize the surface of the microchannels. With these conditions in mind, we

investigated double-emulsion formation using a microcapillary device and series-connected T-junctions.

3.2.1.1 Microcapillary Double Emulsification

Utada and coworkers used cylindrical glass capillary tubes nested within a square glass tube in a configuration that resulted in hydrodynamic focusing of coaxial flows to generate double emulsions [118]. One capillary tube has a narrow inner diameter while the other capillary tube has a tapered point. The two cylindrical glass capillary tubes' outer diameters must match the inner dimension of the square tube in order to facilitate the alignment between the narrow end of one tube and the tapered point of the capillary tubes. When the two capillary tubes are not aligned properly their system suffered and disrupted the double emulsion droplet generation. Additionally, when two tapered capillary tubes were used, alignment of the two tapered points proved to be difficult.

They generated double emulsions that contained either a single internal droplet to form core-shell geometries or double emulsions that contained a number of internal drops with different average sizes and size distributions. However, in order to switch between encapsulating one droplet and encapsulating a number of droplets different device geometries (capillary tubes) had to be used. This may be a reason why their work focused primarily on generating single internal drops since dynamically tuning the internal droplet dimensions over a wide range could have been difficult to demonstrate. They generated encapsulation structures by crosslinking a photopolymerizing polymer

that made up the intermediate fluid of the double emulsion. Typical values of polydispersity were determined to be between 1 and 3%.

3.2.1.2 Series Connected T-junctions

Nisisako and coworkers used a one chip module fabricated by isotropicaly etching a pyrex glass substrate to generate water-in-oil-in-water double emulsions [82, 83, 116]. Their module consisted of two different sized T-junctions connected in series. The upstream T-junction, the smaller of the two junctions, was used to generate the first aqueous droplets. In order to accomplish this using pyrex, which is hydrophilic, a silane-coupling agent was used to render the surface hydrophobic. Downstream at the larger T-junction the external oil droplets were produced at a hydrophilic junction, which encapsulated the aqueous droplets generated at the first junction.

They demonstrated the ability to vary the external droplet diameters over a range between 210 to 150 μm by modifying the external oil flow rate between 4 to 15 ml/h respectively. Additionally they reported that by adjusting the flow rates they could control the number of droplets encapsulated at the second emulsion step. It is unclear, however, whether the size of the internal droplets can be adjusted as easily as the external droplets since in all the work presented the internal droplet diameter was maintained at a constant diameter of 52 μm and was the smallest droplet size reported. The polydispersity for the double emulsions generated was below 3%.

3.3 Series Connected Flow-Focusing and T-junctions

Earlier we demonstrated single monodisperse oil-in-water emulsions using the flow-focusing emulsification design with coefficient of variations under 2.5% for a wide range of droplet diameters. As recently discussed in section 3.2.1.2, T-junctions have proven to produce monodisperse droplets, however, the range of droplet diameters is not as large as that for the flow-focusing technique. Our approach to generating a double emulsion consists of a two-step emulsification process where the first emulsification step (oil-in-water) is generated using flow-focusing, and the subsequent emulsification step (water-in-oil) occurs downstream at a T-junction. In this manner, we combine both the ability to finely tune the drop size and uniformity of the inner droplets over a wide range using flow-focusing while maintaining the capability to generate the larger second droplet, which contains the first emulsion, with high monodispersity at a T-junction. By using silicon-based microfabrication, we also eliminate any alignment issues between the two emulsification steps [118]. Between the first and second emulsification steps, the microfluidic device has integrated channels that provide the added flexibility of introducing other chemicals or particles within the intermediate fluid. The microchannel etch depth at the flow-focusing region is shallow, whereas the microchannels that form the T-junction are deep. A schematic image of the microfluidic double emulsification device is shown in (Fig. 3.12).

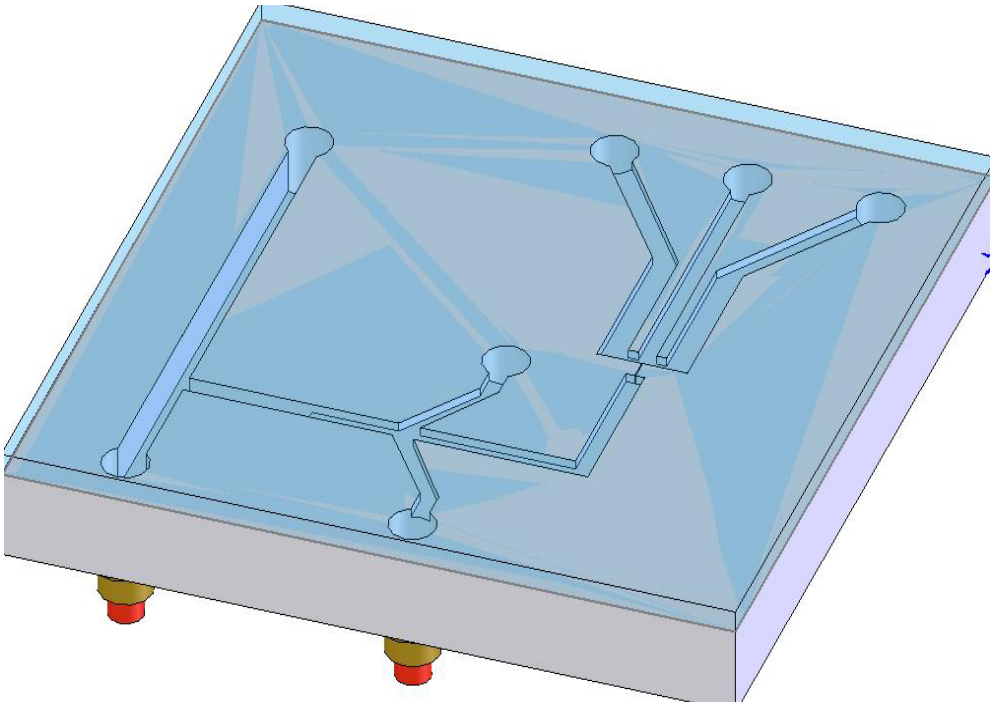

Figure 3.12: A schematic representation of our single chip double emulsification device. Shallow etched channels compose the flow-focusing region while deep etched channels define the T-junction region. Two additional channels between the flow-focusing and T-junction region are integrated in order to provide the added flexibility of introducing other chemicals or particles within the intermediate fluid.

3.3.1 Single Chip Microfabrication

The microfluidic emulsification chip used in this work was fabricated from silicon (100) substrates using a three-step deep reactive ion etch (DRIE) process to form the flow-focusing region first, the T-junction second and lastly, the through-wafer holes. The process flow is depicted in (Fig. 3.13). A 1.2 μm layer of thermally grown silicon dioxide was used as an etching hard mask. The flow-focusing microchannels on the bare silicon substrate were defined using a 2.8 μm layer of I-line photoresist. Following

photolithographic exposure and development of the first layer pattern the photoresist was baked for 2 hours to provide a durable masking layer. The 1.2 μm layer of silicon dioxide in the unprotected areas was etched completely in a Lam silicon dioxide etcher. However, before etching the exposed silicon, a 9 μm layer of SPR 220 photoresist (Shipley) was spun on the wafer and exposed to define the T-junction channels. The photoresist was baked for 1 hour to provide a durable mask. The exposed silicon dioxide was etched completely in a Lam etcher to expose the underlying silicon. The unprotected silicon areas were etched 120 μm deep in the first of three DRIE steps in a STS using the Bosch process. After the etching was complete the photoresist mask was removed using PRS3000 at 90°C for 2 hours. The substrate was then cleaned in piranha, a 4:1 (vol) solution of concentrate sulfuric acid : 30% hydrogen peroxide, to remove any trace organics. The cleaned wafer has both the flow-focusing and T-junction channels defined by the silicon dioxide hard mask. A second DRIE step was used to etch the unprotected silicon areas to a depth of 30 μm. As a result, the flow-focusing microchannels have a depth of 30 μm while the T-junction channels are 150 μm deep (120 μm first etch plus 30 μm the second etch). This masking technique is required when two different etch depths are desired.

Before patterning the backside of the wafer with photoresist to define the etch locations for the fluidic through-holes, the wafer was bonded to an oxidized silicon handle wafer using Cool Grease™ (AI Technology) as the adhesion layer. The device substrate was bonded to the handle wafer with the microchannels facing down. The

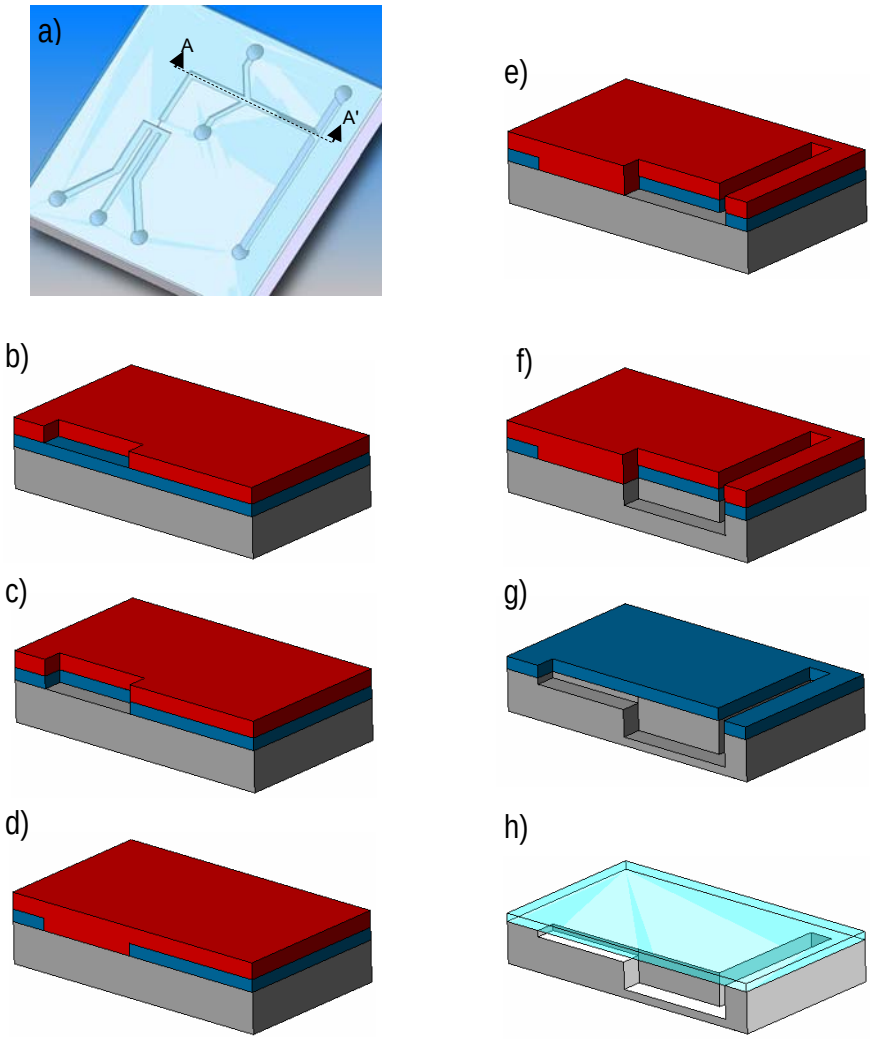

Figure 3.13: Fabrication process flow of the double emulsification device. (a) Schematic of the double emulsification design. The relevant cross-sections are taken along A─A'. (b) Photoresist is patterned to define the shallow microchannel regions (flow-focusing area). (c) The oxide layer is etched to provide a etch mask (this mask is used after step f). (d) Thick photoresist is spun onto wafer. (e) Photoresist is patterned to define the deep microchannel regions (T-junction area), and the oxide layer is etched to provide the first silicon etch mask. (f) A deep silicon etch defines the T-junction region. (g) Photoresist is removed to expose the entire oxide mask. A shallow silicon etch defines the flow-focusing region and etches the deep channels to a final depth. (h) Oxide mask is removed and the wafer is encapsulated with a glass coverslip.

backside of the wafer was then patterned with a 9 μm layer of SPR 220 photoresist and the third DRIE step was used for the through-wafer etch to create both the fluidic ports and the functionalizing port. The bonded wafers were then separated by immersing the pair in acetone at room temperature for 30 minutes under ultrasonication.

The substrate was cleaned in piranha, and subsequently immersed for 30 seconds in concentrated hydrofluoric acid (49%) to remove the native oxide. An image of the completed double emulsification device is shown in (Fig. 3.14). The channels were sealed by anodic bonding of a pyrex wafer using a Suss SB6 Anodic Bonder as described previously (not shown in Fig. 3.14).

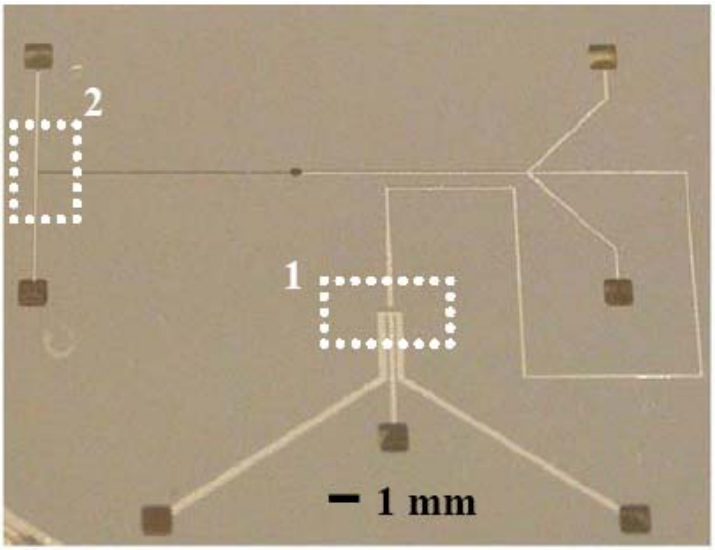

Figure 3.14: Image of fabricated double emulsification device highlighting the flow-focusing (1) and T-junction (2) regions. Two additional channels between the flow-focusing and T-junction region are integrated in order to provide the added flexibility of introducing other liquids or particles within the intermediate fluid. A functionalizing through-wafer port is located at the intersection where the shallow and deep channels meet.

3.3.2 Surface Functionalization

Our chip is naturally hydrophilic since the silicon channels are coated with native oxide, so the first emulsification step (oil-in-water) generated at the flow-focusing orifice needs no surface modification. In order to create the second emulsification (water-in-oil) at the T-junction downstream, the hydrophilic silicon/pyrex channels are selectively functionalized with a hydrophobic siliconizing agent AquaSil™ (Hampton Research Inc.). AquaSil™ is a monomeric octadecylsilane derivative that in general is applied by immersion in a bath. In our case the surface functionalizer was selectively flowed through the T-junction channels to render them hydrophobic. To achieve this we connected a tube to the functionalization through-wafer hole (Fig. 3.15). The two outlet ports found at the T-junction side of the chip were connected to a vacuum pump while all the other ports were left open to atmospheric pressure. The vacuum was turned on and allowed to run for 5 minutes to establish a pressure difference and subsequently the tube connected to the functionalizing port was placed in the siliconizing agent. The vacuum forced the fluid to flow only through the T-junction channels. Once all the siliconizing agent was flowed through the chip DI water was then flushed through the T-junction to remove any excess siliconizing fluid. The vacuum was allowed to continue to pump after the DI water rinse in order to dry the microchannels. Lastly, the entire chip was heated at 100°C for 20 minutes to cure the silicone coating.

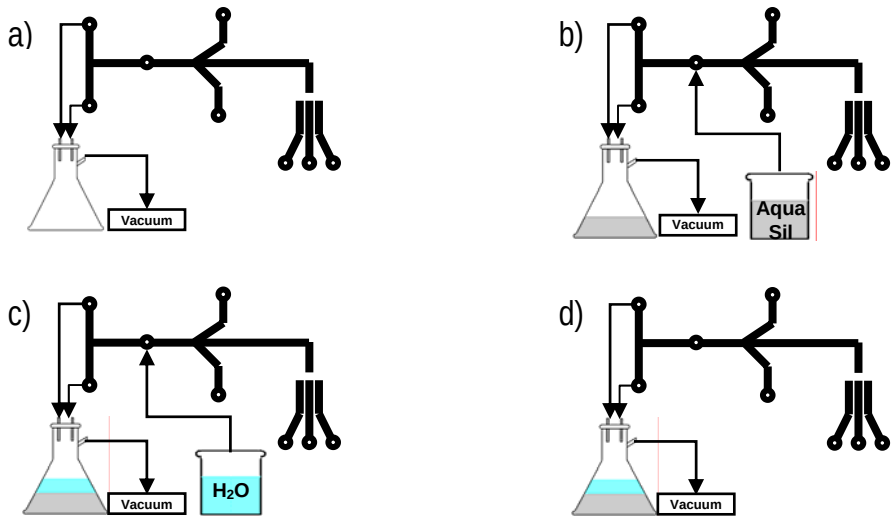

Figure 3.15: Illustration of channel functionalization. a) Vacuum is connected to the T-junction outputs while all the other ports are left open to atmospheric pressure. b) AquaSil™ is introduced through the functionalization through wafer hole. c) DI water is flushed through the microchannels. d) Vacuum is allowed to run until microchannels dry.

3.3.3 Liquids and Surfactants Used

The stability of double emulsions in general is poor because a double emulsion contains more interface area, making them more thermodynamically unstable than single emulsions. In some cases this is desired for time-release drug delivery. However, in other cases such as emulsion templating high stability is desired in order to maintain longer product shelf life. When generating oil droplets in water at the flow-focusing region, we used hexadecane for the discontinuous phase while poly-vinyl alcohol PVA (Sigma-Aldrich) surfactant solubilized in water at a concentration of 2% (w/v) was used for the continuous phase. When generating the second emulsification step at the T-junction, the to-be-dispersed phase, or in other words the intermediate phase is the

Water/PVA solution while Lecithin (Sigma-Aldrich) surfactant solubilized in hexadecane at a concentration of 0.5% (w/v) served as the continuous phase. Figure 3.16 depicts the liquid combinations used.

When preparing double emulsions, it is critical to select the correct surfactants otherwise stability of the emulsions will suffer. To aid in selecting the surfactant, the hydrophilic-lipophilic balance (HLB) number is useful. If an emulsifier has a low HLB number, there are a low number of hydrophilic groups on the molecule and it will have more of a lipophilic character that makes it oil soluble and cause the oil phase to dominate and form a water-in-oil emulsion. In the other case, a higher HLB number indicates that the emulsifier has a large number of hydrophilic groups on the molecule and therefore is more hydrophilic in character which makes it water soluble and causes

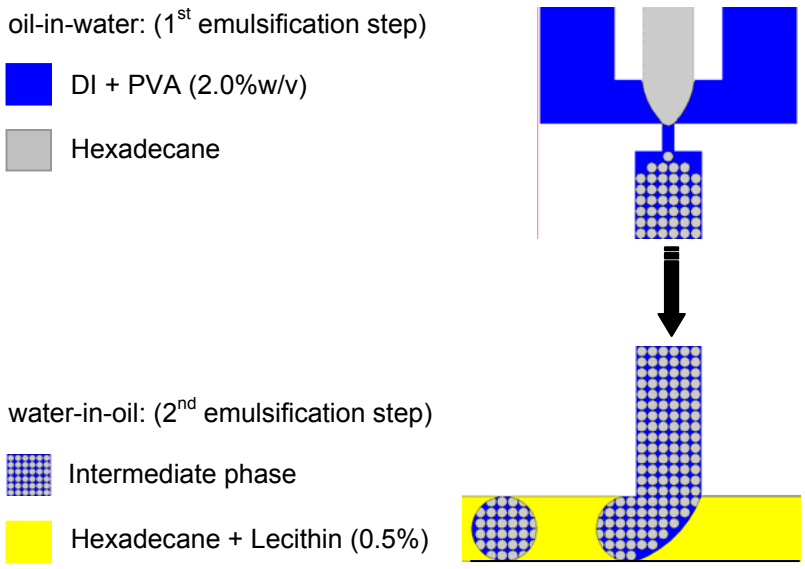

Figure 3.16: Illustration of the liquids and surfactants used in the two-step emulsification process.

the water phase to dominate and form a oil-in-water emulsion. Water-in-oil emulsions can be made with surfactants having HLB numbers from 2 to 6, whereas oil-in-water emulsions can be made with surfactants having HLB numbers from 8 to 12.

3.4 Double Emulsions Experimental Results

3.4.1 Droplet size verses flow rate

A micrograph of our fabricated device is shown in (Fig. 3.17a). Operation of the microfluidic double emulsion chip is based on a two-step emulsification process, where a water phase finally serves as the intermediate fluid. Generation of hexadecane droplets in water, stabilized using 2% (w/v) polyvinyl alcohol in the water phase is shown in Figure 3.17b [105, 120], and generation of water droplets in hexadecane, stabilized using 0.5% (w/v) lecithin in the hexadecane phase, is shown in (Fig. 3.17c).

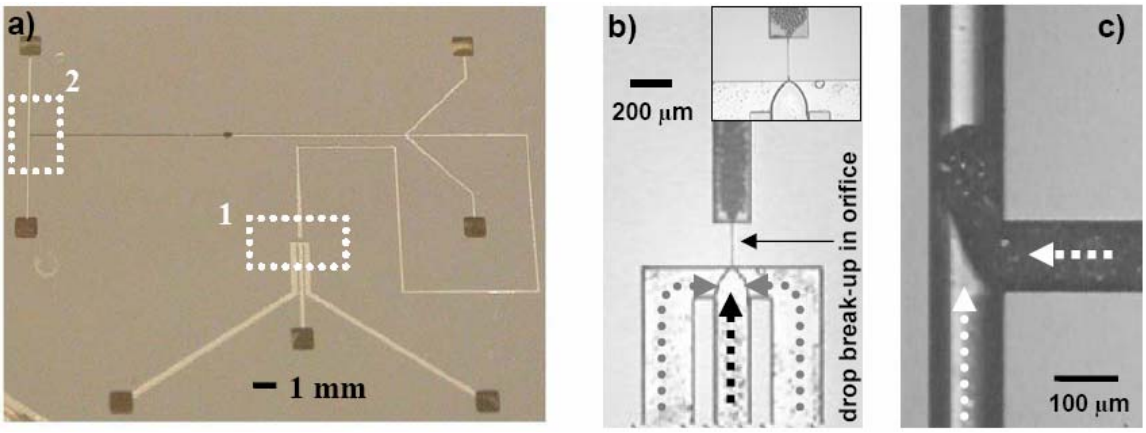

Figure 3.17: a) Fabricated chip. b) A continuous phase (●) flowing through the two outer channels focuses a stream of the dispersed phase (■) from the inner channel into an orifice, resulting in droplet break-up. Close-up of the emulsion generation is shown in the inset image. **c)** The initial emulsion (□) is subsequently re-emulsified by a continuous phase (○) at the T-junction, creating the double emulsion.

By setting a constant volumetric flow rate for both the inner oil flow ($Q_{\text{hexadecane}}$ = 0.4 μL/min) and the outer water flow (Q_{water} = 0.55 μL/min), we produce initial monodisperse oil-in-water emulsions that have a droplet polydispersity less than 2.4% [105], while maintaining a high droplet volume fraction. Once the flow-focusing region is stable we image the double emulsion droplet generation using a high speed Cohu 2700 video camera with exposure times as short as 100 μs. A sequence of micrograph frames depicting the drop break-up sequence is shown in Figure 3.18, and micrographs of the generated monodisperse double emulsions are shown in (Fig. 3.19).

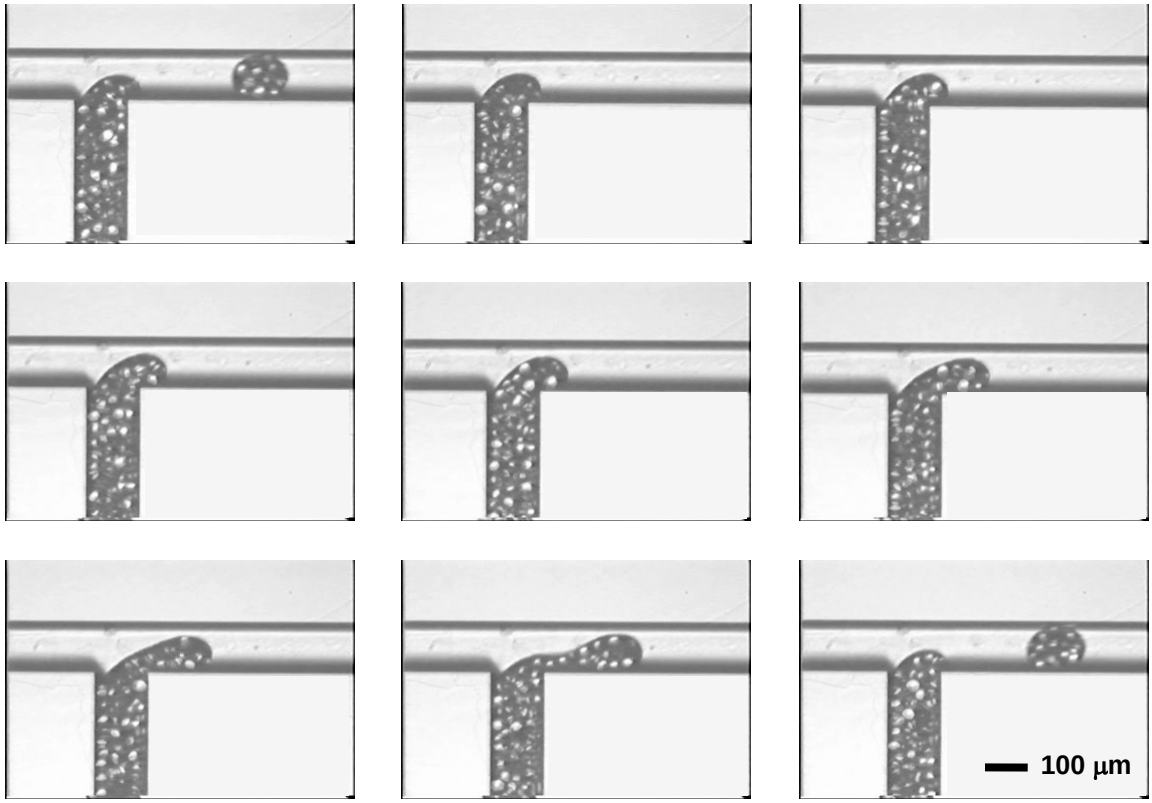

Figure 3.18: Sequential still frames taken of the double emulsification drop break-up at a T-junction (from left to right, top row to bottom row). The first oil-in-water emulsion is dispersed in a continuous oil phase to form oil-in-water-in-oil emulsions. The outer droplet diameter is 120 μm.

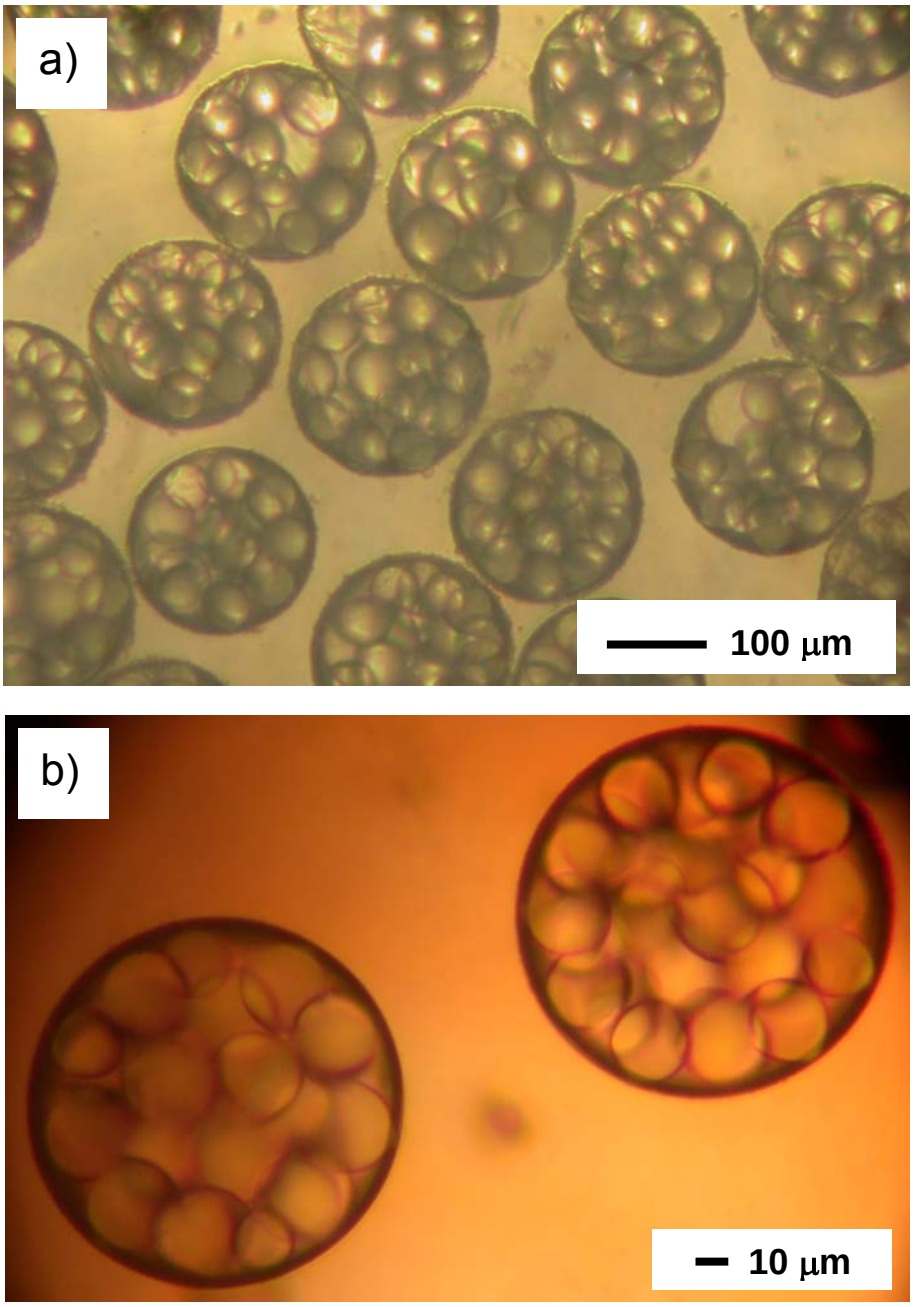

Figure 3.19: Micrographs taken of the double emulsions. a) Demonstrating high inner and outer droplet uniformity. b) Close-up of the oil-in-water-in-oil emulsions. Inner oil and outer water droplets have an average diameter of 27 μm and 120 μm respectively.

Figure 3.20 shows the average second emulsification, water-in-oil, droplet diameters vs. hexadecane/lecithin flow rate. The initial emulsified oil-in-water flow is maintained at a constant volumetric flow rate of ($Q_{\text{oil-in-water}}$ = 1.5 µL/min) while varying the hexadecane/lecithin flow rate (Q_{water} = 1 ─ 65 µL/min). The plot demonstrates that double emulsions with diameter sizes varying from 240 µm down to approximately 80 µm are attainable using a T-junction. The average monodispersity values measured were all below 4.8%.

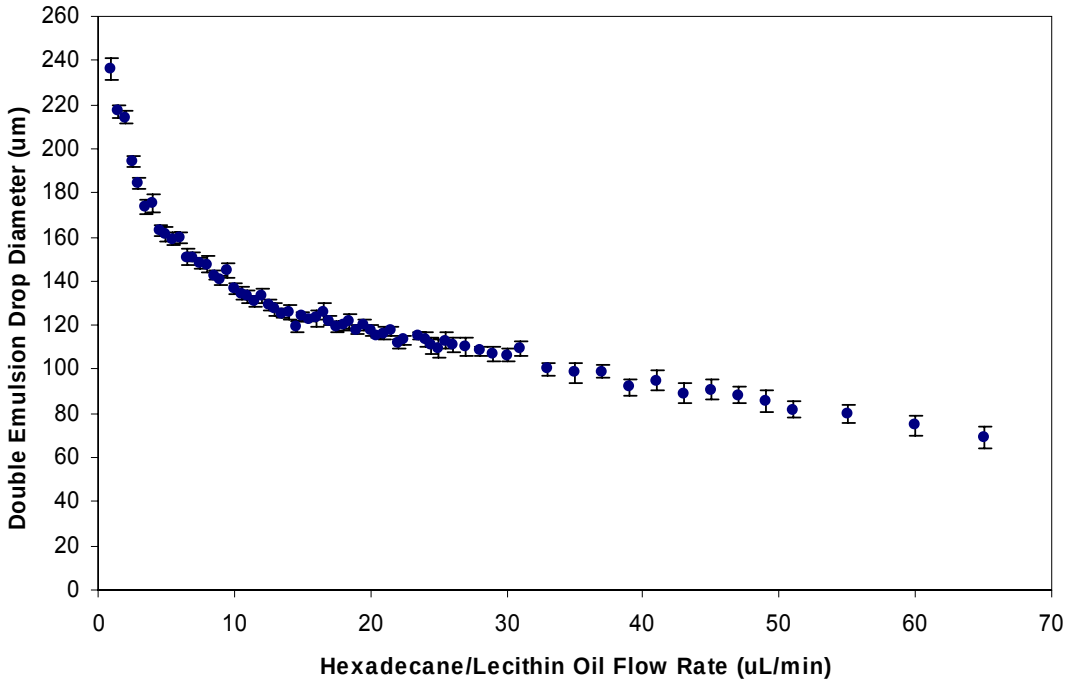

Figure 3.20: The average outer diameter of the double emulsion droplets as a function of the hexadecane/lecithin flow rate. The hexadecane/lecithin oil represents the final continuous phase that is responsible for re-emulsifying the initial emulsion into a double emulsion at the T-junction. Monodispersity values lower than 4.8% were measured.

3.5 Conclusions

In summary, we have characterized both air-in-water, and oil-in-water single emulsification. The flow-focusing emulsification device provides highly monodisperse bubbles and droplets for a wide range of flow rates. When generating air-in-water foams, the air and water flow rate settings are set by the bubble diameter scaling laws. If air-in-water foams are to be used for templating pores, or any other application, one needs to consider the desired bubble size, since it is difficult to generate bubbles below hundreds of microns. These foams were not stable for more than 24 hours, which is a significant drawback. Additionally, it is important to allow the system to reach an equilibrium state before recording or collecting the droplets.

When generating oil-in-water emulsions the capillary number should be investigated since it provides a starting point for setting the oil and water flow rates. In addition, if the surfactant concentration is varied for the same oil-liquid system the capillary number also provides the location where the generated droplets transition from polydisperse to highly monodisperse drops. Generating oil droplets on the order of hundreds to tens of microns was achieved. The oil droplets in water were stable for months without any noticeable coalescence.

Double emulsions also were easily generated using the series connected flow-focusing and T-junction devices on a single chip. It was demonstrated that the flow-focusing device used to generate the first emulsification had a large range of monodisperse inner oil droplet diameters ranging from hundreds of microns down to tens

of microns. In a similar fashion, the T-junction demonstrated encapsulation of the first emulsion to form oil-in-water-in-oil double emulsions with droplet sizes ranging between hundreds of microns down to tens of microns with high uniformity. The integrated channels allowed for more functionality in the future to encapsulate nanoparticles, or introduce reactive chemistries, within the intermediate phase.

With the flow-focusing and the flow-focusing plus series connected T-junction emulsification devices characterized, we can now turn to the reactive synthetic chemistries necessary for the benign (room temperature, neutral pH) gelation of the continuous phase of the oil-in-water emulsions. It is critical to demonstrate that the oil droplets can maintain their spherical structure, as a pore template, during the silica gelation process.

Chapter 4

Emulsion Templated Porous Silica

4.1 Introduction

Pioneering technologies of porous materials with high surface area date back to the 60's with the discovery of zeolite [121], metal oxides in the 70's through the 80's [122], and the development of Mobil Crystalline Material (MCM) by Exxon Mobil in the 90's [123]. Much of this work was geared towards the refining and petrochemical processes. Interest in porous materials has since not slowed; rather, interest in creating materials with uniform pore sizes at larger length scales has motivated continued research. Currently, there is great demand for ordered macroporous silica-based materials with uniform pore sizes ranging from 50 nm to tens of micrometers. However, the drawbacks to conventional methods of generating silica materials are that elevated temperatures and alkaline conditions for synthesis are required. It is therefore of interest to develop a method to generate a porous silica material at near neutral pH, ambient temperature, and pressure. Porous silica generated under these conditions opens a variety of industrial and research applications, including bioseparation filters, catalytic supports,

and tissue supports since biological media require benign conditions. Another application receiving attention is three-dimensional photonic crystals [124-127]. In all these applications, tight control of the pore size distribution is critical.

This chapter begins by recovering results published in the literature with respect to techniques used to generate templated porous materials, including silica. Subsequently addressed, is nature's process by which living organisms produce silica (biosilicification) and the proteins responsible for the material formation. In particular, we survey recent work published on diatoms to better understand the biological organic and inorganic processes used by diatoms to create their ornate porous silica shell under benign conditions. We also discuss how diatoms inspired us to develop a biomimetic approach to create synthetically derived silica-based porous materials/particles using emulsions as templates at near neutral pH, ambient temperature, and pressure. We detail our efforts in combining biomimetic chemistry with template-directed synthesis and microfluidics to produce high-quality macroporous silica with the aim that in the future, custom materials may be produced *in situ* within lab-on-a-chip systems and functionalized for use in reaction and separation modules.

4.2 Templated Porous Materials

A number of successful approaches have used self-assembly to organize a pore template around which material was then deposited [128-134]. Close-packed emulsion droplets and bubbles served as a template for silica, titania, and metal oxides through sol-gels; upon heat treatment to evaporate the droplets and densify the gel, macroporous

ceramics such as silica and titania were formed. When the emulsion droplets used were equally sized, the resulting materials possessed monodisperse pore sizes, ranging from 50 nm to several micrometers. In other work, porous polymer materials were formed by polymerizing the material surrounding the emulsion droplet [135-138].

A number of research groups have since extended this emulsion-templating technique by employing colloidal assemblies of silica and polymer spheres as templates to form ordered mesoporous polymers and titania photonic crystallites [124, 139, 140]. Other research groups have since investigated methods of packing colloidal dispersions of an evaporated droplet containing "n" silica or polymer spheres into higher ordered cluster configurations [141, 142]. As "n" is varied, the geometry of the cluster is changed and as a result, the clusters can be tailored into desired crystals that can be used as templates.

The benefits of using emulsion droplets as opposed to colloidal dispersions as pore templates is that the emulsion droplets can easily be removed by evaporation or dissolution. In addition, the droplets are deformable which allows volume fractions in excess of the close packing limit of rigid microspheres (74%) [62]. However, there is a drawback to using emulsions and colloids to prepare macroporous silica using these techniques since harsh conditions are required to form the porous material: high alkaline conditions (pH > 10) and elevated temperatures (T > 450°C). For this reason, we look to the diatom's method of generating silica under benign conditions.

4.3 Silica Biomineralization

Much attention of late has been focused on elucidating nature's mechanisms of silica formation [21, 33, 143]. Silica is the second most abundant mineral type formed by organisms [144]. The simplest soluble form of silica is the monomer, orthosilicic acid, which is a silicon atom tetrahedrally co-ordinated to four hydroxyl groups with a chemical formula ($Si(OH)_4$). In the ocean, silica primarily exists as orthosilicic acid. Algae, sponges, and mollusks, for example, perform biosilicification reactions under benign chemical conditions and ambient temperature to create silica by absorbing and incorporating the silica precursors taken up from seawater.

We focused on diatom biosilicification because diatoms are a group of unicellular brown algae whose ornate shells are composed of amorphous silica [36]. As mentioned in Chapter 1, the mechanisms by which the diatom's intricate architectures are created are not fully understood. However, researchers have isolated two sets of organic macromolecules from purified diatom biosilica: the first are post-translationally modified proteins named silaffins, and the second are long-chain polyamines of different lengths [145]. Most of these molecules have been found to act as catalysts for silica precipitation; when either native silaffin-1A or the polyamines are added to the silica precursor, orthosilicic acid, a network of nanospheres precipitates in minutes at ambient temperature. The catalytic activity of both the native silaffin-1A and the polyamines (both positively-charged) are known to aggregate the negatively-charged silica particles from the orthosilicic acid into silica clusters. The resulting solid silica material was found to contain both silica and the biocatalyst incorporated into the material.

In order to mimic this process, a silicon precursor is needed, similar to the seawater used by diatoms. A positively charged biocatalyst at a neutral pH, is required in order to nucleate negatively charged silica particles found in seawater.

4.4 Diatom Inspired Emulsion – Templating Approach

In this and the subsequent sections, we describe the benign, room temperature and neutral pH, synthesis of micro/nanoporous silica structures, using processes inspired by the mechanisms used by diatoms to build their complex silica shells. These structures can serve as porous membranes or large surface area catalysts in microfluidic systems. As micro/nanoemulsions are believed to be central to the diatom's synthetic mechanism [24], we used emulsions to template macroporous silica using bioinspired synthetic catalysts. The biomimetic approach that we use to create macroporous silica materials is as follows:

1) Use the microfluidic emulsification chip to generate a monodisperse oil-in-water emulsion to serve as the pore template.
2) Allow the droplets to hexagonally close pack.
3) Introduce diatom-inspired reactive chemistries into the continuous phase of the emulsion which gels the liquid.
4) Remove the oil template resulting in the formation of a pore. This approach is illustrated in (Fig 4.1).

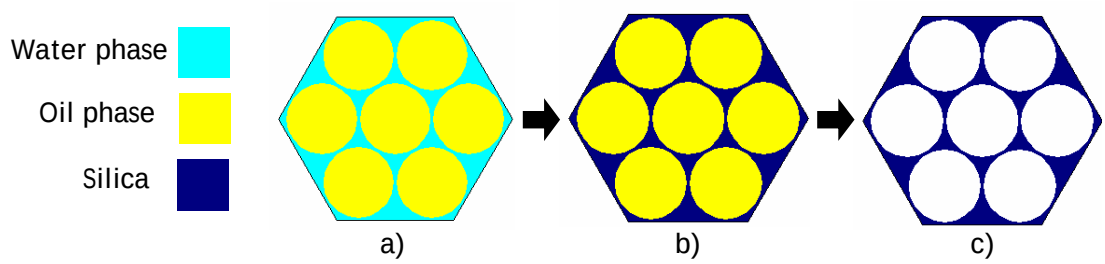

Figure 4.1: Emulsion templating approach, a) emulsification chip creates monodisperse emulsion and droplets are close packed, b) biomimetic reactive chemistries are introduced in the water phase to form silica gel around emulsion droplets, c) emulsion template is removed and material is calcinated to form the glassy macroporous silica material.

4.5 Applications for Diatom Inspired Porous Silica

Preparation of monodisperse silica has drawn more attention in recent years because of their technological applications in the fields of ceramics, catalytic supports, chromatographic adsorbents, bioseparation filters, abrasives, and three-dimensional photonics just to name a few. Our aim is to use porous silica for applications such as on-chip filters for bioseparation, high surface catalysts for enzyme immobilization, and as photonic crystals. For biological applications, it is important that the silica is generated under benign conditions so as to provide an environment that will not damage the sample.

2.3.5.1 Bioseparation

The most effective approach in understanding a biological process (cells) is to study purified individual molecules such as enzymes, nucleic acids, or structural proteins.

In this manner the purified components can be characterized without interference from other molecules present in the intact cell. Traditional purification methods begin with mechanically homogenizing the cells (breaking cells apart) and dispersing their contents in a buffered solution [146]. The suspension is then centrifuged at various speeds and times in order to separate the cells contents, as illustrated in (Fig. 4.2a). Lower speeds and shorter times are required for centrifuging the larger particles, whereas greater speeds and longer times are required when separating the smaller contents. Typical values for speed and time used are (1000 g, 10 minutes) for large particles and (150000 g, 3 hours) for small particles. Major drawbacks to this method are that the initial sample volumes required are on the order of milliliters and the process is both energy and time intensive. Our aim is to generate customizable porous membrane filters on-chip that would allow for the specific purification of certain cellular contents depending on the size of the pores generated, as shown in (Fig. 4.2b). The benefits of an integrated lab-on-a-chip approach are that small microliter sample volumes are required, the membrane pores

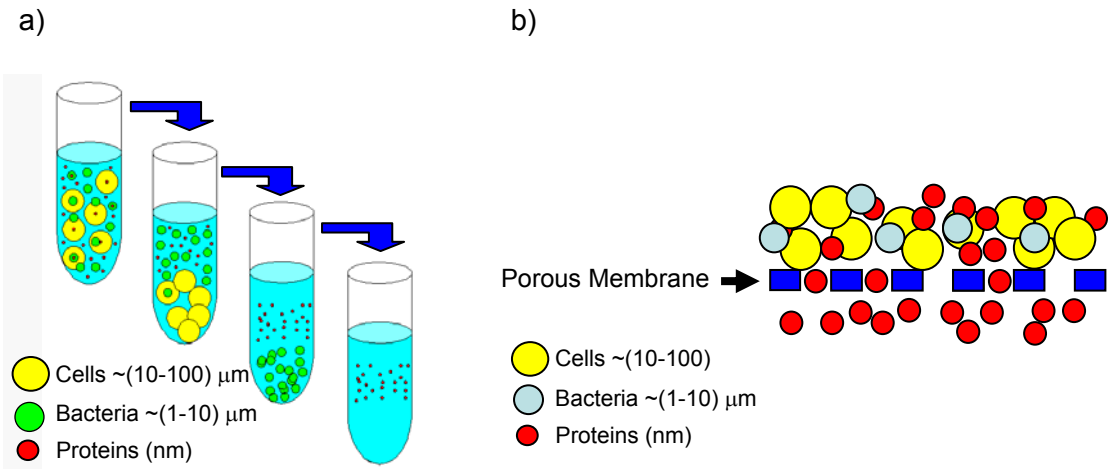

Figure 4.2: Illustration comparing traditional bioseparation methods using: a) a sequence of centrifuging steps, and b) the lab-on-a-chip concept of creating an on-chip customizable porous membrane within a microfluidic channel to separate a cells contents depending on the pore size created.

are tailorable to isolate different cellular contents, and less time and energy are required.

4.5.2 Enzyme Immobilization

Enzymes are highly specialized proteins that catalyze chemical reactions efficiently and selectively under mild conditions of temperature and pH. The function of an enzyme is to accelerate the rate of a reaction. A simple enzymatic reaction can be written as follows:

$$E + S \Leftrightarrow ES \Leftrightarrow EP \Leftrightarrow E + P$$

where E, S and P represent the enzyme, substrate, and product, and ES and EP are transient complexes of the enzyme with the substrate and the product. The substrate is

defined as the molecule bound to the active site and acted upon by the enzyme [146]. In Figure 4.3, the substrate molecule is passed through the immobilized enzyme support, and the products due to the catalytic reaction are collected downstream. The benefits to immobilizing enzymes onto porous supports within a lab-on-a-chip system are that it minimizes the enzymes lost (washed away with the product), enzyme degradation can be reduced (depending on the method used to bind the enzyme), and sample volumes used are reduced. As a result, immobilized enzymes lower the overall cost of the catalytic reaction.

Enzyme immobilization is an application where porous materials are attractive due to their high surface area. Enzymes are generally fixed onto functionalized

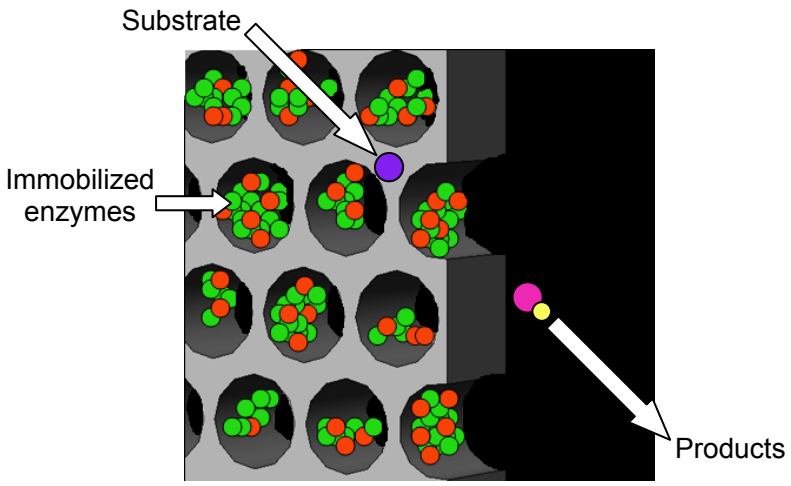

Figure 4.3: A schematic view of immobilized enzymes on a porous silica support. The substrate is flowed through the support. The enzymes catalyze a reaction and the products are collected downstream.

porous materials through adsorption [147, 148], encapsulation [149, 150], and covalently bonding [151]. A variety of biomolecules have been encapsulated in silicates, but the harsh conditions required to form the silica limited their activity [152].

Previous work [153] has demonstrated high immobilized enzyme activity when native proteins from diatoms were used to catalyze the formation of porous silica. These results support our long-term vision of creating synthetically catalyzed emulsion-templated porous silica using diatom-inspired conditions to immobilize enzymes within the pores of the silica material while maintaining a high enzyme activity. The benefits of a synthetic approach is that once a synthetic catalyst selected and demonstrated to catalyze the formation of silica large volumes of the synthetic catalyst can be produced, as opposed to the difficult isolation and purification of the catalyst responsible for the silica precipitation in diatoms.

4.6 Biocatalyst Selection

In order to synthetically form silica at room temperature and neutral pH we must look for a catalyst that will aggregate silica at a pH near neutral. Other groups have used synthetic bioinspired catalysts for silica precipitation [29, 32]. Since the silica-precipitating silaffin-1A and polyamines found in diatoms are cationic, several cationically-charged synthetic molecules were tested for silica precipitation in a silica precursor solution. Several cationic molecules gave silica precipitates of nanosized spherical particles, including poly-l-lysine, poly-l-arginine, and the unmodified 19 amino

acid sequence found in silaffin-1A ("pR5"). The catalytic activity of these molecules was explained by their cationic charges, as they can aggregate the negatively-charged silica particles into clusters. For example, the activity of poly-l-lysine, which gives silica spheres in 10-30 s, is believed to be due to the cationic lysine, an important amino acid in silaffin proteins. We decided to use triethylenetetramine (TETA) as our bio-catalyst because it was soluble in water and was previously demonstrated to precipitate silica from orthosilicic acid at near neutral pH within minutes [34, 35]. In order to determine the most straightforward method to solidify the outer aqueous material around our emulsion template into a silica using TETA as our bio-catalyst, we examined sol-gel processes.

4.7 Sol-Gel Chemistry

The sol-gel process is a versatile technique for forming various amorphous materials, specifically ceramics and glasses such as silica. We pursued sol-gel processing to create our silica because as the name implies, it involves the transition of inorganic networks through the formation of a colloidal suspension (sol) and gelation of the sol to form a network in a continuous liquid phase (gel) and finally transitions into a dried ceramic material through evaporation of the solvent (Fig. 4.4).

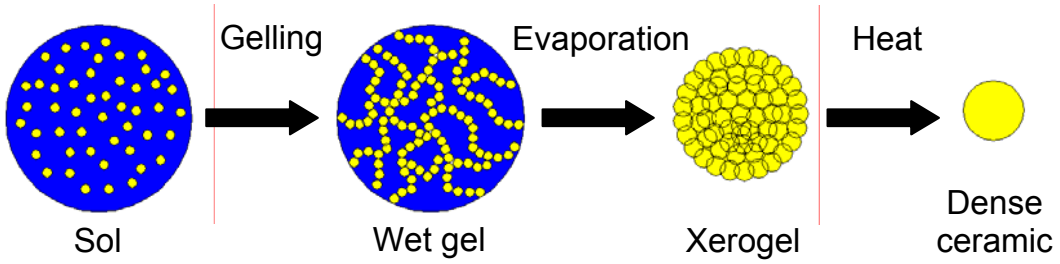

Figure 4.4: Illustration depicting the sol-gel process. The silicon precursor is hydrolyzed to form a colloidal suspension (sol), the particles then condense to form a new phase (gel), as the gel continues to dry by evaporation it is possible to obtain porous solid matrices (Xerogels). Lastly, by heating at high temperatures the gelled material densifies into a high purity oxide.

The sol is made of solid particles that have a diameter of few hundred nm, usually inorganic metal salts, suspended in a liquid phase. The silicon precursors for synthesizing these colloids consist of a metal or metalloid element of which metal alkoxides are most popular because they react readily with water (hydrolyze). The most widely used metal alkoxides are the alkoxysilanes, such as tetraethoxysilane (TEOS) and tetramethoxysilane (TMOS) where (R = C_2H_5, CH_3) for TEOS and TMOS respectively (Fig 4.5).

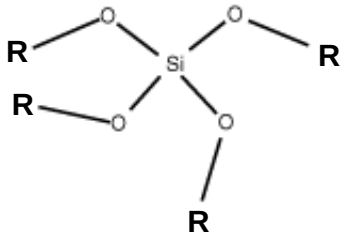

Figure 4.5: Structure formula for the silicon precursor prior to hydrolysis where R represents the end group.

Other alkoxides such as aluminates, titanates, and borates are also commonly used in the sol-gel process. At the functional group level, three reactions are generally used to describe the sol-gel process: hydrolysis (Eq. 4.1), alcohol condensation (Eq. 4.2), and water condensation (Eq. 4.3). Both the hydrolysis and condensation reactions are as follows:

Hydrolysis: ($R = C_2H_5$, CH_3, etc…)

$$\equiv Si\text{-}OR + H_2O \leftrightarrow \equiv Si\text{-}OH + ROH \quad (4.1)$$

Condensation:

$$\equiv Si\text{-}OR + HO\text{-}Si \equiv \leftrightarrow \equiv Si\text{-}O\text{-}Si\equiv + ROH \quad (4.2)$$

$$\equiv Si\text{-}OH + HO\text{-}Si \equiv \leftrightarrow \equiv Si\text{-}O\text{-}Si\equiv + H_2O \quad (4.3)$$

The hydrolysis reaction is accomplished through the addition of water which replaces the alkoxide groups (OR) with hydroxyl groups (OH). As a result the negatively charged sol is produced, more specifically silanol groups (Si-OH) are formed along with alcohol

(ROH) as a by-product. After hydrolyzing the silicon precursor, a condensation reaction begins to occur. There are two forms of condensation. In the first case, an alkoxysilane (Si-OR) group reacts with a silanol group to form a siloxane bond (Si-O-Si) and again alcohol is produced as a by-product. In the second case, a silanol group reacts with another silanol group to form a siloxane bond, only this time water is produced as a by-product. As the number of siloxane bonds increase, these individual molecules begin to bridge and aggregate the sol into a network which forms the gel. If the hydrolysis/condensation process were allowed to proceed a gel will form within 24 hours. However, there are a number of factors that affect the rate of hydrolysis and condensation reactions, such as, pH, reagent concentrations, catalyst nature (charge) and concentration, temperature and time of reaction. Most of these factors will be addressed in later sections. It should be noted that in sol-gel processes as explained above, the by-products of the hydrolysis and condensation process are water and alcohol and as a result stretch the networked siloxane bonds. However, during the evaporation and heating stages of the sol-gel, the water and alcohol are evaporated which permits the siloxane bonds to relax and consequently the material densifies as shown in (Fig. 4.4).

4.8 Gelation Process Flow

Having surveyed sol-gel processes, it was our aim to demonstrate that by carefully selecting the silicon precursors and the bio-inspired catalyst we could successfully gel the aqueous phase of a monodisperse oil-in-water emulsion generated

using the microfluidic flow-focusing emulsification chip. In order to prove the emulsion templating concept, it was decided that the initial silica gel experiments would be done in bulk in order to facilitate varying the reactive chemistries, the pH, and both the silicon precursor and catalyst concentrations. Additionally, bulk materials would allow for easier material inspection using either an optical microscope or a scanning electron microscope (SEM). Our process flow is depicted in Figure 4.6, which illustrates the oil-in-water emulsion being collected off-chip in a vial. The silicon precursor and the bio-catalyst are introduced into the vial and gently mixed so as to not disturb the emulsion. Once the gel is formed, it is aged in order to densify the gel. An ethanol exchange is then used to remove the hexadecane oil template. The gelatin-like plug is removed from the vial, the sample is sectioned and calcinated sequentially to prepare the sample for SEM inspection.

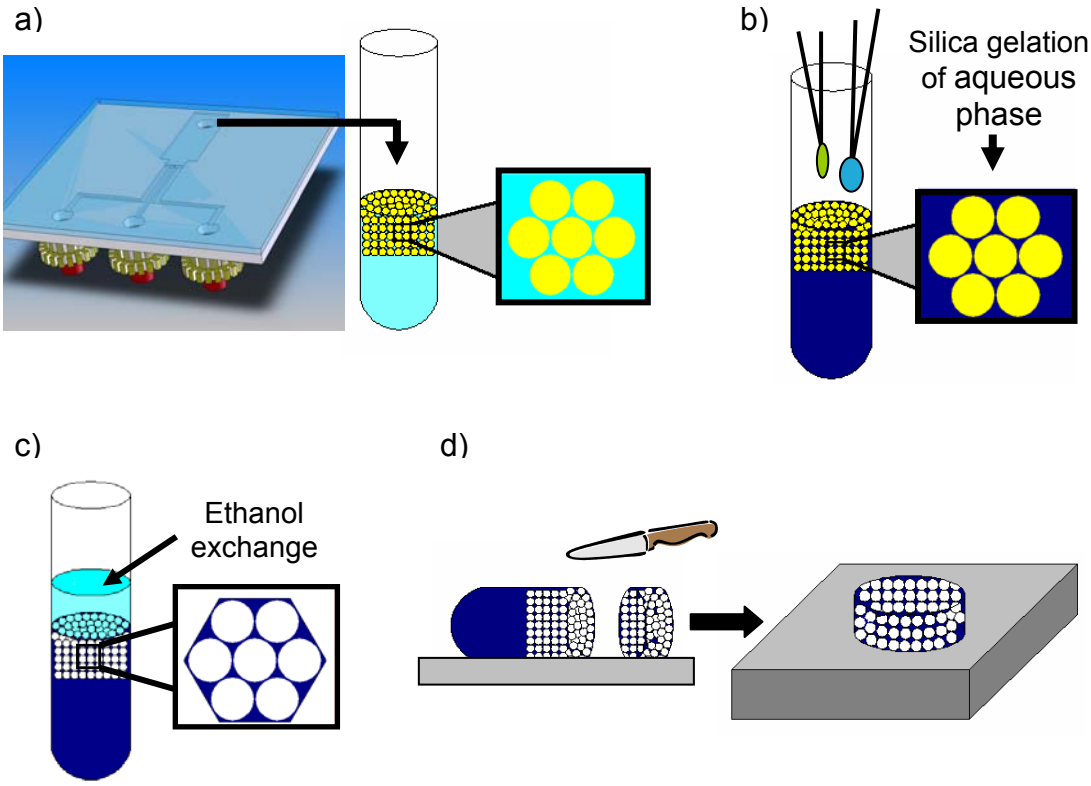

Figure 4.6: Emulsion templating process flow. (a) The oil-in-water monodisperse emulsion droplets are collected in a vial and allowed to close pack, (b) the reactive chemistries are introduced into the aqueous phase to initiate the silica gelation, (c) after the gel solidifies into a gelatin-like silica material an ethanol exchange is used to solubilize the hexadecane template, (d) The gelatin-like silica is sectioned with a razor blade into thin strips. The strips are placed on a silicon substrate in order to calcinate the silica into a glassy material by heating at 400°C.

4.8.1 Reaction Conditions

To determine the correct silicon precursor and bio-catalyst concentrations to gel the aqueous phase of the emulsion at neutral pH and room temperature, we varied both the concentrations of the silicon precursor and the bio-catalyst. The concentration of the

tetramethoxysilane (TMOS) silicon precursor we chose to use was varied between 1.9mM ─ 1M while the concentration of the triethylenetetramine (TETA) bio-catalyst in de-ionized water was varied between 0.0665 ─ 66.5mM. For the silica gelation, (0.9997, 0.9977, 0.9816, and 0.848 mL) of 1mM HCl was combined with (0.0003, 0.0023, 0.018, and 0.152 mL) of TMOS to hydrolyze the precursor and form orthosilicic acid, $Si(OH)_4$, at a final concentration of (0.0019, 0.0156, 0.125, and 1M) respectively. The results shown in Table 4.1 describe the initial pH value for each chemical concentration used, the resulting pH value for the reaction, a brief description of the gelation process, and the time required for the reaction to gel completely. All reactions were done by mixing 200 μL of each chemical in a vial. Vial (T2) which had the 1M and 6.65mM of the hydrolyzed TMOS silicon precursor and the TETA bio-catalyst respectively demonstrated a reasonable gelling time of approximately 12 ─ 15 minutes at a near neutral pH of 6. All the other vials took greater than 16 hours to gel and were further away from the neutral pH range that we set out to demonstrate. As a result, the concentrations used to produce vial (T2) were used for the following emulsion-templating studies.

TETA Concentration

TMOS Concentration

	66.5mM pH = 11	6.65mM pH = 10	.665mM pH = 9	.0665mM pH = 6
1000mM pH = 3.5	T1 The reaction precipitated immediately and remained a runny gel. The reaction turned white. pH = (7-7.5)	T2 The reaction precipitated white particles after 25 seconds and became a solid gel at ~12-15 minutes. The vial is cloudy. pH = 6	T3 The reaction in the vial remained clear. No noticeable precipitation. pH = 5. Still liquid after >16hrs	T4 Vial remained clear during reaction. No noticeable precipitation. pH = 4. Still liquid after >16hrs
125mM pH = 3.5	T5 The reaction turned milky white immediately. Could not see any large particles. pH = 10. Still not gelled after >16hrs	T6 The reaction began to precipitate white particles after 1 minute. pH = 7. Only particles, but no gelling after >16hrs	T7 The reaction in the vial remained clear. No noticeable precipitation. pH = (5.5—6). Still liquid after >16hrs	T8 The reaction in the vial remained clear. No noticeable precipitation. pH = 5. Still liquid after >16hrs
15.6mM pH = 4.5	T9 The reaction looks clear. No noticeable precipitation. pH = 10. Still liquid at >16hrs	T10 The reaction looked clear initially, then turned cloudy after 90 seconds. pH = 9. Still liquid after >16hrs	T11 The reaction looks clear. No noticeable precipitation. pH = 6. Still liquid at > 16hrs	T12 The reaction looks clear. No noticeable precipitation. pH = 5. Still liquid at > 16hrs
1.9mM pH = 4.5	T13 The reaction looks clear. No noticeable precipitation. pH = 11. Still liquid at >16hrs	T14 The reaction looked clear. No noticeable precipitation. pH = 10. Still liquid at >16hrs	T15 The reaction looks clear. No noticeable precipitation. pH = 6. Still liquid at > 16hrs	T16 The reaction looks clear. No noticeable precipitation. pH = 5. Still liquid at >16hrs

Table 4.1: Varied silicon precursor and bio-catalyst concentrations necessary to gel aqueous phase at neutral pH and room temperature. Vial (T2) demonstrated a reasonable gelling time of approximately 12 — 15 minutes at a near neutral pH of 6.

4.8.2 Emulsion Templated Gels

Monodisperse emulsions with droplet diameters on the order of tens of microns were collected off-chip in a vial and used as templates around which silica gel was formed in the biomimetic reaction. The emulsion droplets self-assembled into close-packed ordered lattices due to the buoyancy of the oil droplets in the water phase. Gelation was induced using the biomimetic catalyst, TETA, chosen for its similarity to natural polyamines found to catalyze silica precipitation in diatoms [33]. The catalytic activity of this molecule can be explained by its polycationic charge at neutral pH, which aggregates the negatively-charged particles of the silica sol into clusters. To initiate the gelation, 200 μL of orthosilicic acid (1M) and 80 μL of the biomimetic catalyst solution (6.65mM) were added to 200 μL of a monodisperse hexadecane-in-water emulsion (6% (w/v) SDS). Using these volumes the result is gelation within 8 min at neutral pH and ambient temperature. A subsequent heat treatment at 50°C for 12 h allowed the reactions to proceed to completion. The heat treatment densifies the gel and evaporates a portion of the organics. Micrographs of sectioned gels taken after the aging step are shown in (Fig. 4.7). The emulsion templates maintained their shape during the gelling process and a polydispersity less than 2.4% was measured for these samples.

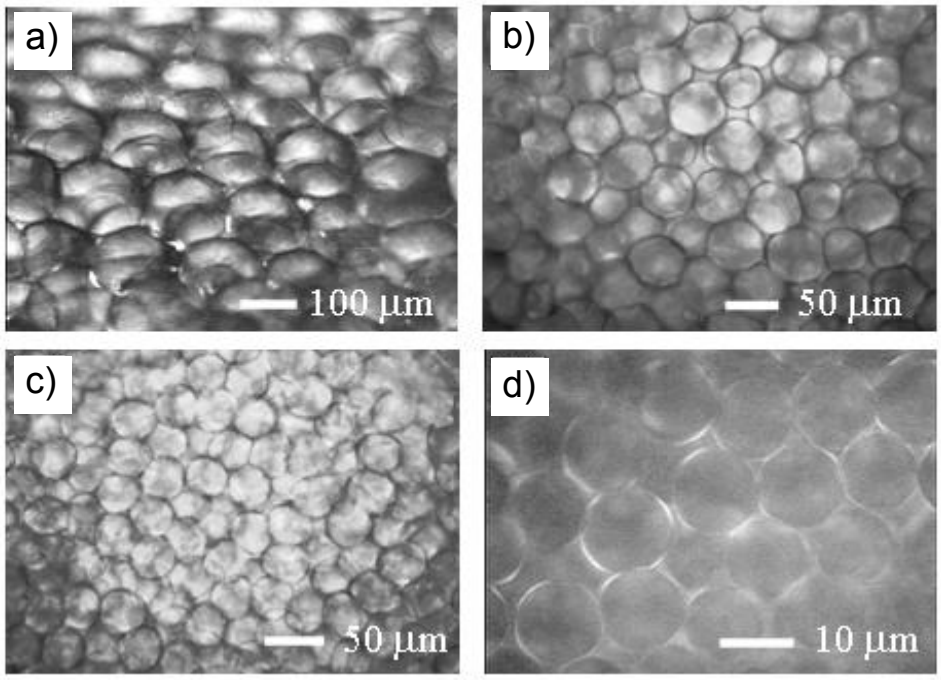

Figure 4.7: Macroporous silica gel templated around monodisperse chip-generated emulsions with average drop diameters: a) 120 µm, b) 48 µm, c) 34 µm, and d) 11 µm.

4.8.3 Calcinated Bulk Macroporous Silica

Before calcinating the emulsion-templated gels, a control was generated under similar gelling conditions to compare both the untemplated and emulsion-templated silica gels. The control was created by mixing 200 µL of orthosilicic acid (1M) and 200 µL of the biomimetic catalyst solution (6.65mM) and subsequently aged at 50°C for 12 hours and finally calcined at 400°C (ramp rate 12°C/min) for 4 h in air. Calcining served to densify the gel, remove the organic content and convert the material into glassy silica. SEM micrographs of the control are shown in Figure 4.8 depicting a smooth surface.

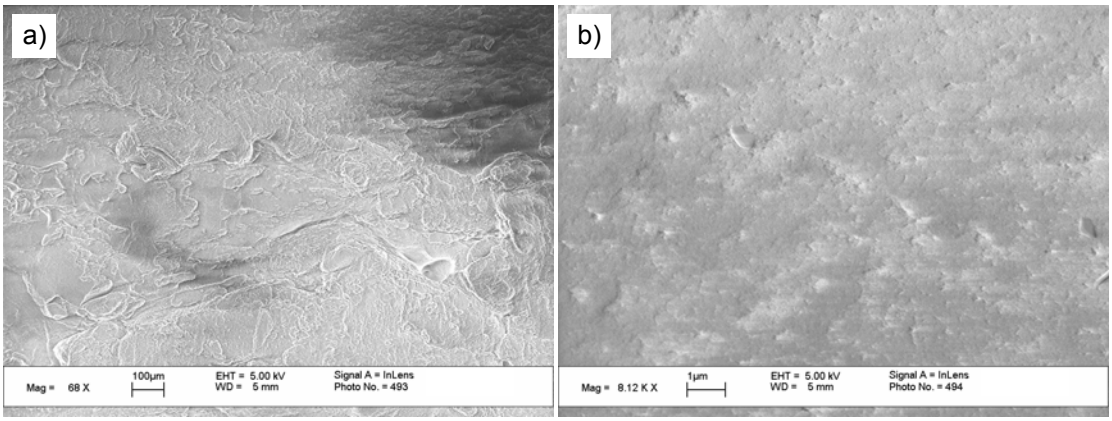

Figure 4.8: SEM micrographs of the control untemplated silica gel of both: a) a global view and, b) a zoomed in view of the nonporous material.

The emulsion-templated silica gels were then calcinated under the same conditions used for the untemplated control gels. Micrographs of the emulsion-templated glassy porous silica are shown in Figure 4.9, demonstrating pores sizes roughly 10 ─ 50 µm in diameter. The images clearly show that the pores are not circular as expected; rather they appear to have collapsed during the calcination step.

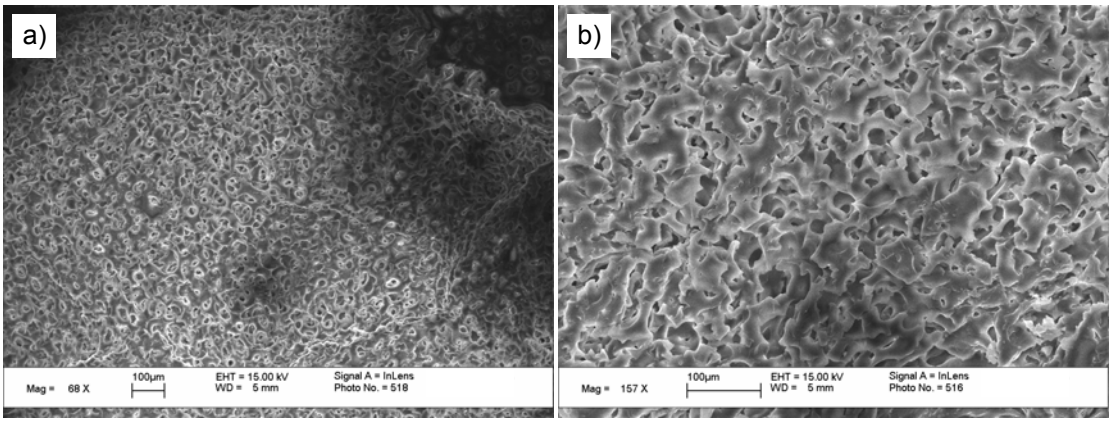

Figure 4.9: SEM micrographs of the emulsion-templated silica gel of both: a) a global view and, b) a zoomed in view of the porous glassy material.

To minimize pore collapse, a less aggressive ramp rate (2°C/min) was used to help reduce the thermal shock experienced by the silica sol-gel during the evaporation of the water, alcohol, and the organics which makes up the majority of the gel. In addition, the calcination step was done for 8 hours rather than 4 hours to provide a longer duration to insure the complete removal of any residual organics left behind from the hexadecane oil droplets. An emulsion-templated silica gel with a large polydispersity (greater than 10%) was aged as previously stated and calcinated using the new conditions. The results are shown in the micrographs of Figure 4.10, which demonstrate that the pores no longer collapse and maintained their circular shape. The pores range between 1 ─ 20 μm in diameter and multilayered pores are visible through the uppermost pores. It is evident that there are cracks in the glassy material of which may be a direct result of either the sectioning of the gel or the calcination process.

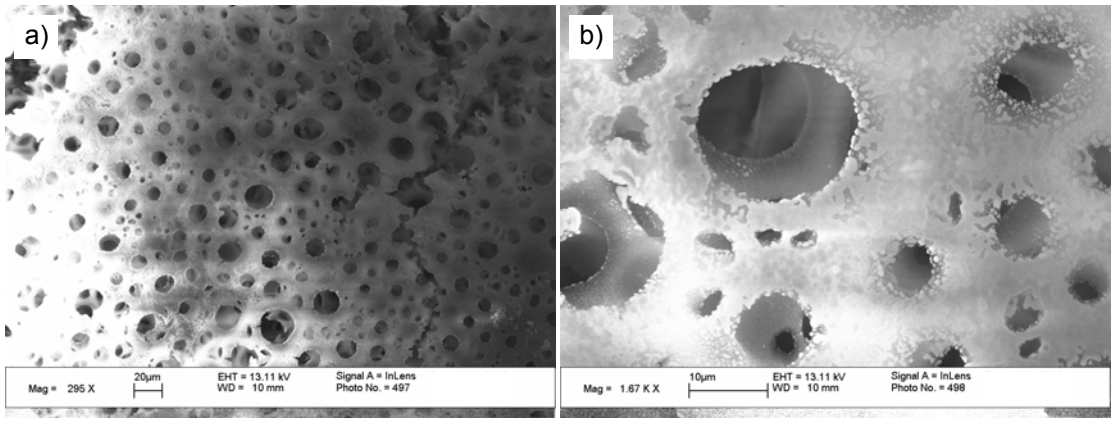

Figure 4.10: SEM micrographs of the emulsion-templated silica gel calcinated at a slower ramp rate (2°C/min). a) The pores have a polydispersity greater than 10%. b) The close-up image depicts multilayered pores on the order of tens of microns in diameter.

Upon calcining monodisperse silica gels similar to the ones shown in Figure 4.7, we observed a densification of ~50 ─ 70%; similar results were reported in [128]. The silica pore structure generally retained the hexagonal close-packing of the emulsion template after calcination. In addition to monodisperse pores at the μm-scale, it is likely the silica matrix also contains a pore network at the nm-scale as sol-gel silica is naturally mesoporous (2 ─ 50 nm) [128]. SEMs of templated silica of two pore sizes are shown in (Fig. 4.11).

We have demonstrated a powerful new technique to create ordered macroporous materials efficiently, by combining template-directed synthesis and biomimetic chemistry with microfluidics. If synthesized within lab-on-a-chip systems, functionalized porous silica will also be valuable for reaction, separation, and sample preparation modules

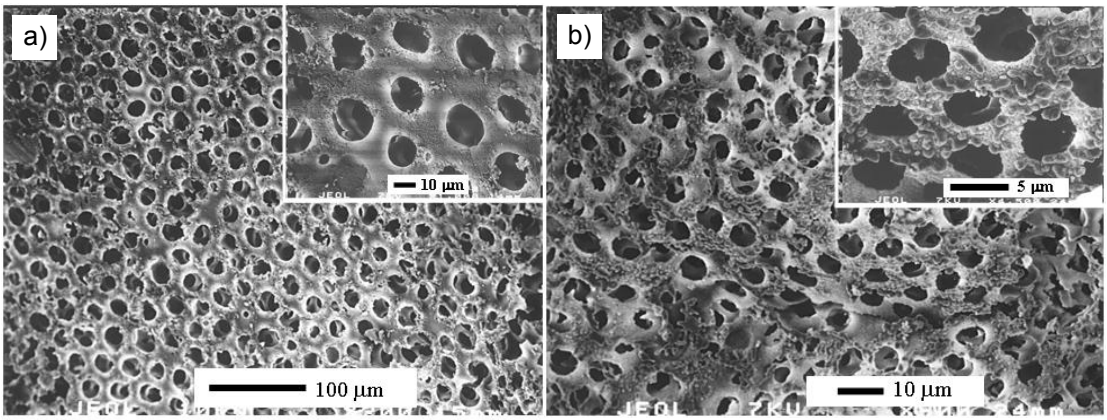

Figure 4.11: SEM micrographs of emulsion-templated porous silica: a) average pore diameter 17 μm, corresponding to ~70% shrinkage from the original gel. b) Average pore diameter 5.6 μm, corresponding to ~53% shrinkage from the original gel. Close-ups of the pores are shown in the inset SEMs.

described earlier. This work opens the possibility of in-use customization of critical microsystem components.

In Chapter 3, we addressed double emulsions along with the fabricated single chip emulsification device that consisted of a flow-focusing region in series with a T-junction. In between these two regions, integrated microchannels were designed to allow for the delivery of reactive chemistries and other materials such as nanoparticles. Therefore, by using the innermost oil droplets in a double emulsion as a template the silicon precursor and the bio-catalyst can be delivered downstream into the intermediate phase between the first and second emulsification steps to gel the intermediate phase and produce an emulsion-templated silica particle. This approach can be used to fabricate particles with porosity at different scales and particles with added functionality by incorporating nanoparticles to stud the silica.

4.9 Double Emulsion Templated Silica Gels and Particles

This section describes a new approach to the formation of macroporous silica particles generated through a two-step emulsification process using a single microfluidic device. We combine biomimetic chemistry to modify the intermediate fluid of the double emulsion and microfluidics to produce high-quality template-directed macroporous silica particles. In the future these three dimensional porous particles may be produced *in-situ* within lab-on-chip systems for reaction and separation modules, or collected and dispensed from an ink-jet system to produce complex arrangements such as scaffolds.

Using the characterized single emulsification device described in chapter three, generation of hexadecane droplets in water, stabilized using 2% (w/v) polyvinyl alcohol in the water phase served as the first emulsification step while generation of water droplets in hexadecane, stabilized using 0.5% (w/v) lecithin in the hexadecane phase served as the second emulsification step. By setting a constant volumetric flow rate of both the inner oil flow ($Q_{hexadecane}$ = 0.4 μL/min) and the outer water flows (Q_{water} = 0.55 μL/min), we produce the initial monodisperse oil-in-water emulsions that have a droplet polydispersity less than 2.4% as previously characterized [105], at the flow-focusing region. The system was allowed to stabilize for 30 minutes before any of the reactive chemistries were introduced.

Between the formation of the first and second emulsification steps, orthosilicic acid (1M) and the biomimetic catalyst triethylenetetramine (6.7mM) were both introduced into the intermediate phase separately using the two integrated microchannels at a constant volumetric flow rate of ($Q_{chemistries}$ = 0.4 μL/min). At the T-junction, a water-in-oil emulsion was generated which encapsulated the reactive chemistries with the intermediate phase causing it to form a templated silica gel around the inner monodisperse oil droplets as shown in (Fig. 4.12).

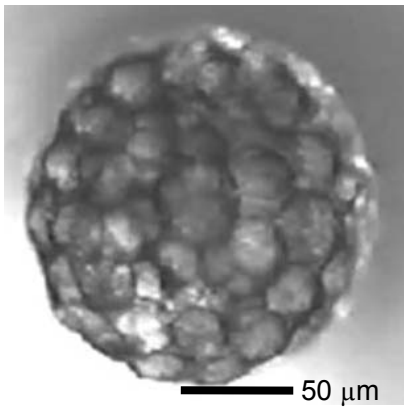

Figure 4.12: Micrograph of a gelled double emulsion droplet. The intermediate phase inside the larger droplet forms a silica gel templated around the inner emulsion droplets of diameter ~30 μm.

The double emulsion-templated gels were aged exactly the same as the bulk gels. Subsequent calcination of the gelled droplets at 400°C for 8 h removes the organic content and converts the material into glassy porous silica particles [128]. After calcination, we observe a densification of ~50%. SEM micrographs of a double-emulsion-templated porous silica particle are shown in (Fig. 4.13). The SEMs show that the outermost silica shell is smooth. Additionally, each of the encapsulated droplets which reside at outermost point of the shell has a small pore. The pores are more than likely formed as a result of the solvents from the innermost encapsulated droplets exiting the particle during calcination. Taking a closer look inside the silica particle reveals individual rough shells (spheres) that are not interconnected to one another, but rather they are loosely bunched together inside the outermost silica shell. An investigation focusing on both the dependence of silicon precursor and the bio-catalyst concentrations

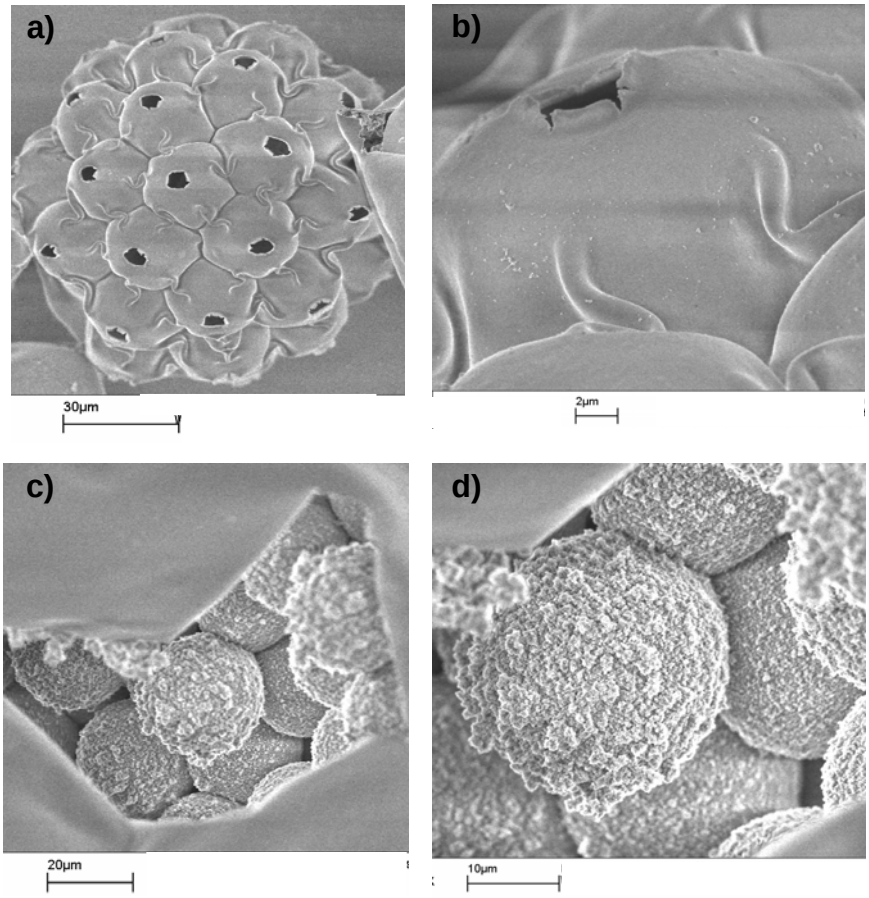

Figure 4.13: SEM micrographs of emulsion-templated double emulsion porous silica particles: a) inner droplets have a diameter of ~30 µm, b) a close-up depicts the smooth silica walls and small pore diameters of ~5 µm, c) a crack in the surface of a silica particle reveals silica templated around previously encapsulated emulsion droplets, d) a close-up of the encapsulated emulsion-templates demonstrates that the droplets are not interconnected and are loosely bunched together inside the outermost silica shell.

may aid in explaining whether a lack of silicon or bio-catalyst caused inner shells to form around each encapsulated droplet instead of forming a solid silica material with interconnected internal pores similar to the bulk macroporous silica cases.

4.9.1 Gold Studded Double Emulsion-Templated Silica Particles

The incorporation of gold nanoparticles within the intermediate phase of the double emulsion so as to embed the silica and form nanocomposite materials/particles was investigated. Metal nanoparticles immobilized in this manner can be used as catalysts and have the potential for improving the efficiency, selectivity, and yield of the catalytic processes. The higher surface-to-volume ratio means that much more of the catalyst is actively participating in the reaction. The potential for cost savings is significant from a material, labor, and time standpoint. Traditional methods fix nanoparticles onto a porous support through an adsorption process. A drawback of this method is that the nanoparticles wash away during the reaction due to the weak bond to the support. An immobilized nanoparticle in our approach has the potential to mean less waste and fewer impurities, which could lead to reduced environmental impacts.

To embed the intermediate phase with metal nanoparticles a monodisperse 20 nm gold colloid (Sigma-Aldrich) was used. All of the volumetric flow rates which include the oil and water flow-focusing channels, the two microchannels used to deliver the orthosilicic acid/gold nanoparticles mixture and the TETA bio-catalyst, were kept fixed. In this manner the final composition within the generated double emulsion could be maintained at (50, 25, 20, and 5)% (v/v) of orthosilicic acid, oil-in-water emulsion, TETA bio-catalyst, and gold nanoparticles, respectively. Earlier work using bulk materials demonstrated that these volumes allowed for the gelation of the silica at room temperature, near neutral pH, and within 30 minutes.

The gold embedded double emulsion-templated silica gels were aged and calcinated as previously described. Micrographs taken after the calcination procedure, shown in Figure 4.14, were quite intriguing. It was expected that images taken would look similar to Figure 4.14 (a and b), showing the gold nanoparticles embedded along the surface; however, it was clearly evident that there was nanowire growth occurring which was not observed in the calcination of gold free silica gels. Traditional nanowire growth is done using a vapor-liquid-solid (VLS) method [154-156]. In VLS, the synthesized nanowires are grown at elevated temperatures within a silane, SiH_4, rich gas environment (used as the silicon source) while a metal nanoparticle serves as the nucleation site during the nanowire growth. In our case, we used metal nanoparticles, much like that of VLS, however we used lower temperatures (T = 400°C), and the ambient atmosphere inside the calcination oven/furnace was only air compared to traditional VLS processes. The nanowires may have potentially grown as a result of the gold nanoparticles nucleating silicon molecules from the silicic acid (TMOS was used as the silicon precursor) at the elevated temperature. The material composition of the nanowires was not embedded in this work.

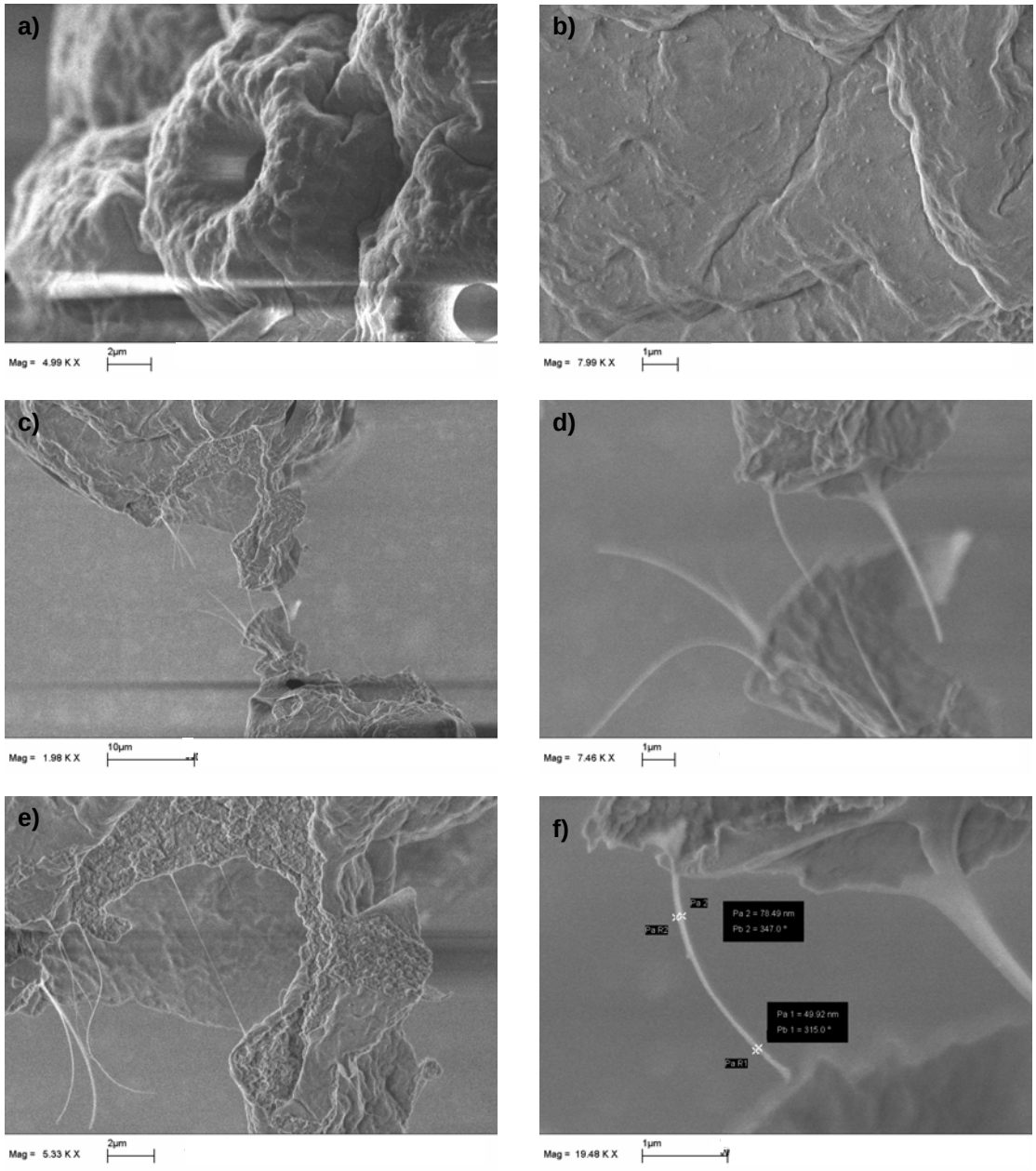

Figure 4.14: Micrographs of nanowire growth that occurred during the calcination procedure at 400°C. Images (a) and (b) illustrate the immobilized gold nanoparticles. Images (c) and (d) show nanowire growth, and images (e) and (f) illustrate nanowires spanning across a broken pores. The nanowires ranged between 25 to hundreds of nm in diameter.

The calcinated samples were placed in a VLS system to promote the continued growth of the nanowires. The nanowire growth was carried out at a temperature of 850°C for 10 minutes using 10% H_2 in argon (Ar) as the carrier gas at a ratio of 50/200. The ratio equals the carrier gas that goes through a bubbler where the amount of the precursor that is picked up is roughly based on the vapor pressure of the precursor to that of the gas that bypasses the bubbler. SEM micrographs of the VLS grown nanowires are shown in (Fig. 4.15). Figures 4.15 (a and b), show a ruptured silica particle exposing individual encapsulated silica shells covered by a rug-like growth of nanowires. A possible reason for the ruptured silica particle is the quick thermal cycle experienced during the VLS process. A slower ramp rate may help minimize the number of ruptured silica particles, as was seen with the bulk emulsion-templating. Figures 4.15 (c through f), present a survey of different silica particles specifically observing the randomness of the nanowire growth as a result of the silica being amorphous. Since the silica does not have a long range crystal orientation the nanowires are shown making random 90 degree turns, others are shown either having spilt into two nanowires, or having intersected. Additionally, nanowires with lengths on the order of milli-meters were observed.

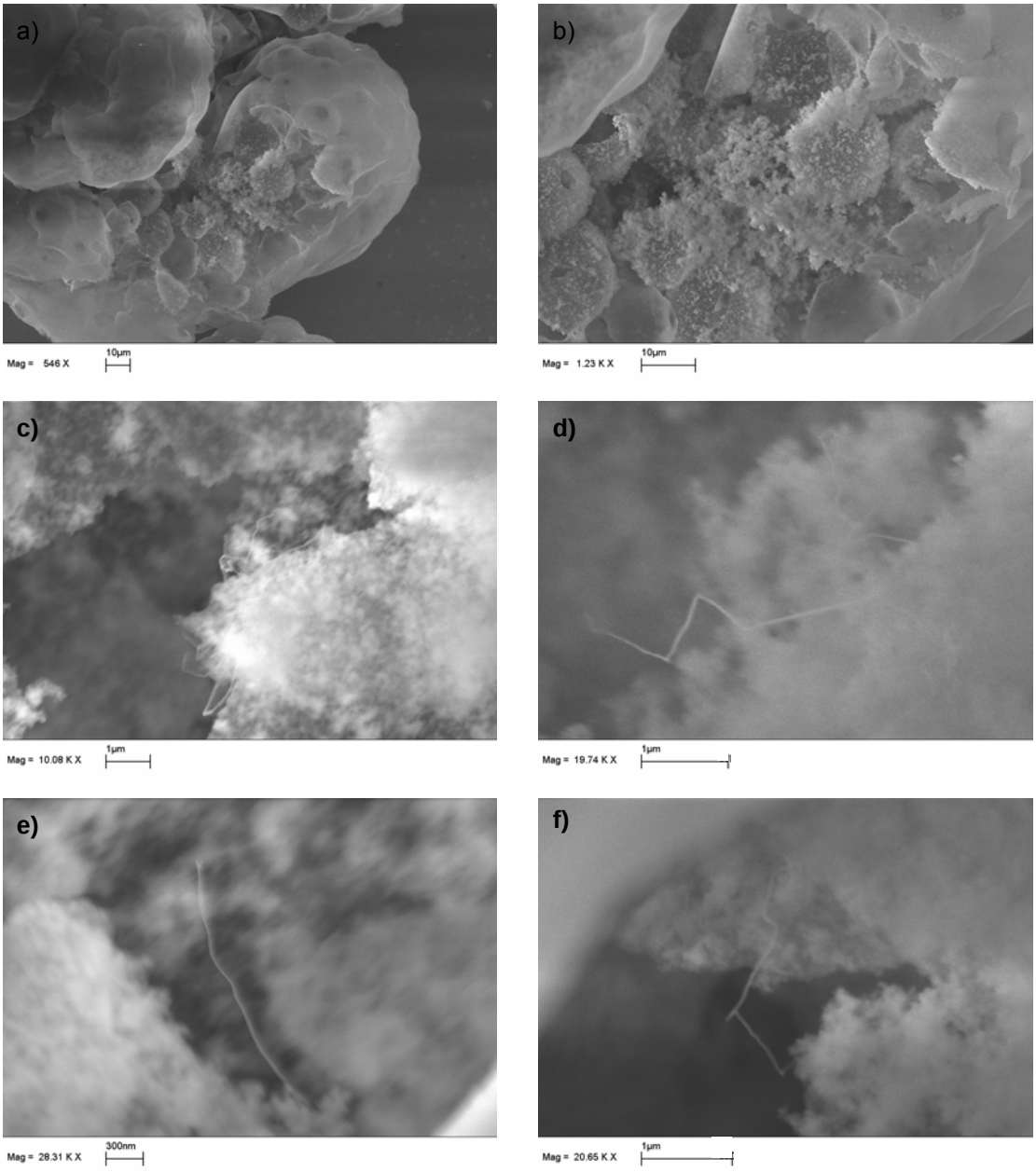

Figure 4.15: Micrographs of VLS nanowire growth. Images (a) and (b) illustrate a ruptured silica particle and a rug-like nanowire growth. Images (c through f) demonstrate the random growth of the nanowires as a result of the silica crystal orientation being amorphous.

4.10 Conclusions

We have demonstrated a new technique to create ordered macroporous materials/particles efficiently, by combining template-directed synthesis and biomimetic chemistry with microfluidics. By using hydrolyzed TMOS as our silicon precursor and TETA as the bio-catalysts we demonstrated gelling at neural pH and room temperature. With the addition of the channels between emulsification steps we have added the flexibility of not only introducing the reactive chemistries on-chip but also the functionality of introducing other materials such as nanoparticles to stud the silica particles. If synthesized within lab-on-a-chip systems, functionalized porous silica will also be extremely valuable for microsystems, in particular for reaction, separation, and sample preparation modules.

Further investigations are necessary to describe fully the material composition of the nanowire and also to determine how different gold colloid concentrations will effect the nanowire growth. There is a possibility that a lower gold colloid concentration will minimize the rug-like nanowire growth and result in more individually isolated nanowires. However, our first attempt of studding the macroporous silica and nanowire growth were very encouraging.

Having developed a technique to produce emulsion-templated silica and silica particles we are now in a position to attempt to use the biomimetically generated silica for our intended applications of bioseparations and enzyme immobilization. These applications along with other ideas will be described in detail in the following chapter.

Chapter 5

Conclusions and Future Directions

5.1 Summary

When we started this research our aim was to develop a new approach to the formation of macroporous silica. Unlike conventional methods of creating porous silica, which require elevated temperatures and alkaline conditions, we were inspired by nature's mechanisms of silica formation, specifically diatom biomineralization. Diatoms create their ornate outer shells, or frustules, which contain rows of pores or slits arranged in remarkably uniform patterns under benign conditions. As micro/nanoemulsions are believed to be central to the diatom's synthetic mechanism, we developed a biomimetic approach to create synthetically derived silica-based porous materials using bioinspired catalysts and emulsions generated in a microfluidic device as templates at near neutral pH, ambient temperature, and pressure.

In Chapter 2, we reviewed microfluidic techniques used for the generation of emulsions. Using our defined emulsion criteria, each method was described and evaluated in order to determine which was the most promising for our application. It was

determined that the flow-focusing emulsification device satisfied all of our criteria. We developed microfabrication, chip bonding, and fluidic interfacing processes to fabricate our flow-focusing emulsification device, which we used to produce oil-in-water emulsions. Initially we encountered problems concerning debris plugging our orifice and oil induced swelling causing intermittent flow as a result of using PDMS as an adhesion layer. However, we solved these problems by using anodic bonding to encapsulate our device and NanoPort™ assemblies to facilitate the fluidic interfacing between our device and syringe pumps.

Next, in Chapter 3, we investigated the droplet generation and characterization of our microfluidic emulsification device for both air-in-water and oil-in-water emulsions. We first generated air-in-water foams by using a filtered solution of DI water, glycerol (52% (w/w)), and Tween-20 surfactant (2% (w/w)) as the continuous aqueous phase and an empty gas-tight syringe to inject the dispersed gas phase. There were two main drawbacks to air-in-water foams: 1) the smallest droplets producible were 120 μm in diameter, and 2) the gas bubbles coalesced very quickly, which made working with foams as templates difficult. Therefore, we turned our attention to oil-in-water emulsions. We generated oil-in-water emulsions by using DI water with SDS surfactant as the continuous phase and filtered hexadecane oil as the dispersed phase. We were able to generate monodisperse droplets with coefficient of variations lower than 3% over a large range of flow rates. The smallest oil drops producible were 8 μm in diameter, and were stable for months unlike the air-in-water foams. By investigating the capillary number we were able to predict which flow rates generated monodisperse droplets.

Also in Chapter 3, the concepts of double emulsions were introduced. Current two-step emulsification techniques used to produce double emulsions were reviewed and evaluated. We generated oil-in-water-in-oil double emulsions. In order to accomplish this, we developed a series connected flow-focusing and T-junction two-step emulsification device in order to maintain the ability to finely tune the drop size and uniformity of the inner droplets over a wide range using flow-focusing while maintaining the capability to generate the larger second droplet, which contained the first emulsion, at a T-junction. Our microfabrication process and selective microchannel surface fictionalization was described. Characterization of our two-step emulsification devices showed that uniform external droplets ranging between 80 – 240 μm in diameter for flow rates between 1 – 60 μm/min were generated while 27 μm diameter droplets were being encapsulated by the external droplet.

Finally in Chapter 4, we developed a new approach to the formation of macroporous silica, templated using emulsions generated in a microfluidic device. With precise control over the size and uniformity of the emulsion droplets, we were able to tailor the pore size and size distribution of the resulting silica gels. By using triethylenetetramine as a biomimetic catalyst, our gelation reactions occurred within minutes at room temperature and neutral pH, in contrast to conventional sol-gel routes. We subsequently dried the gel at 50°C and calcinated at 400°C yielding glassy materials with spherical pores where the emulsion droplets had been. Monodisperse porous silica with a range of pore sizes from 5-50 μm and polydispersity less than 2.4% was fabricated.

Based on the single emulsion-templating we developed an approach to the formation of macroporous silica particles generated through a two-step emulsification process using a single microfluidic device. Between the first and second emulsification steps, integrated channels provided added the flexibility of introducing reactive chemistries and nanoparticles within the intermediate fluid. The overall size of the fabricated silica particles ranged from 40-120 μm in diameter with measured polydispersity less than 4.8 %. The innermost droplets each had pores with diameters on the order of 5 μm. We also developed a technique of embedding gold nanoparticles in the silica to form nanocomposite particles. Gold nanoparticles were attractive for a number of reasons. Mainly, the embedded particles alone could alter the physical and optical properties; additionally, it provided a catalyst for Vapor-Liquid-Solid (VLS) nanowire synthesis. The majority of work related to nanowire growth has been done on free-standing planar substrates; however our nanowires were synthesizes on non-planar amorphous porous silica.

5.2 Future Directions

Having demonstrated a technique to create ordered macroporous materials, future directions include efforts in creating entire lab-on-a-chip microsystems. If synthesized within lab-on-a-chip systems, functionalized porous silica would be extremely valuable for microsystems, in particular for reaction, separation, and sample preparation modules. This work would open the possibility of in-use customization of critical microsystem

components. In order to fully achieve these complete mircosystems additional work in the following areas are required.

Additional work could encompass an investigation of monodisperse droplet formation at smaller size scales to fabricate silica with pore dimensions down to hundreds of nanometers. A possible method of achieving smaller emulsion droplets would be to microfabricate devices with shallower microchannels, and smaller orifice widths. Work which explores orifice designs in order to create instabilities of the fluid as it flows through the orifice may lead to smaller droplets with higher uniformity over a larger range of flow rates.

Continuing along the lines of microfabrication, silica deposition vesicles etched into the silicon would provide an area where silica formation could occur within a confined geometrical space all on-chip. The vesicle would allow for characterization of the formation of the silica through imaging of the reaction *in-vitro*.

From a biomimetic chemistry point of view, further investigations of the reactive silica chemistries may lead to discoveries of reactions that go from a liquid phase straight into the solid phase, bypassing both the gel phase and the need to heat the gels in order to densify the silica. The technique described is not limited to silica and may be adapted to create a variety of porous materials. If the reaction occurred under benign conditions, it can be envisioned that enzymes could be combined during the reaction, so as to create immobilized enzyme catalytic supports.

The proteins responsible for the precipitation of silica in diatoms are known, and a promising direction would aim to generate enough volume of these native proteins in

order to study the silica formation within a microsystem. This would further the understanding of nature's biomineralization process.

We briefly investigated the synthesis of nanocomposite porous materials which included embedding gold nanoparticles within the silica and synthesizing nanowires by using the cold as a catalyst. However, there is still endless work to do in this area. For example, characterization of the composite materials is necessary to fully understand both the material and optical properties of nanoparticle embedded silica, and nanowires grown on silica nanocomposite materials. Mainly, because this technique of creating nanocomposites may open possibilities of controlling the overall physical and optical properties of the materials and lead to nanocomposites that could be used either as waveguides, or effectively scatter light and as a result be used as pigments in smart acrylics, or in environmentally responsive materials.

In conclusion, using diatoms as inspiration, we developed a powerful new technique to create ordered macroporous materials efficiently, by combing template-directed synthesis and biomimetic chemistry with microfluidics. This technique opens the possibility of tailoring materials specific to their intended applications, such as: bioseparation filters, high surface are catalytic supports, tissue engineering supports, size-exclusion chromatography, and three-dimensional photonics. We envision that our technique will aid in developing a foundation for new micro/nanostructure fabrication technologies for adaptive and repairable microsystems.

Bibliography

1. Barrer, R.M., *Hydrothermal Chemistry of Zeolites.* London: Academic Press, 1982.
2. Zhou, Y., et al., "Efficient Catalysis of Polysiloxane Synthesis by Silicatein α Requires Specific Hydroxy and Imidazole Functionalities". *Angewandte Chemie Intl*. 38, p. 779-782, 1999.
3. Cha, J.N., et al., "Biomimetic synthesis of ordered silica structures mediated by block copolypeptides". *Nature*. 403(6767), p. 289-292, 2000.
4. Weaver, J. C., et al., "Molecular biology of demosponge axial filaments and their roles in biosilicification" *Microscopy Research and Technique.* 62(4), p.356-67, 2003.
5. Roth, K.M., et al., "Bifunctional Small Molecules Are Biomimetic Catalysts for Silica Synthesis at Neutral pH". *J. Am. Chem. Soc.* 127 (1), p. 325 -330, 2005.
6. Foo, C.W.P., et al., "Lessons from seashells: silica mineralization via protein templating". *Trends in Biotechnology*. 22(11): p. 577-585, 2004.
7. Epstein, E., "The Anomaly of Silicon in Plant Biology". Proceedings of the National Academy of Sciences. 91, p. 11-17, 1994.
8. Harrison, C.C., "Evidence for intramineral macromolecules containing protein from plant silicas". *Phytochemistry*. 41(1), p. 37-42, 1996.
9. Perry, C.C. et al., "Model studies of colloidal silica precipitation using biosilica extracts from Equisetum telmateia". *Colloid & Polymer Science.* 281(7), p. 652-664, 2003.
10. Riebesell, U., et al., "Carbon dioxide limitation of marine phytoplankton growth rates". *Nature.* 361(6409), p. 249-251, 1993.
11. Riebesell, U., "Photosynthesis: Carbon fix for a diatom". *Nature*. 407(6807), p. 959-960, 2000.
12. Smetacek, V., "Oceanography: The giant diatom dump". *Nature.* 406(6796), p. 574-575, 2000.
13. Smetacek, V., "A watery arms race". *Nature*. 411(6839), p. 745-745, 2001.
14. Armbrust, E.V., et al., "The Genome of the Diatom Thalassiosira Pseudonana: Ecology, Evolution, and Metabolism". *Science*. 306(5693), p. 79-86, 2004.
15. Field, C.B., et al., "Primary Production of the Biosphere: Integrating Terrestrial and Oceanic Components". *Science*. 281(5374), p. 237-240, 1998.
16. Round, F.E., et al., *The Diatoms: Biology and Morphology of the Genera* London: Cambridge University Press, 1990.

17. Scala, S., et al., “Genome Properties of the Diatom Phaeodactylum tricornutum”. *Plant Physiol*, 129, pp. 993-1002, 2002.
18. Poulsen, N. and N. Kroger, “Silica Morphogenesis by Alternative Processing of Silaffins in the Diatom Thalassiosira pseudonana”. *J. Biol. Chem.* 279 (41), p. 42993-42999, 2004.
19. Bradbury, J., “Nature's Nanotechnologists: Unveiling the Secrets of Diatoms”. *PLos Biol.* 2(10), p. e306, 2004.
20. Kroger, N., et al., “Polycationic Peptides from Diatom Biosilica That Direct Silica Nanosphere Formation”. *Science.* 286(5442), p. 1129-1132, 1999.
21. Kroger, N., et al., “Species-specific polyamines from diatoms control silica morphology”. *Proc. National Academy of Science.* 97(26), p. 14133-14138, 2000.
22. Kroger, N., et al., “Silica-precipitating Peptides from Diatoms. THE CHEMICAL STRUCTURE OF SILAFFIN-1A FROM CYLINDROTHECA FUSIFORMIS”. *J. Biol. Chem.* 276(28), p. 26066-26070, 2001.
23. Kroger, N., et al., “Self-Assembly of Highly Phosphorylated Silaffins and Their Function in Biosilica Morphogenesis”. *Science*. 298(5593), p. 584-586, 2002.
24. Sumper, M., “A Phase Separation Model for the Nanopatterning of Diatom Biosilica”. *Science.* 295(5564), p. 2430-2433, 2002.
25. Sumper, M., “Biomimetic Patterning of Silica by Long-Chain Polyamines”. *Angew. Chem. Int. Ed. Engl.* 43(17), p. 2251-2254, 2004.
26. Sumper, M., et al., “Biomineralization in diatoms: Characterization of novel polyamines associated with silica”. *FEBS Letters*. 579(17): p. 3765-3769, 2005.
27. Patwardhan, S.V., et al., “Macromolecule mediated bioinspired silica synthesis using a diol-modified silane precursor”. *Silicon Chemistry.* 2(5): p. 279-285, 2005.
28. Brunner, E., et al., “Biomimetic synthesis of silica nanospheres depends on the aggregation and phase separation of polyamines in aqueous solution”. *Phys. Chem. Chemical Phys.* 6(4), p. 854-857, 2004.
29. Patwardhan, S.V., et al., “Silicification and biosilicification: Part 5. An investigation of the silica structures formed at weakly acidic pH and neutral pH as facilitated by cationically charged macromolecules”. *Materials Science and Engineering: C*. 23(4), p. 495-499, 2003.
30. Patwardhan, S.V., et al., “Silicification and Biosilicification Part 7: Poly-L-Arginine Mediated Bioinspired Synthesis of Silica”. *Journal of Inorganic and Organometallic Polymers*. 13(4), p. 193-203, 2003.
31. Patwardhan, S.V., et al., “Silicification and biosilicification”. *Polymer Bulletin*. 48(4), p. 367-371, 2002.
32. Patwardhan, S.V., et al., “Silicification and biosilicification: Part 3 The role of synthetic polymers and polypeptides at neutral pH”. *Silicon Chemistry*. 1(3), p. 207-214, 2002.
33. Noll, F., et al., “Nanostructure of Diatom Silica Surfaces and of Biomimetic Analogues”. *Nano Letters* 2(2), p. 91-95, 2002.
34. Mizutani, T., et al., “Silicic Acid Polymerization Catalyzed by Amines and Polyamines”. *Chemistry Letters*. p. 133-134, 1999.

35. Mitzutani, T., et al., "Silicic Acid Polymerization Catalyzed by Amines and Polyamines". *Bulletin of the Chemical Society of Japan*. 71, p. 2017-2022, 1998.
36. Falciatore, A. et al., "Revealing the Molecular Secrets of Marine Diatoms". *Annu. Rev. Plant Biol.* 53, p. 109-130, 2002.
37. Hildebrand, M., "Biological processing of nanostructured silica in diatoms". *Progress in Organic Coatings*. 47(3-4), p. 256-266, 2003.
38. Hildebrand, M., et al., "Nanoscale control of silica morphology and three-dimensional structure during diatom cell wall formation". *J. Mater. Res*. 21(10), p. 2689-2698, 2006.
39. Frigeri, L.G., et al., "Identification of Proteins from a Cell Wall Fraction of the Diatom Thalassiosira pseudonana: Insights into Silica Structure Formation". *Molecular & Cellular Proteomics.* 5, p. 182-193, 2006.
40. Harris, T., "Treading Carefully". *Industrial Minerals*. 431,:p. 52-55, 2003.
41. Patwardhan, S.V., et al., "Bioinspired synthesis of new silica structures". *Chem. Commun*. 10, p. 1122-1123, 2003.
42. Bogush, G.H., et al., "Preparation of monodisperse silica particles: Control of size and mass fraction". *Journal of Non-Crystalline Solids*. 104(1), p. 95-106, 1988.
43. Göltner, C. G., et al., "Mesoporous Silica from Lyotropic Liquid Crystal Polymer Templates". *Angew. Chem. Int. Ed.* 37(5), p. 613-616, 1998.
44. Kim, S.S., et al., "Ultrastable Mesostructured Silica Vesicles". *Science.* 282(5392), p. 1302-1305, 1998.
45. Ding, K., et al., "Engineering the Structural Properties of DNA Block Copolymer Micelles by Molecular Recognition". *Angew. Chem. Int. Ed.* 46(7), p. 1172-1175, 2007.
46. Fowler, C.E., et al., "Interfacial synthesis of hollow microspheres of mesostructured silica". *Chemical Communications*. 19, p. 2028-2029, 2001.
47. Coffman, E.A., et al., "Surface Patterning of Silica Nanostructures Using Bio-Inspired Templates and Directed Synthesis". *Langmuir.* 20(20), p. 8431-8436, 2004.
48. Esquena, J., et al., "Preparation of monodisperse silica particles in emulsion media". *Colloids and Surfaces A: Physicochemical and Engineering Aspects*. 123-124: p. 575-586, 1997.
49. Minehan, W.T., et al., "Synthesis of spherical silica particles by spontaneous emulsification". *Colloids and Surfaces*. 63, p. 181-187, 1992.
50. Sims, S. D., et al., "Morphosynthesis of Macroporous Silica Frameworks in Bicontinuous Microemulsions". *Advanced Materials.* 10(2), p. 151-154, 1998.
51. Walsh, D., et al., "Fabrication of hollow porous shells of calcium carbonate from self-organizing media". *Nature*. 377(6547), p. 320-323, 1995.
52. Antonietti, M., et al., "Synthesis of Mesoporous Silica with Large Pores and Bimodal Pore Size Distribution by Templating of Polymer Latices". *Advanced Materials.* 10, p. 154-159, 1998.
53. Mann, S., et al., "Crystallization at Inorganic-organic Interfaces: Biominerals and Biomimetic Synthesis". *Science.* 261(5126), p. 1286-1292, 1993.

54. Mann, S., "Biomineralization: the form(id)able part of bioinorganic chemistry". *J. Chem. Soc., Dalton Trans.* 21, p. 3953-3961, 1997.
55. Mann, S., "Biomineralization and biomimetic materials chemistry". *Journal of Materials Chemistry*. 5: p. 935-946, 1995.
56. Zhang, Z., et al., "Synthesis of Uniform Silica Rods, Curved Silica Wires, and Silica Bundles Using Filamentous fd Virus as a Template". *Small* 3(3), p. 424-428, 2007.
57. Royston, E., et al., "Characterization of silica-coated tobacco mosaic virus". *Journal of Colloid and Interface Science*. 298(2), p. 706-712, 2006.
58. Davis, S.A., et al., "Bacterial templating of ordered macrostructures in silica and silica-surfactant mesophases". *Nature*. 385, p. 420-423, 1997.
59. Hubert, D. H. W., et al., "Vesicle-Directed Growth of Silica". *Advanced Materials.* 12(17), p. 1286-1290, 2000.
60. Becher, P., *Emulsions: Theory and Practice.* Reinhold Publishing Corporation: New York, USA, 1957.
61. Anna, S.L., et al., "Formation of dispersions using ``flow focusing'' in microchannels". *Applied Physics Letters*. 82(3), p. 364-366, 2003.
62. Sherman, P., *Emulsion Science.* Academic Press: New York, 1968.
63. Squires, T.M., et al., "Microfluidics: Fluid physics at the nanoliter scale". *Reviews of Modern Physics*. 77(3), p. 977-50, 2005.
64. Gravesen, P., et al., "Microfluidics-a review". *Journal of Micromechanics and Microengineering*. 3(4), p. 168-182, 1993.
65. Beebe, D.J., et al., "PHYSICS AND APPLICATIONS OF MICROFLUIDICS IN BIOLOGY". *Annu. Rev. Biomed. Eng.* 4, p. 261-286, 2002.
66. Harrison, D.J., et al., "Micromachining a Miniaturized Capillary Electrophoresis-Based Chemical Analysis System on a Chip". *Science.* 261(5123), p. 895-897, 1993.
67. Jacobson, S.C., et al., "High-Speed Separations on a Microchip". *Anal. Chem.* 66, p. 1114-1118, 1994.
68. Joscelyne, S.M., et al., "Membrane emulsification -- a literature review". *Journal of Membrane Science*. 169(1), p. 107-117, 2000.
69. Rayner, M., et al., "The impact of mass transfer and interfacial expansion rate on droplet size in membrane emulsification processes". *Colloids and Surfaces A: Physicochemical and Engineering Aspects*. 266(1-3), p. 1-17, 2005.
70. Rayner, M., et al., "Using the Surface Evolver to model droplet formation processes in membrane emulsification". *Journal of Colloid and Interface Science*. 279(1), p. 175-185, 2004.
71. Sugiura, S., et al., "Interfacial Tension Driven Monodispersed Droplet Formation from Microfabricated Channel Array". *Langmuir*. 17(18), p. 5562-5566, 2001.
72. Kobayashi, I., et al., "Microscopic observation of emulsion droplet formation from a polycarbonate membrane". *Colloids and Surfaces A: Physicochemical and Engineering Aspects*. 207(1-3), p. 185-196, 2002.

73. Schroder, V., et al., "Production of emulsions using microporous, ceramic membranes". *Colloids and Surfaces A: Physicochemical and Engineering Aspects*. 152(1-2), p. 103-109, 1999.
74. Yasuno, M., et al., "Visualization and characterization of SPG membrane emulsification". *Journal of Membrane Science*. 210(1), p. 29-37, 2002.
75. Vladisavljevic, G.T. et al., "Preparation and analysis of oil-in-water emulsions with a narrow droplet size distribution using Shirasu-porous-glass (SPG) membranes". *Desalination*. 144(1-3), p. 167-172, 2002.
76. Mine, Y., et al., "Preparation and stabilization of simple and multiple emulsions using a microporous glass membrane". *Colloids and Surfaces B: Biointerfaces*. 6(4-5), p. 261-268, 1996.
77. Schroder, V., et al., "Effect of Dynamic Interfacial Tension on the Emulsification Process Using Microporous, Ceramic Membranes". *Journal of Colloid and Interface Science*. 202(2), p. 334-340, 1998.
78. Kobayashi, I., et al., "Silicon array of elongated through-holes for monodisperse emulsion droplets". *AIChE*. 48(8), p. 1639-1644, 2002.
79. Kobayashi, I., et al., "Preparation characteristics of oil-in-water emulsions using differently charged surfactants in straight-through microchannel emulsification". *Colloids and Surfaces A: Physicochemical and Engineering Aspects*. 229(1-3), p. 33-41, 2003.
80. Kobayashi, I., et al., "Novel Asymmetric Through-Hole Array Microfabricated on a Silicon Plate for Formulating Monodisperse Emulsions". *Langmuir*. 21(17), p. 7629-7623, 2005.
81. Thorsen, T., et al., "Dynamic Pattern Formation in a Vesicle-Generating Microfluidic Device". *Physical Review Letters*. 86(18), p. 4163, 2001.
82. Okushima, S., et al., "Controlled Production of Monodisperse Double Emulsions by Two-Step Droplet Breakup in Microfluidic Devices". *Langmuir*. 20(23), p. 9905 – 9908, 2004.
83. Nisisako, T., et al., "Controlled formulation of monodisperse double emulsions in a multiple-phase microfluidic system". *Soft Matter*. 1, p. 23-27, 2005.
84. Sugiura, S., et al., "Effect of Channel Structure on Microchannel Emulsification" *Langmuir*. 18(15), p. 5708-5712, 2002.
85. Sugiura, S., et al., "Characterization of spontaneous transformation-based droplet formation during microchannel emulsification". *Journal of Physical Chemistry B*. 106(36), p. 9405-9, 2002.
86. Nakagawa, K., et al., "Microchannel emulsification using gelatin and surfactant-free coacervate microencapsulation". *Journal of Colloid and Interface Science*. 278(1), p. 198-205, 2004.
87. Sugiura, S., et al., "Effect of interfacial tension on the dynamic behavior of droplet formation during microchannel emulsification". *Journal of Colloid and Interface Science*. 269(1), p. 178-185, 2004.
88. Garstecki, P., et al., "Formation of monodisperse bubbles in a microfluidic flow-focusing device". *Applied Physics Letters*. 85(13), p. 2649-2651, 2004.

89. Gañán-Calvo, A.M., "Generation of Steady Liquid Microthreads and Micron-Sized Monodisperse Sprays in Gas Streams". *Physical Review Letters*. 80(2), p. 285, 1998.
90. Gañán-Calvo, A.M., et al., "Perfectly Monodisperse Microbubbling by Capillary Flow Focusing". *Physical Review Letters*. 87(27), p. 274501, 2001.
91. Meinhart, C.D., et al., "The flow structure inside a microfabricated inkjet printhead". *Journal of Microelectromechanical Systems*. 9(1), p. 67-75, 2000.
92. Le, H.P., "Progress and Trends in Ink-jet Printing Technology". *The Journal of Imaging Science and Technology*. 42(1), p. 49-62, 1998.
93. Gordillo, J.M., et al., "A new device for the generation of microbubbles". *Physics of Fluids*. 16(8), p. 2828-2834, 2004.
94. Link, D.R., et al., "Geometrically Mediated Breakup of Drops in Microfluidic Devices". *Physical Review Letters*. 92(5), p. 054503-4, 2004.
95. Cramer, C., et al., "Drop formation in a co-flowing ambient fluid". *Chemical Engineering Science*. 59(15), p. 3045-3058, 2004.
96. Jensen, M.J., et al., "A numerical study of two-phase Stokes flow in an axisymmetric flow-focusing device". *Physics of Fluids*. 18(7), p. 077103-10, 2006.
97. Brittain, S., et al., "Soft lithography and microfabrication". *Physics World*. 11, p. 31-37, 1998.
98. Seo, M., et al., "Microfluidics: From Dynamic Lattices to Periodic Arrays of Polymer Disks" *Langmuir*. 21(11), p. 4773-4775, 2005.
99. Lewis, P.C., et al., "Continuous Synthesis of Copolymer Particles in Microfluidic Reactors". *Macromolecules.* 38, p. 4536-4538, 2005.
100. Nie, Z., et al., "Polymer Particles with Various Shapes and Morphologies Produced in Continuous Microfluidic Reactors". *J. Amer. Chem. Soc.* 127, p. 8058-8063, 2005.
101. Seo, M., "Continuous Microfluidic Reactors for Polymer Particles". *Langmuir.* 21(25), p. 11614-11622, 2005.
102. Murakami, T., et al., "Dynamics of Polymeric Solid Surfaces Treated with Oxygen Plasma: Effect of Aging Media after Plasma Treatment". *Journal of Colloid and Interface Science*. 202, p. 37-44, 1998.
103. Rogers, T., et al., "Selection of glass, anodic bonding conditions and material compatibility for silicon-glass capacitive sensors". *Sensors and Actuators A: Physical*. 46, p. 113-120, 1995.
104. Cozma, A., et al., "Characterization of the electrostatic bonding of silicon and Pyrex glass". *J. Micromech. Microeng*. 5, p. 98-102, 1994.
105. Zendejas, F.J., et al., "Microfluidic Generation of Tunable Emulsions for Templated Monodisperse Silica". *Transducers Conference; Seoul Korea*, 2005.
106. Cristini, V., et al., "Drop breakup and fragment size distribution in shear flow". *Journal of Rheology*. 47(5), p. 1283-1298, 2003.
107. Cristini, V., et al., "Theory and numerical simulation of droplet dynamics in complex flows-a review". *Lab on a Chip.* 4(4), p. 257-264, 2004.

108. Tan, Y.-C., et al., "Design of microfluidic channel geometries for the control of droplet volume, chemical concentration, and sorting". *Lab on a Chip.* 4(4), p. 292-298, 2004.
109. Benichou, A., et al., "Double emulsions stabilized by new molecular recognition hybrids of natural polymers". *Polymers for Advanced Technologies*. 13(10-12), p. 1019-1031, 2002.
110. Edris, A., et al., "Encapsulation of orange oil in a spray dried double emulsion". *Nahrung/Food*. 45(2), p. 133-137, 2001.
111. Lee, M.-H., et al., "Preparation of Silica Particles Encapsulating Retinol Using O/W/O Multiple Emulsions". *Journal of Colloid and Interface Science*. 240(1), p. 83-89, 2001.
112. Muguet, V., et al., "Formulation of shear rate sensitive multiple emulsions". *Journal of Controlled Release*. 70(1-2), p. 37-49, 2001.
113. Laugel, C., et al., "Modulated release of triterpenic compounds from a O/W/O multiple emulsion formulated with dimethicones: infrared spectrophotometric and differential calorimetric approaches". *Journal of Controlled Release*. 63(1-2), p. 7-17, 2000.
114. Gallarate, M., et al., "On the stability of ascorbic acid in emulsified systems for topical and cosmetic use". *International Journal of Pharmaceutics*. 188(2), p. 233-241, 1999.
115. Bocanegra, R., et al., "Monodisperse structured multi-vesicle microencapsulation using flow-focusing and controlled disturbance". *Journal of Microencapsulation*. 22(7), p. 745-759, 2005.
116. Nisisako, T., et al., "Monodisperse anisotropic polymeric particles generated from a micro co-flow system". *Microelectromechanical Systems (MEMS) Conference: Istanbul, Turkey*, 2006: p. 470-473.
117. Sugiura, S., et al., "Preparation characteristics of water-in-oil-in-water multiple emulsions using microchannel emulsification". *Journal of Colloid and Interface Science*. 270(1), p. 221-228, 2004.
118. Utada, A.S., et al., "Monodisperse Double Emulsions Generated from a Microcapillary Device". *Science.* 308(5721), p. 537-541, 2005.
119. van der Graaf, S., et al., "Preparation of double emulsions by membrane emulsification--a review". *Journal of Membrane Science*. 251(1-2), p. 7-15, 2005.
120. Zendejas, F.J., et al., "Microfluidic Generation of Tunable Double Emulsions for Templated Monodisperse Silica Particles". *Micro-Tas Conference: Tokyo, Japan*, 2006.
121. Davis, M.E., et al., "Zeolite and molecular sieve synthesis". *Chem. Mater.* 4, p. 756-768, 1992.
122. Austin, I.G. et al., "Metallic and Nonmetallic Behavior in Transition Metal Oxides". *Science*, 168(3927), p. 71-77, 1970.
123. Kresge, C.T., et al., "Ordered mesoporous molecular sieves synthesized by a liquid-crystal template mechanism". *Nature*, 359(6397), p. 710-712, 1992.
124. Klein, S.M., et al., "Synthesis of Spherical Polymer and Titania Photonic Crystallites". *Langmuir.* 21(15), p. 6669-6674, 2005.

125. Fuhrmann, T., et al., "Diatoms as living photonic crystals". *Applied Physics B: Lasers and Optics*. 78(3), p. 257-260, 2004.
126. Ishikawa, K., et al., "Formation process of three-dimensional arrays from silica spheres". *AlChE.* 49(5), p. 1293-1299, 2003.
127. Yi, G.-R., et al., "Generation of uniform photonic balls by template-assisted colloidal crystallization". *Synthetic Metals*. 139(3), p. 803-806, 2003.
128. Imhof, A. et al., "Ordered macroporous materials by emulsion templating". *Nature*, 389(6654), p. 948-951, 1997.
129. Manoharan, V.N., et al., "Photonic Crystals from Emulsion Templates". *Advanced Materials.* 13(6), p. 447-450, 2001.
130. Olkhovyk, O., et al., "Periodic Mesoporous Organosilica with Large Heterocyclic Bridging Groups". *J. Am. Chem. Soc.* 127(1), p. 60-61, 2005.
131. Holland, B., "Determination of Both Mesopores and Macropores in Three-Dimensional Ordered Porous Materials by Nitrogen Adsorption". *Journal of Porous Materials.* 10(1), p. 17-22, 2003.
132. Schacht, S., et al., "Oil-Water Interface Templating of Mesoporous Macroscale Structures". 273(5276), p. 768-771, 1996.
133. Imhof, A., et al., "Macroporous materials with uniform pores by emulsion templating". *Mat. Res. Soc. Symp. Proc*. 497, p. 167-172, 1998.
134. Caruso, F., et al., "Nanoengineering of Inorganic and Hybrid Hollow Spheres by Colloidal Templating". *Science.* 282, p. 1111-1114, 1998.
135. Butler, R., et al., "Emulsion Templating Using High Internal Phase Supercritical Fluid Emulsions". *Advanced Materials.* 13(19), p. 1459-1463, 2001.
136. Cameron, N.R., "High internal phase emulsion templating as a route to well-defined porous polymers". *Polymer*. 46(5), p. 1439-1449, 2005.
137. Imhof, A., et al., "Uniform Macroporous Ceramics and Plastics by Emulsion Templating". *Chemical Engineering & Technology.* 21(8), p. 682-685, 1999.
138. Johnson, S.A., et al., "Ordered Mesoporous Polymers of Tunable Pore Size from Colloidal Silica Templates". *Science.* 283, p. 963-965, 1999.
139. Nisisako, T., et al., "Synthesis of Monodisperse Bicolored Janus Particles with Electrical Anisotropy Using a Microfluidic Co-Flow System". *Advanced Materials.* 18(9), p. 1152-1156, 2006.
140. Kim, T.K., et al., "Gas foamed open porous biodegradable polymeric microspheres". *Biomaterials*. 27(2), p. 152-159, 2006.
141. Manoharan, V.N., et al., "Building Materials by Packing Spheres". *MRS Bulletin*. 29(2), p. 91-95, 2004.
142. Manoharan, V.N., et al., "Dense Packing and Symmetry in Small Clusters of Microspheres". *Science.* 301, p. 483-487, 2003.
143. Shimizu, K., et al., "Silicatein alpha : Cathepsin L-like protein in sponge biosilica". *Proc. Natl. Acad. Sci. USA.* 95(11), p. 6234-6238, 1998.
144. Muller, W.E.G., *Silicon Biomineralization: Biology, Biochemistry, Molecular Biology, Biotechnology.* Springer Verlag: 2003.
145. Sumper, M., et al., "Silica formation in diatoms: the function of long-chain polyamines and silaffins". *J. Materials Chemistry.* 14, p. 2059-2065, 2004.

146. Nelson, D.L., et al., *Lehninger Principles of Biochemistry*. W.H. Freeman; 4th edition: April 23, 2004.
147. Fan, J., et al., "Rapid and high-capacity immobilization of enzymes based on mesoporous silicas with controlled morphologies". *Chemical Communications*. 17, p. 2140-2141, 2003.
148. Yiu, H.H.P., et al., "Enzyme immobilisation using siliceous mesoporous molecular sieves". *Microporous and Mesoporous Materials*. 44-45, p. 763-768, 2001.
149. Gill, I., et al., "Bioencapsulation within synthetic polymers (Part 1): sol-gel encapsulated biologicals". *Trends in Biotechnology*. 18(7), p. 282-296, 2000.
150. Avnir, D., et al., "Enzymes and Other Proteins Entrapped in Sol-Gel Materials". *Chem. Mater*. 6(10), p. 1605-1614, 1994.
151. Wu, C.-W., et al., "Protein and enzyme immobilization on non-porous microspheres of polystyrene". *Biotechnology and Applied Biochemistry*. 27: p. 225-230, 1998.
152. Kennedy, J.F., "A future for immobilized cell technology". *Nature*, 299, p. 777-778 1982.
153. Luckarift, H.R., et al., "Enzyme immobilization in a biomimetic silica support". *Nat Biotech*. 22(2), p. 211-213, 2004.
154. Kamins, T., et al., "Self-Assembled Semiconductor Nanowires on Silicon and Insulating Substrates: Experimental Behavior". *Science and Technology of Semiconductor-On-Insulator Structures and Devices Operating in a Harsh Environment*. p. 327-332, 2005.
155. Sharma, S., et al., "Synthesis of thin silicon nanowires using gold-catalyzed chemical vapor deposition". *Applied Physics A: Materials Science & Processing*. 80(6), p. 1225-1229, 2005.
156. Islam, S., et al., "A novel interconnection technique for manufacturing nanowire devices". *Applied Physics A: Materials Science & Processing*. 80(6): p. 1133-1140, 2005.